The Use of Image and Point Cloud Data in Statistical Process Control

Fadel Mounir Megahed

Dissertation submitted to the faculty of the Virginia Polytechnic Institute and State University in partial fulfillment of the requirements for the degree of

Doctor of Philosophy
in
Industrial and Systems Engineering

Jaime A. Camelio, Committee Co-Chair
William H. Woodall, Committee Co-Chair
Kimberly P. Ellis
Joel A. Nachlas

March 26, 2012
Blacksburg, Virginia

Keywords: 3D Laser Scanners, Control Charts, Fault Diagnosis, High Density Data, Machine Vision Systems, Profile Monitoring, and Spatiotemporal Analysis

The Use of Image and Point Cloud Data in Statistical Process Control

Fadel Mounir Megahed

ABSTRACT

The volume of data acquired in production systems continues to expand. Emerging imaging technologies, such as machine vision systems (MVSs) and 3D surface scanners, diversify the types of data being collected, further pushing data collection beyond discrete dimensional data. These large and diverse datasets increase the challenge of extracting useful information. Unfortunately, industry still relies heavily on traditional quality methods that are limited to fault detection, which fails to consider important diagnostic information needed for process recovery. Modern measurement technologies should spur the transformation of statistical process control (SPC) to provide practitioners with additional diagnostic information. This dissertation focuses on how MVSs and 3D laser scanners can be further utilized to meet that goal. More specifically, this work: 1) reviews image-based control charts while highlighting their advantages and disadvantages; 2) integrates spatiotemporal methods with digital image processing to detect process faults and estimate their location, size, and time of occurrence; and 3) shows how point cloud data (3D laser scans) can be used to detect and locate unknown faults in complex geometries. Overall, the research goal is to create new quality control tools that utilize high density data available in manufacturing environments to generate knowledge that supports decision-making beyond just indicating the existence of a process issue. This allows industrial practitioners to have a rapid process recovery once a process issue has been detected, and consequently reduce the associated downtime.

DEDICATION

To my grandma and Montasser, in heaven

And my mum, my guiding light on earth

ACKNOWLEDGMENT

First of all, I would like to express my deepest thanks to Dr. Jaime Camelio for his continued support, trust and encouragement. I am also indebted to Prof. William H. Woodall who taught me all that I know about quality control and process monitoring. Dr. Camelio and Dr. Woodall, this dissertation would not have been possible if it were not for your advice and support.

I would also like to thank my committee members, Dr. Joel Nachlas and Dr. Kimberly Ellis for their valuable comments, and for bringing different perspectives to this work. Dr. Nachlas introduced me to change-point methods, which became a fundamental component of Chapter 3. Dr. Ellis's continued coaching has helped me grow as an academic.

In addition, I would like to thank my colleagues and friends in the iMAS lab, especially Lee Wells and Jeremy Rickli who have helped me a lot during my graduate research and taught me how to be a graduate researcher. I would also like to thank Mrs. Hannah Parks and the rest of the ISE staff who made me feel home here in Virginia Tech.

I owe my deepest gratitude to the faculty of the Mechanical Engineering Department in the American University of Cairo, where I did my undergraduate studies. Without you, I would have never had the knowledge to ever-succeed on this level.

I would like to thank my best friends in Cairo for being there for me every day in my life and more importantly for being there for my family when I could not. Amal, Dina, Fatma, Gamil, Mokhtar, Nourhan, Omar, and Yahia; no words are enough to show my gratitude for you.

Andrew Henry, thank you for being there for me and for being a great friend. Finally, I would like to thank my greatest friend, supporter and role-model Lora Cavuoto. Without you, I could have never made it, and I could have never been able to withstand being all these many thousand miles away from my family, friends and my beloved country. You are the best and will always be family.

TABLE OF CONTENTS

LIST OF FIGURES

LIST OF TABLES

PREFACE

This dissertation is submitted in partial fulfillment of the requirements for the Doctor of Philosophy in Industrial and Systems Engineering. It involves the research work performed starting in late May 2009 until early February 2012 in the iMAS lab, a part of the Center for High Performance Manufacturing in the ISE department in Virginia Tech. Some of the ideas in this work, as in any research, are based on the research of others, and I have done my best to provide references to these sources.

In the spring semester of 2009, I had the idea of utilizing control charts combined with digital image processing to detect faults and trends in manufacturing processes. Dr. Woodall suggested reviewing the current literature as a starting point. This process led to finding out that the majority of the techniques in the literature were developed in isolation and had many limitations. Consequently, this seemed to be an interesting research paper idea and I wrote the original draft. However, Dr. Woodall used a lot of his expertise to further develop this paper; he guided me to classify image-based control charting techniques according to control chart type rather than by application. In addition, Dr. Camelio provided feedback, especially with regards to the use of Perceptron® systems. It should also be noted that the *Journal of Quality Technology* reviewers and the editor have also provided feedback, which resulted in the current form of the paper that is shown in Chapter 2.

After finishing up the draft for the review paper, I was taking Dr. Woodall's advanced SQC class in Spring 2010. In this class, we read a journal paper per week and discussed them in class. I was introduced to the topic of public-health surveillance in that class and made the comment that these ideas can be very easily extended to image-based systems, which was the area of research that interested me. As I talked about that idea in class and in the lab, Lee Wells became very interested and asked me if he could join this research project to assist with programming and identifying the metrics needed for performance evaluation. I modified and ran the code to obtain the results needed for the paper and modified it to produce the video that I used in my dissertation proposal. Using these results, I wrote the first draft of the paper. Then, Lee, Dr. Camelio and Dr. Woodall

provided their feedback which I used to further improve the paper. This resulted in the current form of the paper, which can be found online on the *QREI* website.

In May 2010, Dr. Camelio talked to Lee about looking into 3D laser scan data for SPC purposes. In one of our lab meetings, Lee told me that he was thinking of implementing a multinomial CUSUM approach to that problem. However, I told him that a profile monitoring approach is probably easier and more intuitive. Therefore, we looked into the use of Q-Q plots. I reviewed the literature, interpreted the results, and wrote the paper, while Lee wrote the simulation code. This work was then presented by Dr. Camelio at the *SAE 2010 Aerospace Manufacturing and Automated Fastening Conference & Exhibition*. From there, the next step was to do experimental studies to showcase how the method can be implemented in a manufacturing setting. I designed the experiment and Cory Niziolek, an undergraduate researcher in iMAS, helped with the scanning process. Dr. Woodall added his input on the statistical methods in the paper. As in the previous papers, the manuscript was revised based on the referees' comments. The version presented in this dissertation reflects a draft based mostly on my work and does not include the final revisions for publication done by Lee Wells. This paper is now under second review at the *Journal of Intelligent Manufacturing*.

Writing this dissertation has been extremely challenging; however, in the process my knowledge about statistical process monitoring and digital image processing have increased a lot. The multi-disciplinary focus of this work has lead to the incorporation of many statistical, computer science, and industrial engineering concepts, which made the dissertation more complete.

1 Introduction

The goal of my dissertation is to investigate how high-density imaging data from machine vision systems or three-dimensional laser scanners can be incorporated into the statistical process control (SPC) framework. Such images can economically provide thousands of data points representing the geometry, surface finish and/or color of manufactured parts. This type of data allows for a more accurate depiction of the quality of these parts when compared to traditional SPC methods that usually focus on monitoring a few pre-defined quality characteristics. Capturing the image-based aesthetic quality characteristics enables industrial practitioners to better monitor and control their manufacturing process to lower variation and decrease the number of nonconforming items produced. In addition, the efficient use of digital images can significantly reduce the time required for fault diagnosis/correction since digital images can provide a greater amount of process/product data. Accordingly, this data should be analyzed more effectively such that practitioners can have a control charting scheme that reflects the dual-objective of SPC, i.e., rapid fault detection capability and an ability to provide diagnostic information after the detection of process shifts. Through the use of imaging data in SPC, I foresee a quality control system that can provide 1) a rapid fault detection capability, 2) insight on the root-cause of a process shift, 3) assistance to industrial practitioners in making more informed quality control decisions, and 4) means to reducing the risk of catastrophic machine failures.

1.1 Motivation

The availability of data pertaining to the quality performance of manufacturing systems continues to increase. More importantly, emerging imaging technologies, e.g. machine vision systems (MVSs) and 3D laser scanners, diversify the types of data being collected pushing data collection beyond historically discrete dimensional data. These large and diverse datasets increase the challenge of extracting useful information. In addition, industry still relies heavily on traditional quality methods that are limited to fault detection. The process of identifying the root-cause of process problems is still heavily reliant on operators and engineers on the shop-floor. Identifying the root-causes for these

faults is not only time-consuming, but can also be very difficult. A recent survey in *The Economist* shows that "workers are already overloaded: 62% of them say that the quality of what they do is hampered because they cannot make sense of the data that they already have ..." (The Economist (Dec 2011)). Consequently, it is important to investigate how data can be used to generate a better understanding and knowledge of the performance of manufacturing systems. This follows the recommendations of the President's Council of Advisors on Science and Technology who stated that "advanced manufacturing … [depends] on the use and coordination of information, automation, computation, software, sensing, and networking …" (PCAST (2011)).

1.2 Significance

The effective use of high-density image data can significantly improve the performance of quality monitoring methods in manufacturing and service systems. In addition, the high-density information inherent in this data type could provide guidance in identifying the root-cause for process shifts and, as a result, reduce the downtime required to return the process to its in-control state. This is especially important since Fitchett and Sondalini (2006) reported that about 5-8% of production time is lost due to unplanned downtime as shown in Figure 1.1. These unplanned downtimes are extremely costly, for example, Reilly (2005) reported that every minute of production downtime in an automotive assembly plant costs an estimated $21,000, which would result in about $13 million in expenses per year per plant. Through the use of image-based monitoring approaches, practitioners would be able to monitor both dimensional and aesthetic quality characteristics, which would consequently reduce the possibility of producing defective products and/or failing to capture process deterioration when compared to solely monitoring dimensional characteristics. Overall, this dissertation provides a framework to capture dimensional and aesthetic quality characteristic groups by bringing together methodologies from statistical process control, digital image processing, epidemiology, and statistics.

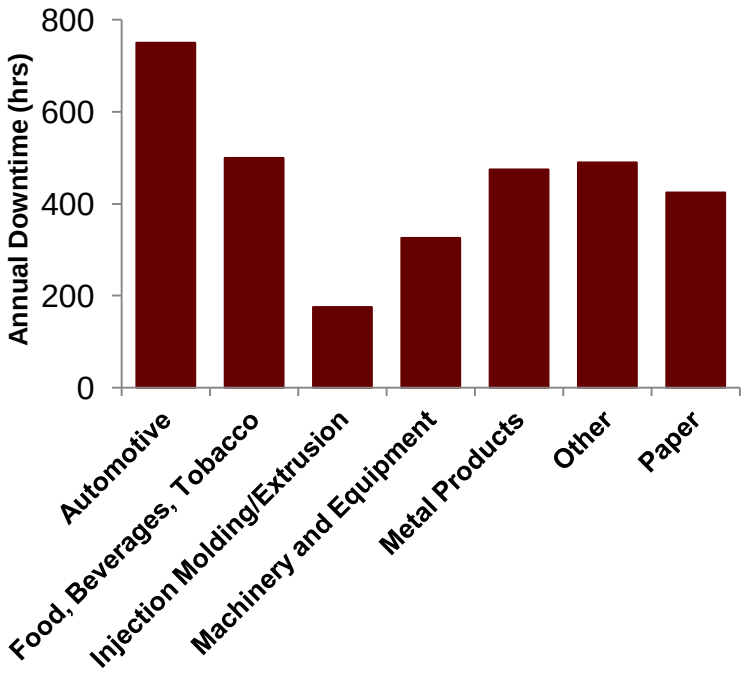

Figure 1.1: Annual Downtime in Hours Assuming 24/7 Production Environments (Adapted from Fitchett and Sondalini (2006))

1.3 Research Objectives

The goal of this dissertation is to create new quality control tools that utilize the availability of high density data in manufacturing environments to generate knowledge that supports fault diagnosis rather than only indicating the existence of a process problem. Under this main goal, four critical topics are addressed in this dissertation:

1. *Identifying and proposing metrics for the evaluation of the performance of image-based control charting methodologies*: The majority of the image-based control charting techniques that are presented in the literature are evaluated through their performance in a specific application, which makes their comparison difficult, if not impossible. Therefore, it is important to identify how to evaluate the performance of different image-based control charting methods to allow practitioners to better understand their advantages and their limitations.
2. *Developing a spatiotemporal framework for image monitoring*: Image data is inherently spatiotemporal. One image provides information pertaining to the location/size of faults on a manufactured part. On the other hand, capturing the

variation from one image to another can provide valuable information regarding when a process problem occurs. Unfortunately, the available literature on grayscale image monitoring has only considered only the first of these two features, which reduces the benefits captured in this type of data. The methodology presented in this dissertation will not only detect process problems, but will also provide useful diagnostic information such as the estimates of the change-point, fault location and size.

3. *Detecting unspecified faults through the use of point clouds*: A new methodology is proposed for utilizing laser scanners' ability to provide an entire depiction of the surface of a manufactured part in order to capture unspecified faults. Typically, the dimensional quality of products is assessed through measuring a few predetermined points on the surface, which makes practitioners unable to detect faults that do not affect these sampling points.
4. *Identifying process issues through spatial analysis of point clouds*: Once a process shift is detected, 3D scanning software is used to identify the location of the defect(s) that caused the proposed control charting methodology to signal.

1.4 Dissertation Layout

This dissertation is comprised of five major chapters.

Following the introductory first chapter, the second chapter provides a review of image-based control charts that have been proposed for a number of industrial and medical applications. This chapter shows the novelty and significance of the work presented in this dissertation. It should be noted that chapter two is paper that was published in 2011 in the *Journal of Quality Technology* and recognized as the most downloaded JQT paper in 2011.

Chapter three provides a framework for using grayscale images for fault detection and diagnosis through the use of a spatiotemporal method that is based on the generalized likelihood ratio (GLR) control chart. The performance of this control chart is evaluated through computer simulations, which show how the method performs under various out-of-control conditions. A lab study is presented to show the method can be applied to

industrial images. The reader should note that this chapter is based on a paper that was accepted to *Quality and Reliability Engineering International* and now appears on-line at the journal's website.

The fourth chapter shows how point cloud data obtained from 3D laser scanners can be used to detect and locate unknown faults that affect the surface of manufactured parts. As in the previous chapter, computer simulations and a lab study are used to illustrate the performance of the control charting method. This chapter is a draft of a paper that is currently under second review in the *Journal of Intelligent Manufacturing*.

Chapter five is the concluding chapter for this work. It summarizes the contributions and provides ideas for future research.

2 A Review and Perspective on Control Charting with Image Data

2.1 Abstract

Machine vision systems are increasingly being used in industrial applications due to their ability to provide not only dimensional information, but also information on product geometry, surface defects, surface finish, and other product and process characteristics. There are a number of applications of control charts for these high dimensional image data to detect changes in process performance and to increase process efficiency. We review control charts which have been proposed for use with image data in industry, and in some medical device applications, and discuss their advantages and disadvantages in some cases. In addition, we highlight some application opportunities available in the use of control charts with image data and provide some advice to practitioners.

2.2 Introduction

Recently there have been a number of industrial and medical device applications where control charts have been proposed for use with image data. The papers on this topic have appeared in a wide variety of subject matter fields, independent of previous related work. A primary purpose of our paper is to review these applications and the proposed methods. Our goal is to bring this work on the use of control charting for image data into better focus and to encourage further work in this area.

Control charts were proposed by Walter A. Shewhart in the 1920s as a simple and yet effective method to visualize and detect the occurrence of assignable causes of variability in manufacturing processes. It is well documented in the quality control literature that his control charts are most effective in detecting moderate to large shifts in the parameter being monitored. To improve the performance of the Shewhart control charts in detecting other types of unusual patterns, supplementary run rules were introduced (see, e.g., the Western Electric Company (1956)). There are several image-based approaches that are designed to aid in control chart pattern interpretation; see, for example, Arpaia et al.

(1999) and Lavangnananda and Piyatumrong (2005). These image-based tools are not included in our review since their inputs are standard control chart data patterns rather than industrial or medical images. It should also be noted that we do not cover the application of control charts to video sequence data for digital image processing purposes such as for detecting noise-obscured signals in a sequence of frames, as in Vihonen et al. (2008), or for scene recognition purposes as in Elbasi et al. (2005). We believe that 3D-laser scanning represents much of the future of industrial measurement since it can rapidly provide thousands (or millions) of data points representing the entire geometry of a part. Megahed et al. (2010b) introduced the application of control charting to 3D laser scanning data and highlighted some future research opportunities on this subject. This type of data collection and analysis, however, is also not covered in our paper.

We assume that the reader is familiar with the construction and use of control charts (for detailed introductions see Wheeler and Chambers (1992), Woodall and Adams (1998), or Montgomery (2008)). On the other hand, it is not assumed that the reader is familiar with the issues involved with image data. Therefore, a brief overview of image data processing is given in Section 2.3. In Section 2.4, we provide a discussion on some of the general differences between image-based control chart applications and more standard control charting. We then offer some general advice to practitioners. Then there are several sections on various types of methods proposed for monitoring with image data, along with their advantages and disadvantages in some cases. Finally, our conclusions are given in Section 2.12.

2.3 An Overview of Machine Vision Systems

A machine vision system (MVS) is a computer system which utilizes one or more image-capturing devices (e.g., cameras or X-ray devices) to provide image data for analysis and interpretation. The system involves the image capturing step, the analysis of the image data, taking appropriate action based on the image analysis, and learning from experience so that the system's future performance can be enhanced.

In spite of some similarities between human and machine vision, there are significant differences between them. As Zuech (2000) stated, current machine vision systems are

primitive when compared to the human eye-brain capability since, for example, current MVSs are susceptible to variations in lighting conditions, reflection, and minor changes in texture, among other variations, to which the human eye can easily adjust and compensate. Despite these limitations, the use of MVSs is superior to visual inspection with respect to 1) monitoring processes with high production rates; 2) performing multiple simultaneous tasks with different objects; 3) their ability to cover all the ranges of the electromagnetic spectrum, as in the use of magnetic resonance imaging (MRIs) and X-rays in medical applications; and 4) the lack of susceptibility to fatigue and distraction. In some cases use of MVSs is cheaper than the use of human inspectors and it is expected that the cost of MVSs will continue to decrease over time. These advantages position the use of MVSs as a much more attractive option than the use of human visual inspection in many cases, which explains their widespread and increasing use in industrial and medical applications. Therefore, there is a need for some statistical process control (SPC) monitoring techniques.

The acquisition of an image is the first step in any application of machine vision. An image is often represented as a function $f(x, y)$ or a vector $\mathbf{f}(x, y)$, where x and y represent the spatial coordinates on the image plane, and the value (or values) at any location (x, y) is commonly known as the intensity (or intensities). In digital images x, y, and the intensities take only non-negative integer values. As the resolution of the image capturing device increases, the image is divided into more elements (i.e., pairs of x and y) and thus the total number of elements (pixels) increases. On the other hand, the intensity values depend on whether the image is black and white (binary), grayscale, or in color. In the case of a binary image, each pixel can only have an intensity of either 0 (black) or 1 (white). If the image is grayscale, then $f(x, y)$ can take any integer value between 0 (black) and 255 (white) for 8-bit images. Finally, when the image is in color, $\mathbf{f}(x, y)$ is a vector of three individual components corresponding to red, green, and blue (RGB) with values between 0 and 255 for each component. Thus, in all three cases each image can be viewed as a collection of multivariate, spatially distributed observations with dimensionality that depends on the number of pixels and the type of image. For 16-bit images, the intensity values can take values between 0 and 2^{16}-1.

Images in industrial applications are most often grayscale or binary images. These images are cheaper to obtain and analyze. In addition, there is limited time to analyze images in industrial settings with high production rates, so there are advantages in using simple analysis methods.

The intensity values for neighboring pixels within an image are often highly correlated. This correlation can result in a considerable amount of data redundancy, where the information contained at any given pixel location in an image is relatively small since its intensity can often be predicted accurately from the neighboring pixels.

Color (RGB) images are just one example of a larger class of hyper-spectral images. A hyper-spectral image consists of a stack of aligned (i.e., congruent) images, each of which covers a certain wavelength band. Together these congruent images form a three-way matrix (x, y, $\mathbf{f}(x, y)$). It should be noted that $\mathbf{f}(x, y)$ is vector of the different wavelength intensities captured by the image capturing device. For example, the representation of an RGB image in its three-way matrix form is illustrated in Figure 2.1. In part due to the correlated nature of the information contained across the different congruent images, hyper-spectral images are usually referred to as multivariate images.

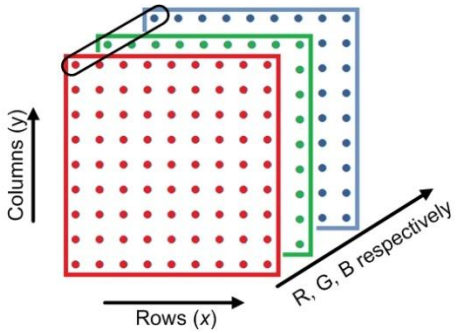

Figure 2.1: A color image representation in three wavelength channels (RGB).
The ellipse indicates the Red, Green, and Blue intensity values for a given pixel

After an image is captured, it must be analyzed so that information can be extracted. Gonzalez and Woods (2007) divided this process into three levels, 1) low-level processes comprised of basic operations of noise reduction, image compression, and contrast enhancement, where the inputs and outputs are images; 2) mid-level processes where the inputs are images and the outputs are attributes extracted from images such as edges,

objects, and contours; and 3) high-level operations aimed at understanding and making sense of the data. For binary/grayscale images, the process of information extraction is referred to as digital image processing or image analysis. There are quite a few books on this topic, including Nalwa (1993), Jähne (2005) and Gonzalez and Woods (2007). Multivariate images are often analyzed through some multivariate statistical framework, such as principal component analysis (PCA) or partial least squares (PLS) regression, for dimension reduction. The analysis process for multivariate images is commonly known as multivariate image analysis (MIA). We discuss MIA monitoring approaches in more detail in Section 2.10. For more information on the well-developed area of MIA, the reader is referred to Geladi and Grahn (1996), Grahn and Geladi (2007), and Pereira et al. (2009).

Machine vision systems are widely used in a variety of industries for inspection purposes where "good" items are to be separated from "bad" ones. Megahed and Camelio (2010) categorized MVS inspection applications into the following three groups: 1) medical applications, where MVSs are used in detecting and diagnosing abnormalities in different body parts (e.g. Liu et al. 1996); 2) transportation and construction applications, where MVSs are used in the identification and measurement of cracks, surface indentations, and protrusions in different construction materials and structures (e.g., Schmitt et al. (2000)); and 3) industrial applications. Malamas et al. (2003) reviewed in considerable detail the industrial use of MVSs to detect dimensional defects (comparing the product's shapes and dimensions with respect to the design tolerances), structural defects (checking for missing components in product assemblies), surface defects (inspecting surfaces for scratches, cracks, improper finish, and roughness), and operational defects (verifying the proper operation of inspected products). Despite their importance, we do not cover inspection applications in our paper unless control charts are directly involved.

2.4 General Differences from Standard SPC

The use of image-based control charts differs somewhat from the use of more traditional control charts. These differences can be attributed to a number of factors, which include the type of data being monitored, the rationale behind using control charts, and how the control charts are applied. Preliminary analysis of image data is required before control

charting methods can be used. Noise reduction, image compression, and other types of data processing may be necessary with image data before any monitoring can be done. This analysis is typically much more extensive than that required in standard control charting applications. Data processing speed can become an issue with 100% inspection.

Human inspectors do not respond with equal sensitivity to all visual information. Gonzalez and Woods (2007) discussed how humans search for distinguishing features within an image, such as edges and/or textural regions, and mentally combine them into recognizable groupings. A person then uses prior knowledge to complete the image interpretation process. Feature detection operations or multivariate analysis is needed with MVS data to perform an analogous type of interpretation.

In some applications image-based control charts are not used to detect changes in images over time, but in specifying where any flaws have occurred spatially on the objects being imaged. In these applications, the X-axis on the control chart can correspond to the location on the image. This is much different from traditional control chart practice where time or the sample number is plotted on the X-axis. These applications are based on a sliding window technique where the window (with a size based on target defect size to be detected) is moved progressively over the whole image area. A statistic is calculated for every window and a "spatial" control chart (due to the fact that the X-axis refers to the window's position within an image) is used for detecting defects. Spatial control charts are described in detail in Section 2.9. The reader should note that the majority of the image-based control charting methods discussed in this paper follow the standard SPC approach. Accordingly, unless otherwise specified, the X-axis of the discussed image-based control chart will correspond to either time or image number.

In process monitoring, it is very beneficial to carefully distinguish between the Phase I analysis of historical data and the Phase II monitoring stage. With Phase I data, one is interested in checking for stability of the process and in estimating in-control parameter values for constructing Phase II methods (see, e.g., Woodall (2000)). Phase I methods are usually evaluated by the overall probability of a signal, whereas run-length performance is typically used for comparison purposes in Phase II, where the run length is the number

of samples before a signal is given by the control chart. In general, for current papers on image-based control charts, there is often not a clear distinction made between the two phases. Exceptions include much of the work on MIA monitoring approaches, Lyu and Chen (2009), and the approach of Wang and Tsung (2005).

2.5 Advice to Practitioners

There are many practical decisions that must be made when using images for process monitoring. These include the choice of the image-capturing device, the frequency of imaging, the set-up of the imaging to avoid lighting, alignment, and other problems, the software to use for image analysis, the preliminary image processing, and the type of monitoring method to employ. There are no currently existing guidelines for guiding the practitioner through all of these decisions. It may be possible to use images taken in industry for some other purpose, such as inspection or item alignment, for process monitoring. Our advice to practitioners who are to implement image-based monitoring is to find the paper (or papers) on the most similar applications in order to obtain implementation ideas. Because there is no standard approach to image monitoring in most cases, practitioners will have to adapt methods to their particular applications.

The choice of a method will be driven to a large extent by the purpose of the monitoring. Often imaging is used for feature extraction, e.g., to obtain dimensional data on the imaged object. In this case, standard control charting methods are used on the obtained data just as if they had come from a source other than through imaging. Of course the measurement system must be evaluated through a gage R&R or other approach. This feature-extraction use of image data is the most straightforward and should be used when the focus is on known features, such as dimensional variables. This approach has been used for roughly twenty years in the automotive industry, e.g., with Perceptron® measurement systems (www.perceptron.com). A concern with extracting known features from images is that some unknown features, or other ignored information in the images, could be important because images allow for the detection of localized faults (e.g. the presence of an extra punched hole) which do not necessarily affect the extracted features.

In some applications, however, uniformity of the image is the ideal situation, as when checking a metal surface for flaws. In this case some measure of the number and size of flaws must be obtained and monitored. In other cases, such as in fabric monitoring, the ideal image has a specified pattern and any variations from this pattern are to be detected and located within the image. Spatial control charts are designed for this purpose. If the image is not expected to be uniform or with a particular specified regular pattern, there may still be requirements on the overall pattern, as in the monitoring of cultured marble countertops. In this case MIA may be most useful. Finally, in some cases it is not the images that are monitored over time so much as the image capturing device. In medical applications, for example, one obviously does not expect images to be consistent over time when different patients are being imaged. The overall image quality and consistency, however, can be measured and monitored.

Practitioners should be aware that many of the papers on image monitoring are rather difficult to understand. In a number of cases no careful justification is given for the monitoring approach. In our view, a considerable amount of work is needed in image monitoring to give it a more coherent structure and to provide guidelines for implementation. MIA is an exception in this regard, but it is applicable only under certain conditions and for certain purposes. MIA-based methods are discussed in more detail in Section 2.10.

2.6 Univariate Control Charts for Industrial Image Data

We first consider some univariate methods that were designed for use with successive binary or grayscale images.

Horst and Negin (1992) were among the first to discuss the advantages of using control charts with industrial image data, although we expect that control charts were used with image data in industry prior to the publication of their article. Horst and Negin (1992) argued that the use of Shewhart charts and histograms with machine vision data could lead to significant productivity improvements in web process applications, e.g., with paper, textiles, and plastic films. Emphasis was given to processes for which the in-process and post-process manufacturing steps need to be accomplished “in register” with

a visual feature such as a watermark. Their paper gave an overview of how control charts could be used with web production processes and included an example related to dimensional control.

Tan et al. (1996) used a MVS to sample and measure the quality characteristics (length, width, and area) of an extruded food product, specifically corn puffs, as a part of total statistical process control system. An X-bar control chart was used to monitor the size of the product. Corrective actions were determined using a proportional and integral (PI) control scheme to minimize the product size variations arising from variations in the moisture content of the corn. Considerable improvement was thereby achieved in product size uniformity.

Armingol et al. (2003) combined machine vision inspection techniques and control charts in developing an online inspection system for manufactured metallic parts. In their approach, they first accounted for illumination changes through a transformation of the pixel values of the image. Illumination changes can be due to problems in the positioning of the camera or changes in the light source. Then M (equal to number of pixels) individual-moving range (I-MR) control charts were constructed for each of the pixel locations to detect any abnormal changes in the image at each of the pixel locations. In their example, they constructed 439,296 control charts for the pixel values using control limits at plus and minus six standard deviations (estimated based on 20 images representing Phase I Data) to decrease the number of false alarms. In the case of a signal, the size and the location of the defect was based on the control charts that signaled. The construction of a control chart for every pixel location, however, does not account for the inter-pixel redundancy of neighboring pixels. In addition, this resulting huge number of control charts can require an excessive amount of computational time that may not allow for online monitoring in real time.

Nembhard et al. (2003) developed a MVS for monitoring color transitions in plastic extrusion processes using a forecasting algorithm. They transformed the original RGB data into grayscale using the hue as the metric, where the hue was calculated as the average of the red, green, and blue intensities. Their methodology integrates traditional

SPC tools for variable data with a forecasting system based on the exponentially weighted moving average (EWMA) statistic. Their algorithm utilizes process knowledge of whether a new color has been added to the extruder or not. In the absence of a color addition, their algorithm captures an image, eliminates the background, applies the hue transformation, and calculates the error between the actual image intensity values and the forecasted intensity values. The forecast errors are then plotted on a Shewhart control chart. On the other hand, if a new color has been added to the extrusion process, then their MVS would identify the end of the color transition stage so that the color of the produced product would be acceptable.

Liang and Chiou (2008) designed a MVS to automatically monitor the tool wear of coated drills. Their tool measurement system consisted of a macro lens and a ring light-bulb in addition to the camera and suitable computer software. The authors segmented (separated) the cutting tool from the background using a suitable threshold pixel intensity value that was based on their Taguchi method experimentation. This was followed by a number of digital image processing steps where they used edge detection techniques. Then they used an X-bar chart with three sigma limits to automatically select the upper and lower curvature threshold values which were needed to identify the vertices that represent the current profile of the cutting tool. Afterwards, the crater wear width, which reflects the amount of tool wear, was calculated using commercially available software.

2.7 Multivariate Control Charts for Industrial Image Data

Typically manufacturing processes are characterized by more than one quality characteristic. In these situations, the simultaneous monitoring of several quality characteristics often yields better results than monitoring each of these characteristics separately. This joint monitoring can be accomplished using multivariate control charts. A thorough review of multivariate control charting was provided by Bersimis et al. (2007). In this section, we will review some of the literature available on the use of multivariate control charts for industrial image monitoring.

Tong et al. (2005) used Hotelling T^2 control charts to monitor integrated circuit (IC) defects on a wafer map. It should be noted that a wafer is the building block of

semiconductor manufacturing, where several hundred integrated circuits (ICs) are simultaneously fabricated on one wafer. A wafer map is a visual display used in semiconductor manufacturing to show the locations of the defective IC chips on the wafer. Even though the wafer map is not based on an image, we include the approach by Tong et al. (2005) among our discussion of the literature because wafer maps possess many of the same spatiotemporal characteristics as industrial image data. Thus, some of the methods of analysis for wafer maps may be modified for use with image data.

The rationale behind the adoption of the Hotelling T^2 control chart by Tong et al. (2005) to monitor integrated circuit defects instead of a traditional defects control chart (c-chart) is based on previous research in the field of semiconductor manufacturing. Hansen et al. (1997) showed that IC defect positions on a wafer map are highly correlated since defective chips often occur in clusters or display systematic patterns. The defect clustering pattern can reflect the causes of the IC defects and therefore clustering indices (CIs) have been developed to accurately represent the clustering phenomenon (e.g., Jun et al. (1999)). The defect counts often cannot be modeled by a Poisson distribution and the corresponding traditional c-charts can have high false alarm rates, as shown by Friedman and Albin (1991).

The method proposed by Tong et al. (2005) is based on the number of defects and the CI as the two quality characteristics to be monitored. Tong et al. (2005) monitored these two quality characteristics using a Hotelling T^2 control chart. In the case of a signal in the T^2 control chart, Tong et al. (2005) suggested the decomposition of the T^2 statistic based on the method by Mason et al. (1997) to identify the cause of the signal. It must be determined whether a control chart signal is associated with an increased number of defects, due to the clustering of the defects, or associated with both.

Liu and MacGregor (2006) developed an MVS for monitoring the appearance and aesthetics of manufactured products with engineered stone countertops used as an example. A primary purpose of their paper was to extend the use of MVSs to the appearance of items that contain “visible patterns such as stripes, swirls, and ripples with varying characteristics in their shapes, sizes, and intensities.” Their methodology is

composed of the following three major steps: extraction of textural features from product images using wavelet transformations, quantitative estimation of the product appearance using principal component analysis (PCA), and monitoring the product appearance based on the most significant principal components. They used control charts in the last two stages of their methodology. In the second stage, a squared prediction error (SPE) plot was used to ensure that the variability of the countertop slabs was well modeled by the PCA model. In the last stage Hotelling T^2 and SPE control charts were used to detect off-specification countertops.

In another application, Lin (2007a, b) used wavelets and multivariate statistical approaches, including the Hotelling T^2 control charts, to detect ripple and other types of defects in electronic components, in particular surface barrier layer (SBL) chips of ceramic capacitors. The wavelet characteristics were used to describe the surface texture properties and then the author proposed a Hotelling T^2 control chart to judge the existence of a defect based on combining the different texture properties. In a later paper, Lin et al. (2008) conducted a comparison between the capabilities of a wavelet-Hotelling T^2 control chart approach and a wavelet-PCA-based approach in detecting surface defects in light-emitting diode (LED) chips. Their results showed that the wavelet-PCA based approach was more effective for their application.

Recently, Lyu and Chen (2009) integrated image processing technologies and multivariate statistical process control charts to design an automated visual inspection expert system, which could be used in mass production manufacturing systems as a part of the inspection process. As in many of the papers on this topic, their approach could be divided into a digital image processing step and a step where the control charts are applied. In the digital image processing stage, they suggested transforming the grayscale image into a binary image and then applying edge detection methods to further reduce the dimensionality of the data. Afterwards, the binary image was analyzed and the required dimensional quality characteristics were obtained and plotted on a multivariate control chart. They suggested the use of the chi-square control chart, Hotelling T^2 control chart, or a multivariate exponentially weighted moving average (MEWMA) control chart with the necessary control limits calculated based on Phase I data. In their application, they

inspected the inner and outer diameters of concentric circles using image processing techniques and used multivariate control charts for detecting special cause variations in the sample mean vector. In their illustrative example they used 20 samples as Phase I data and then applied their Phase II method on the remaining 15 samples.

2.8 Profile Monitoring for Industrial Image Data

Profile monitoring is the use of control charts for cases in which the quality of a process or product can be characterized by a functional relationship between a response variable and one or more explanatory variables. For detailed reviews on the subject, readers are referred to Woodall et al. (2004) and Woodall (2007). Image monitoring could be considered as a natural extension of profile monitoring methods to cases where the explanatory variables indicate the location of the intensity measurement(s) within the image. In general it is worth noting that the papers written on image monitoring can be considerably more difficult to understand than the papers on monitoring profiles involving only one explanatory variable. One tends to have much more data with image applications, a complicating spatial component, more complex analysis methods, and more wide-ranging potential purposes of the monitoring.

In profile monitoring one also has to decide if a particular feature of the profile is to be monitored, e.g., the maximum value, or whether the entire profile function should be monitored. If one chooses to monitor specific features, then standard control charting methods can be used directly. To monitor the entire profile function, one has to first model the function and take different approaches depending on whether parametric or nonparametric methods are used.

Wang and Tsung (2005) used profile monitoring techniques to detect changes in grayscale images using a Q-Q plot, which reflected the relationship between a current image sample and a baseline conforming image sample. The authors used their method in a case study to detect defects in mobile-phone liquid crystal display (LCD) panels. Their technique, however, can serve only as a fault detection tool since the pixel locations were ignored, thus removing any information on the type, size, or location of any defect(s).

Woodall (2007) suggested that the monitoring of product shapes is a very promising area of profile monitoring research since the shape of manufactured items is very often an important aspect of quality. Profile monitoring approaches using shape data can be more efficient than standard engineering methods for monitoring shape data because in many cases the engineering approaches do not use all of the information in the data. Colosimo et al. (2010) and Colosimo and Pacella (2011) extended the application of profile monitoring techniques to three dimensional surfaces using coordinate measuring machine data. For example, Colosimo et al. (2010) dealt with a more complex dataset than those traditionally considered in profile monitoring approaches in their application to monitor the surface quality of metallic surfaces. Their proposed approach combined a regression model with spatially correlated noise with univariate and multivariate control charts. They successfully tested their approach on metallic cylindrical items produced by turning on a lathe.

2.9 Spatial Control Charts for Industrial Image Data

The authors of the papers, discussed in this section, proposed control charting methods in a nonstandard way since the horizontal axis of each control chart represents a position in the image, not time. The control charts are used spatially by moving a mask (or window) across the image and then calculating and plotting a statistic each time the mask is moved. Typically the mask positions do not overlap and there is an implicit assumption that defects are just as likely to occur in one region of the image as in any other region of the same size. The size of the mask depends on the expected size of the defects to be detected, with smaller defective regions requiring smaller mask sizes.

Jiang and Jiang (1998) used a digital image processing system to inspect oil seals for conformance to size specifications and used modified I-MR charts to detect surface defects and their locations on the oil seals. They based their I-MR control charts on the gray level of pixels along analyzed circles superimposed on images of the oil seal.

In another application, Jiang et al. (2005) developed a method for the inspection of the uniformity of high-grade LCD monitors that involves analysis of variance (ANOVA) and spatial control charts to detect the type, size, and location of any defects. Their approach

did not utilize image processing techniques per se, but instead used a luminance meter, a light sensitive device, to collect the needed data for analysis. Their measurement process was to divide the LCD panel into a number of different blocks, each with an area of 1000 pixels. Data collection was done in a darkroom with the panel switched to a white background. ANOVA methods were used to identify areas significantly different from other areas in a panel. The EWMA chart was used to detect small differences in various panel areas and to detect the position and size of any defects. Since this method could have easily been implemented using image processing techniques where each block's intensity would be calculated through the mean intensity values of the pixels within that block, this paper falls within the image-based control chart literature. An illustration of an EWMA chart presented by Jiang et al. (2005) is shown in Figure 2.2. Despite the capability of their method to identify the defect type, location, and size, there are two limitations in this research. First, it would be difficult to detect a defective area partially overlapping two or more of the testing blocks. Also, there were no general guidelines for determining the value of the EWMA parameter λ. The authors determined their smoothing parameter value of 0.80 by trial and error.

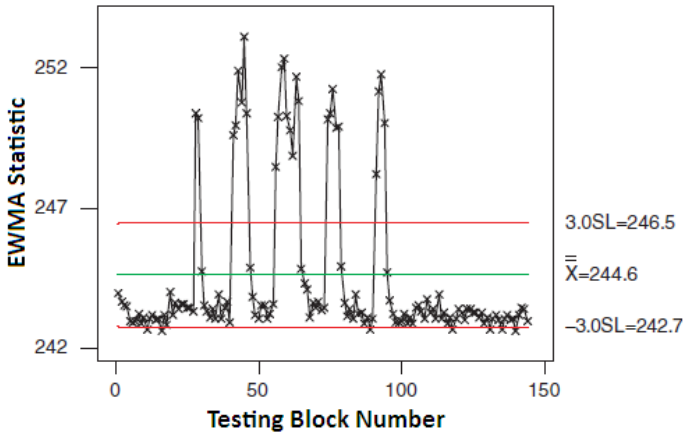

Figure 2.2: EWMA Chart for Detecting LCD defects.

(Adapted from Jiang et al. (2005)) Reprinted with permission from *Taylor & Francis Group*.

Copyright 2005 International Journal of Production Research.

In a similar application, Lu and Tsai (2005) used machine vision and a spatial X-bar chart to tackle the problem of detecting defects in LCD panels. Their approach first removed the repetitive background texture of LCD panels by transforming the image matrix into

the eigenvector space and removing the larger eigenvectors that captured the textural structure. Then the image was reconstructed from the resulting eigenvector space to check for defects. The defect detection scheme was based on a spatial X-bar chart, which can be applied to their reconstructed image since the variation in the intensity of the pixels was small. Thus the spatial control chart was used in distinguishing defects from the uniform background region. They used Chebyshev's theorem to determine the limits for their control chart with 4-σ limits so that their false classification percentage was around 6%.

Lin and Chiu (2006) recommended the use of the Hotelling T^2 control chart, among other methods, to detect MURA defects in LCD monitors. MURA defects are lighting variations on what should be uniform luminance over a surface. More specifically, they used the multivariate Hotelling T^2 statistic to combine the various coordinates of the color models to detect small color variations in the LCD panels. This was a spatial control chart procedure in the sense that the images of size 256x256 pixels were divided into 5x5 pixel subregions with a T^2 statistic calculated and plotted for each subregion.

Defects on thin film transistor (TFT) panels are classified into two categories, macro and micro defects. Lu and Tsai (2005) provided examples for each of the two defect categories. They defined the appearance of macro defects as regions of high contrast with irregular shapes and sizes such as MURA (unevenness in the TFT panels), SIMI (stains on TFT panels) and ZURE (misalignment of TFT panels). On the other hand, micro defects include pinholes, fingerprints, particles and scratches, which are generally very small and hard to detect using human inspectors. Accordingly, an effective machine vision system should be able to detect both defect categories. This goal has yet to be achieved and the available literature for image-based control charts has initially focused more on detecting the macro defects. It should be noted, however, that detecting macro, especially MURA, faults is not an easy task as they often have no clear contour or contrast (Taniguchi et al. (2006)).

Tunák and Linka (2008) provided a robust technique for detecting the occurrence and location of defects in woven fabrics with a plain weave structure using grey system

theory, which has been proposed as an alternative to the use of probability and fuzzy methods. For information on grey system theory, see Deng (1989). By observing that any woven image is periodic in nature and therefore can be considered to have directional texture, Tunák and Linka (2008) used second-order texture statistics because they allow for maintaining both brightness and spatial information. Specifically they used the grey level co-occurrence matrix, GLCM, of grey system theory first introduced for fabric monitoring by Haralick et al. (1973). Tunák and Linka (2008) used classification and regression tree techniques to extract the following five significant features from their matrix: energy, correlation, homogeneity, cluster shade, and cluster prominence. Since the presence of a texture defect causes regular structural changes and, consequently, statistical changes, the authors used a spatial Hotelling T^2 chart to combine multiple texture features and detect defects. Their approach is illustrated in Figure 2.3. The spatial Hotelling T^2 charts involved ten quality characteristics, each of the five features in both the warp and weft directions. Weft is the yarn which is drawn under and over perpendicular to the warp yarns to create a fabric, as illustrated in Figure 2.4.

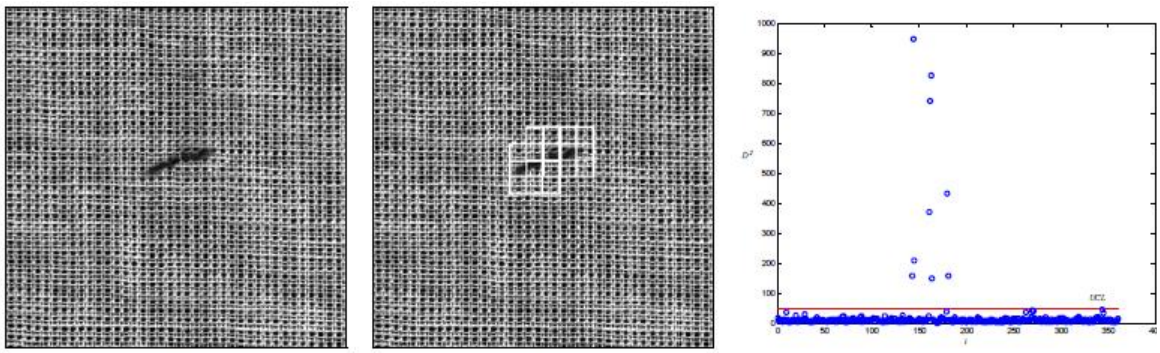

Figure 2.3: **(**a) Foreign body defect, (b) the marking of out of control windows based on T2 control chart, (c) plotting the quality characteristics on the T2 control chart.

(Adapted from Tunák and Linka (2008)) Reprinted with permission from Hong Kong Institution of Textile and Apparel (HKITA). Copyright 2008 Research Journal of Textile and Apparel.

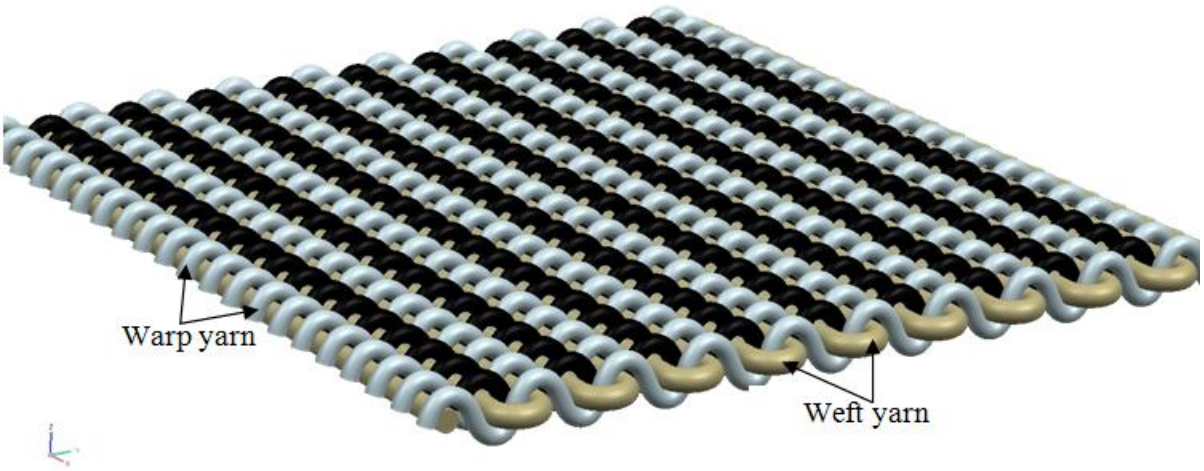

Figure 2.4: A schematic of the warp and weft directions for fabric

Tunák et al. (2009) improved the defect detection capability on plain weave structures by relaxing some of the earlier assumptions and adding more features to the SPC algorithm. Their proposed algorithm can account for the misplacement of the yarn on the image, e.g., possible rotation of the image. In addition, it can be used not only to detect defects associated with the change of weaving density of weft yarns, but also to monitor weaving density in the direction of the length of the fabric. Fabrics could also have different patterns, such as plain, twill, and satin. In order to achieve this flexibility, the authors followed a different approach than that of Tunák and Linka (2008). In particular, after the image is captured Tunák et al. (2009) performed contrast enhancement to increase the distinction between the woven fabric and the background. Then the authors applied a two-dimensional discrete Fourier transformation (2-D DFT) on the image matrix since this representation was found to be well-suited in representing the directionality of the periodic patterns. Through some manipulation of the parameters involving the 2-D DFT and its inverse, the resulting images can be made to contain only warp or weft set of yarns. Therefore, the restored images can be used for the automatic assessment of weaving density. The authors then used a spatial X-bar control chart on the weaving density as a tool to find sites of potential defects. A sample of their results is illustrated in Figure 2.5.

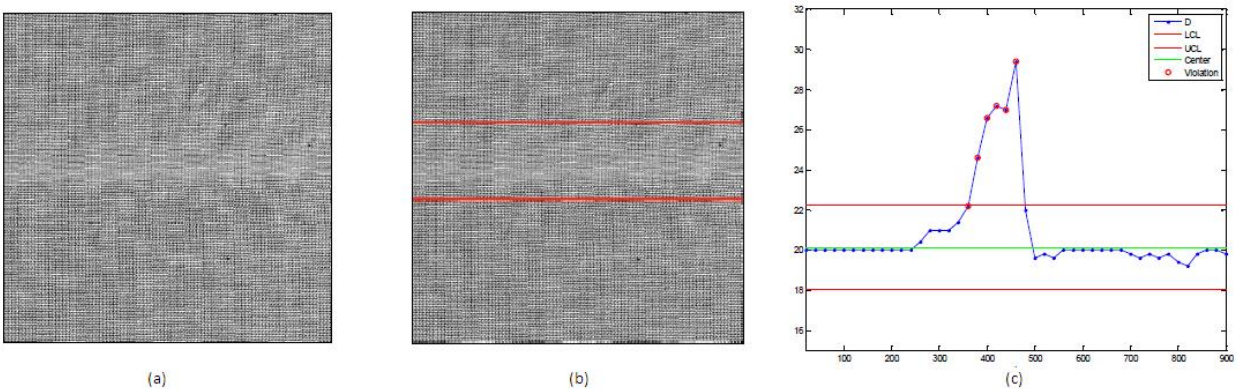

Figure 2.5: (a) Image of woven fabric in a plain weave with defective weft stripe, (b) defective region, (c) control charts for weaving density of weft yarns
(Adapted from Tunák et al. (2009)). Reprinted with permission from Springer Science+Business Media. Copyright 2009 Polymers and Fibers.

Anagnostopoulos et al. (2001) showed that one of the main difficulties with computer-based fabrics quality monitoring is the huge diversity in the types of fabrics and their defects. They provided a detailed list of fifteen different textile faults and their causes. Fabric monitoring methods based on more standard approaches, as opposed to the use of grey system theory, remain to be developed.

2.10 Control Charts and Profile Monitoring Approaches in MIA

In MIA the images involve measurements taken for at least three different wavelengths. Before any monitoring is done, there is usually a dimension reduction step based on principal component analysis (PCA) or partial least squares regression.

Bharati and MacGregor (1998) proposed an on-line approach for extracting information from multivariate spectral images collected over time. The methods can be used for measurements with three or more measured wavelengths where one receives a sequence of images over time and wants to detect and isolate specific features from the images. In their approach, they aggregated the data over pixel locations and used PCA to identify the two principal components that explained most of the variation in the vectors of wavelength intensities. Then they monitored the pixel frequencies corresponding to certain specified features in the score space of the first two principal components. Image masks were developed in the score space to correspond to each feature of interest in the

original image space to be monitored. When any of the pixel frequencies in any specified mask area exceeded a predefined threshold, there would be a signal to allow the operator to look for assignable causes for this change. In order to illustrate the fault diagnosis aspect, the authors showed how these changes could be traced back to show their spatial locations on the original image. Thus, the operator/engineer would know the change in the pixel frequency and location, which would facilitate the root-cause analysis aspect of fault diagnosis. Standard control charting methods can be applied to the pixel frequencies over time corresponding to each feature being monitored.

An example of the use of principal component image masks and how they relate to the original image is illustrated in Figure 2.6. The pixels in each of the two masks in Figure 2.6(a) correspond to flaws of the type shown in Figure 2.6(b).

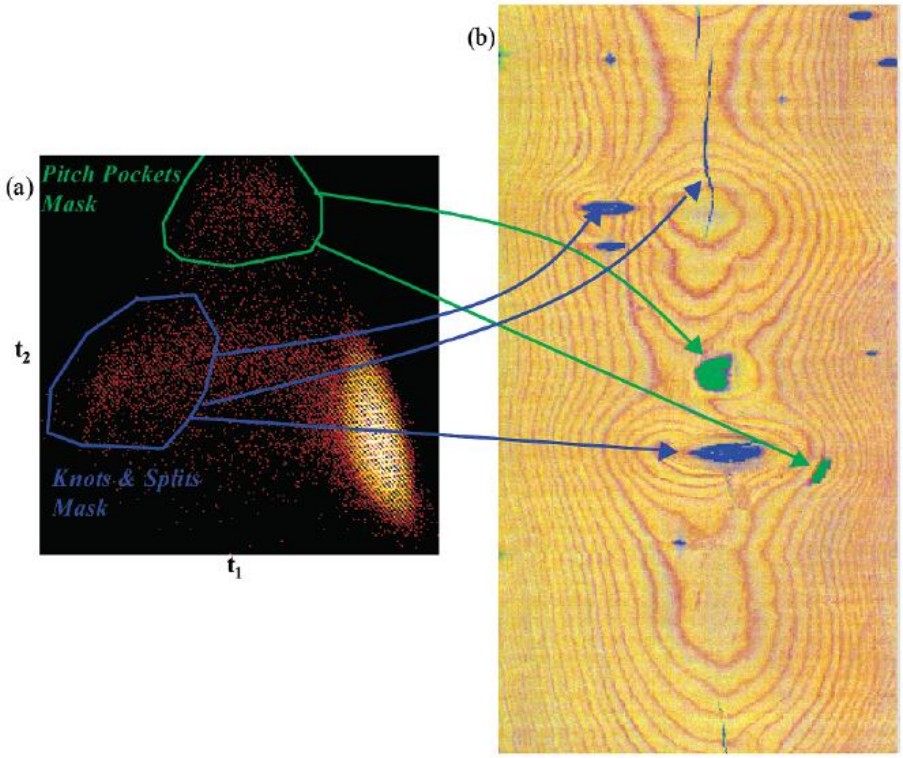

Figure 2.6: (a) Principal component t1-t2 score plot of lumber image with polygon masks of the upper and lower left point clusters. (b) Original image (converted from color) with overlay of highlighted pixels from the two classes outlined in part a.

(From Bharati et al. (2003)) Reprinted with permission from Industrial and Chemistry Research. Copyright 1998 American Chemical Society.

MacGregor et al. (2001) provided additional discussion of the approach of Bharati and MacGregor (1998). They mentioned several industrial applications, which included texture/roughness analysis and monitoring of sheet and film products, monitoring of different gels and faults in polymer films, and the quality category classification of wood products. Bharati et al. (2003) applied the method of Bharati and MacGregor (1998) to the automatic quality grading of softwood lumber boards. In this application, they constructed three frequency-based one-sided (individual sample) control charts, where the control limits were based subjectively on unacceptable quality levels. For example, the control limit of their control chart shown in Figure 2.7(a) has been set at 4912 pixels (which is 2% of the total number of pixels in each lumber image). The authors stated that the control limits must be selected in practice to balance the consequences of classification errors. Two other control charts are shown in Figure 2.7(b) and Figure 2.7(c). The authors recommended always plotting the squared prediction error (SPE) of each image on a control chart to check to see whether or not the model is valid for that image.

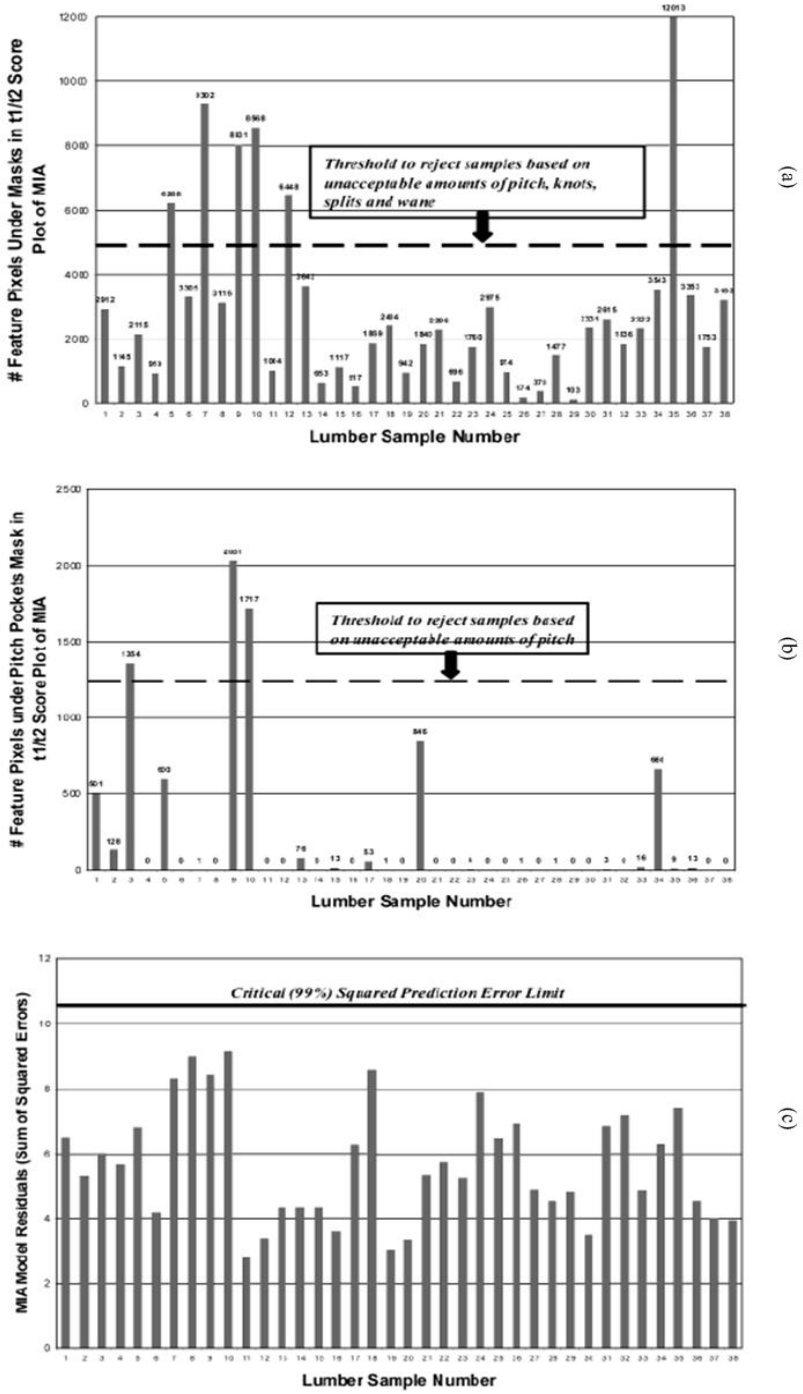

Figure 2.7: (a) Control chart of total number of pixels belonging to all modeled lumber defects (pitch, knots, splits, wane, and bark) in 38 lumber sample images, (b) Control chart of pixels belonging to the pitch pocket lumber defect in 38 lumber sample images, (c) Residual (sum of squared prediction errors) plot of MIA model used on 38 lumber sample images.

(Adapted from Bharati et al. (2003)) Reprinted with permission from *Industrial and Chemistry Research*. Copyright 1998 American Chemical Society.

In two interesting applications of monitoring industrial processes with MIA methods, Yu et al. (2003) developed an online MVS for monitoring and controlling industrial snack food quality and Yu and MacGregor (2004) monitored flames in an industrial steam boiler system. Even though control charts were not employed in these papers, they are useful in better understanding the MIA on-line monitoring methods. In addition, Kourti (2006) provided an excellent review paper on the role of multivariate analysis in process analysis, which included a review of some MIA surveillance methods and mentioned applications not only of electronic vision, but also electronic versions of taste, hearing, and smell. MIA monitoring approaches were also briefly discussed by Kourti (2005).

Liu et al. (2005) developed a MIA-based MVS to monitor the froth of a flotation process, which is one of the most widely used separation processes in mineral processing to separate valuable metals from ore. Their approach involved MIA methods based on PCA analysis with a residuals control chart used to check the validity of the model over time. The residuals control chart was used to prevent the operators from taking corrective actions based on abnormal images resulting from camera problems, lighting problems, or other unusual conditions. This is beneficial because the problem would then be in the images rather than in the process.

Graham et al. (2007) used MIA based on principal component analysis to measure and predict the ladle eye phenomenon in metallurgy with the "eye" referring to the region where liquid metal is exposed to the atmosphere. Their MIA approach is similar to the approach by Bharati and MacGregor (1998). After the MIA stage, they used a Hotelling T^2 control chart to monitor the validity of their ladle eye area predictions and to test for outliers and/or poor image preprocessing.

Facco et al. (2008) developed a MIA method that is based on a two-level nested PCA model for monitoring the surface quality of photolithographed devices in semiconductor manufacturing. In their paper, they recommended the use of control charts (such as the Hotelling T^2 control chart and a residuals chart) to characterize the quality features of the image after it has been transformed into the principal component subspace. They applied two spatial residuals control charts (the horizontal axis was the pixel number) to monitor

the surface roughness on different locations on the semiconductor since roughness on the edges of the produced parts was much smaller than in the associated valleys. Two different schemes were required to monitor each of these features separately.

2.11 Control Charts for Medical Image Devices

In this section we review the use of control charts with medical image data. These control charts are usually employed to ensure that medical imaging devices are functioning properly, as opposed to detecting changes in the items or processes being imaged, as done in the industrial applications. Readers are referred to Pearson and Lawson (2007) for a more comprehensive discussion on the topic of quality assurance for medical imaging devices. We did not find any papers on the use of control charting methods to monitor successive images taken of a single patient to detect changes in health status.

Knight and Williams (1992) used V-mask CUSUM charts and conventional Shewhart charts to monitor the performance of gamma-cameras based on quantitative measures of uniformity of the produced images under a uniform (flood) source. A gamma camera is a device used to image gamma radiation-emitting radioisotopes. The applications include early drug development and nuclear medical imaging to view and analyze images of the human body or the distribution of medically injected, inhaled, or ingested radionuclides emitting gamma rays. In their analysis, they calculated nine uniformity statistics and plotted Shewhart charts and the V-mask CUSUM charts for each of these statistics.

Orwoll et al. (1993) suggested a multi-rule Shewhart control chart to be used in monitoring the long-term precision of the dual-energy x-ray absorptiometry (DXA) scanners from bone measurement density (BMD) measurements obtained from the DXA scans. More specifically, they applied three run rules to the traditional Shewhart chart with BMD as their quality characteristic. The rules used were four consecutive measurements more than one standard deviation on one side of the mean; two consecutive measurements more than two standard deviations on one side of the mean; and ten consecutive measurements on the same side of the mean. Their approach was able to detect small changes in the performance of the machines under consideration.

Accordingly, their quality control protocol provided the ability to detect changes objectively and to adjust for variations in performance over the long-term.

Lu et al. (1996) compared five different quality control procedures for ensuring the functionality of DXA scanners. These five procedures were 1) visual inspection; 2) a Shewhart control chart with sensitizing rules; 3) a Shewhart chart with sensitizing rules with a filter for clinically insignificant mean changes; 4) a moving average chart and standard deviation chart; and 5) a CUSUM control chart. Their measurements were based on scan data and on simulated data. From their analysis, they found that the CUSUM approach was the best because it had good sensitivity for detecting changes with a low false alarm rate. In their conclusion, they suggested that the use of the more intuitive (for medical personnel) Shewhart charts can be acceptable at the individual testing sites if their scanner performance is followed up by CUSUM charting monitoring at a central quality assurance center.

Similarly, Garland et al. (1997) compared the scanner's built-in quality assurance system, visual inspection, a multi-rule Shewhart chart, and CUSUM control charts in establishing the best procedure for the quality assurance of DXA scanners. They utilized three criteria for analysis, the number of faults detected out of eight non-mechanical faults, the true positive fraction, and the Type I error rate. Their analysis was based on simulated (phantom) image data. Based on their criteria, they found that visual inspection, the multi-rule Shewhart chart, and the CUSUM control chart performed much better than the scanner's built-in quality assurance system. In another comparison for DXA machines, Pearson and Cawte (1997) found that the multi-rule Shewhart control chart performed as well as or better than the CUSUM control chart based on their simulated data set and their operating characteristic curve criteria.

Simmons et al. (1999) developed a quality assurance protocol that can be used in evaluating the functional Magnetic Resonance Imaging (fMRI) system performance. The evaluation of the fMRI system performance is achieved through monitoring the quality characteristics of the fMRI, mainly a signal-to-noise ratio (SNR) and a signal-to-ghost ratio (SGR), through two separate X-bar charts with run rules. A ghost image is a fainter

second image of an object being viewed. The control charts allowed for the detection of trends reflecting deterioration in the performance of the fMRI machine that were undetected using other quality assurance methods. Stöcker et al. (2005) also discussed the quality assurance of fMRI systems, but did not discuss control charting.

Chiu et al. (2004) developed a quality assurance protocol for detecting system malfunctioning and assessing the comparability of four image cytometers in a multicenter clinical trial. A cytometer is a device for counting and measuring the number of cells within a specified amount of fluid, such as blood, urine, or cerebrospinal fluid. They constructed an X-bar and R control chart for each of the four quality characteristics that they measured at each of the four clinical centers involved in the study. They also recommended the use of a Hotelling T^2 control chart to combine the four quality characteristics into one statistic for plotting.

2.12 Conclusions and Recommendations

We view image-based analysis and control charting as a very promising area of application within statistical quality control. Image monitoring is a natural extension of profile monitoring, an application and research area of increasing importance. Image-based monitoring adds the capability of monitoring a wide variety of quality characteristics, such as dimensional data, product geometry, surface defect patterns, and surface finish, in real-time. There are also applications of control charting in monitoring the performance of the imaging devices themselves. As the use of imaging increases, there will be an increasing number of practical applications where the concepts of statistical quality control can play an important role.

Some research opportunities in the analysis of image data for quality improvement include the study of the statistical properties and performance of many of the control charting methods. The justifications for many of the proposed methods are not clear. Work is needed to improve the performance of existing methods as well as understand the differences between competing approaches. Spatial control charts, for example, might be designed to provide greater sensitivity to locations in images where flaws are more likely to occur. In addition, some of spatiotemporal monitoring ideas in public health

surveillance for cluster detection and other purposes, such as those discussed by Sonesson (2007), Rogerson and Yamada (2009), and Jiang et al. (2010), may have applications in image monitoring.

2.13 References

Anagnostopoulos, C.; Vergados, D.; Kayafas, E.; Loumos, V.; and Stassinopoulos, G. (2001). "A Computer Vision Approach for Textile Quality Control". *The Journal of Visualization and Computer Animation,* 12 (1), pp. 31-44.

Armingol, J. M.; Otamendi, J.; de la Escalera, A.; Pastor, J. M.; and Rodriguez, F. J. (2003). "Statistical Pattern Modeling in Vision-Based Quality Control Systems". *Journal of Intelligent and Robotic Systems* 37, pp. 321-336.

Arpaia, P.; Betta, G.; Langella, A.; and Sacco, E. (1999). "Measurement Process Control by Means of Algorithms Based on Digital Image Processing". *IEE Proceedings-Science Measurement and Technology* 146, pp. 27-34.

Bersimis, S.; Psarakis, S.; and Panaretos, J. (2007). "Multivariate Statistical Process Control Charts: An Overview". *Quality and Reliability Engineering International* 23, pp. 517-543.

Bharati, M.H. and MacGregor, J.F. (1998). "Multivariate Image Analysis for Real-Time Process Monitoring and Control". *Industrial and Engineering Chemistry Research* 37, pp. 4715-4724.

Bharati, M.H.; MacGregor, J.F.; and Tropper, W. (2003). "Softwood Lumber Grading through on-Line Multivariate Image Analysis Techniques". *Industrial and Engineering Chemistry Research* 42, pp. 5345-5353.

Chiu, D.; Guillaud, M.; Cox, D.; Follen, M.; and MacAulay, C. (2004). "Quality Assurance System Using Statistical Process Control: An Implementation for Image Cytometry". *Cellular Oncology* 26, pp. 101-117.

Colosimo, B. M.; Mammarella, F.; and Petro, S. (2010). "Quality Control of Manufactured Surfaces". *Frontiers in Statistical Quality Control 9*, edited by H. J. Lenz, P. -Th. Wilrich, and W. Schmid, Physica-Verlag, pp. 55-70.

Colosimo, B. M. and Pacella, M. (2011). "Analyzing the Effect of Process Parameters on the Shape of 3D Profiles". *Journal of Quality Technology* (To appear).

Deng, J. l. (1989). "Introduction to Grey System Theory". *The Journal of Grey System* 1, pp. 1-24.

Elbasi, E.; Long, Z.; Mehrotra, K.; Mohan, C.; and Varshney, P. (2005). "Control Charts Approach for Scenario Recognition in Video Sequences". *Turkish Journal of Electrical Engineering and Computer Sciences* 13, pp. 303-309.

Facco, P.; Bezzo, F.; Romagnoli, J.A.; and Barolo, M. (2008). "Using Digital Images for Fast, Reliable, and Automatic Characterization of Surface Quality". *Workshop on Nanomaterials Production, Characterization and Industrial Applications*. Milano, Italy.

Friedman, D. J. and Albin, S. L. (1991). "Clustered Defects in IC Fabrication: Impact on Process Control Charts". *IEEE Transactions on Semiconductor Manufacturing* 4, pp. 36-42.

Garland, S.W.; Lees, B.; and Stevenson, J.C. (1997). "DXA Longitudinal Quality Control: A Comparison of Inbuilt Quality Assurance, Visual Inspection, Multi-Rule Shewhart Charts and CUSUM Analysis". *Osteoporosis International* 7, pp. 231-237.

Geladi, P. and Grahn, H. (1996). *Multivariate Image Analysis*. Chichester, New York: Wiley.

Gonzalez, R. C. and Woods, R. E. (2007). *Digital Image Processing*. Harlow : Prentice Hall.

Graham, K.J.; Krishnapisharody, K.; Irons, G.A.; and MacGregor, J. F. (2007). "Monitoring Ladle Eye Dynamics Using Multivariate Statistical Methods". *Proceedings of the Iron & Steel Technology Conference*. Indianapolis, IN.

Grahn, H. and Geladi, P. (2007). *Techniques and Applications of Hyperspectral Image Analysis*. Hoboken, NJ: John Wiley & Sons.

Hansen, M. H.; Nair, V. N.; and Friedman, D. J. (1997). "Monitoring Wafer Map Data from Integrated Circuit Fabrication Processes for Spatially Clustered Defects". *Technometrics* 39, pp. 241-253.

Haralick, R.; Dinstein, I.; and Shanmugam, K. (1973). "Textural Features for Image Classification". *IEEE Transactions on Systems, Man, and Cybernetics* 3, pp. 610-621.

Horst, R. L. and Negin, M. (1992). "Vision System for High-Resolution Dimensional Measurements and on-Line Inspection: Web Process Application". *IEEE Transactions on Industrial Applications* 28, pp. 993-997.

Jähne, B. (2005). *Digital Image Processing*. Springer: Berlin.

Jiang, B.C. and Jiang, S.J. (1998). "Machine Vision Based Inspection of Oil Seals". *Journal of Manufacturing Systems* 17, pp. 159-166.

Jiang, B.C.; Wang, C.-C.; and Liu, H.-C. (2005). "Liquid Crystal Display Surface Uniformity Defect Inspection Using Analysis of Variance and Exponentially Weighted Moving Average Techniques". *International Journal of Production Research* 43, pp. 67-80.

Jiang, W.; Han, S. W.; Tsui, K-L.; and Woodall, W. H. (2010). "Spatiotemporal Surveillance in the Presence of Spatial Correlation" to appear in *Statistics in Medicine*.

Jun, C.-H.; Hong, Y.; Kim, S. Y.; Park, K.-S.; and Park, H. (1999). "A Simulation-Based Semiconductor Chip Yield Model Incorporating a New Defect Cluster Index". *Microelectronics Reliability* 39, pp. 451-456.

Knight, A. C. and Williams, E. D. (1992). "An Evaluation of Cusum Analysis and Control Charts Applied to Quantitative Gamma-Camera Uniformity Parameters for Automated Quality Control". *European Journal of Nuclear Medicine and Molecular Imaging* 19, pp. 125-130.

Kourti, T. (2005). "Application of Latent Variable Methods to Process Control and Multivariate Statistical Process Control in Industry". *International Journal of Adaptive Control and Signal Processing* 19, pp. 213-246.

Kourti, T. (2006). "Process Analytical Technology Beyond Real-Time Analyzers: The Role of Multivariate Analysis". *Critical Reviews in Analytical Chemistry* 36, pp. 257-278.

Lavangnananda, K. and Piyatumrong, A. (2005). "Image Processing Approach to Features Extraction in Classification of Control Chart Patterns". *Proceedings of the 2005 IEEE Mid-Summer Workshop on Soft Computing in Industrial Applications*, Espoo, Finland, pp. 85-90.

Liang, Y.-T. and Chiou, Y.-C. (2008). "Vision-Based Automatic Tool Wear Monitoring System". *Proceedings of the 7th World Congress on Intelligent Control and Automation*, Chongqing, China, pp. 6031-6035.

Lin, H.-D. (2007a). "Automated Visual Inspection of Ripple Defects Using Wavelet Characteristic Based Multivariate Statistical Approach". *Image and Vision Computing* 25, pp. 1785-1801.

Lin, H.-D. (2007b). “Computer-aided Visual Inspection of Surface Defects in Ceramic Capacitor Chips”. *Journal of Materials Processing Technology* 189, pp. 19-25.

Lin, H.-D.; Chung, C.-Y.; and Lin, W.-T. (2008). "Principal Component Analysis Based on Wavelet Characteristics Applied to Automated Surface Defect Inspection". *WSEAS Transactions on Computers* 3, pp. 193-202.

Lin, H.-D. and Chiu, S. (2006). "Computer-Aided Vision System for Mura-Type Defect Inspection in Liquid Crystal Displays". *Lecture Notes in Computer Science* 4319, pp. 442-452.

Liu, J.; MacGregor, J.F.; Duchesne, C.; and Bartolacci, G. (2005). "Flotation Froth Monitoring Using Multiresolutional Multivariate Image Analysis". *Minerals Engineering 18*, pp. 65-76.

Liu, J. and MacGregor, J.F. (2006). "Estimation and Monitoring of Product Aesthetics: Application to Manufacturing of ‘Engineered Stone’ Countertops". *Machine Vision and Applications* 16, pp. 374-383.

Liu, Z. Q.; Austin, T.; Thomas, C. D. L.; and Clement, J. G. (1996). "Bone Feature Analysis Using Image Processing Techniques". *Computers in Biology and Medicine* 26, pp. 65-76.

Lu, C.-J. and Tsai, D.-M. (2005). "Automatic Defect Inspection for LCDs Using Singular Value Decomposition". *The International Journal of Advanced Manufacturing Technology* 25, pp. 53-61.

Lu, Y.; Mathur, A.K.; Blunt, B.A.; Glüer, C.C.; Will, A.S.; Fuerst, T.P.; Jergas, M.D.; Andriano, K.N.; Cummings, S.R.; and Genant, H. K. (1996). "Dual X-Ray Absorptiometry Quality Control: Comparison of Visual Examination and Process-Control Charts". *Journal of Bone and Mineral Research* 11(5), pp. 626-637.

Lu, C-J. and Tsai, D-M. (2005). “Automatic Defect Inspection for LCDs using Singular Value Decomposition”. *The International Journal of Advanced Manufacturing Technology* 25 (1), pp. 53-61.

Lyu, J. and Chen, M. (2009). "Automated Visual Inspection Expert System for Multivariate Statistical Process Control Chart". *Expert Systems with Applications* 36, pp. 5113-5118.

MacGregor, J.F.; Bharati, M.H.; and Yu, H. (2001). “Multivariate Image Analysis for Process Monitoring and Control”. *Process Imaging for Automatic Control*, H. McCann and D. M. Scott, Eds., Proceedings of SPIE 4188, pp. 17-26.

Malamas, E. N.; Petrakis, E. G.; Zervakis, M.; Petit, L.; and Legat, J.-D. (2003). "A Survey on Industrial Vision Systems, Applications and Tools". *Image and Vision Computing* 21, pp. 171-188.

Mason, R. L.; Tracy, N. D.; and Young, J. C. (1997). "A Practical Approach for Interpreting Multivariate T^2 Control Chart Signals". *Journal of Quality Technology* 29, pp. 396-406.

Megahed, F.M. and Camelio, J.A. (2010a). "Real-Time Fault Detection in Manufacturing Environments Using Face Recognition Techniques". *Journal of Intelligent Manufacturing*. (To appear)

Megahed, F. M.; Wells, L. J.; and Camelio, J. A. (2010b). “The Use of 3D Laser Scanners in Statistical Process Control”. *SAE Conference on Aerospace Manufacturing and Automated Fastening Conference & Exhibition*, Wichita, Kansas.

Montgomery, D. C. (2008). *Introduction to Statistical Quality Control*. Sixth Edition. Hoboken, N.J.: John Wiley & Sons.

Nalwa, V. S. (1993). *A Guided Tour of Computer Vision*. Reading, Mass.: Addison-Wesley.

Nembhard, H.B.; Ferrier, N.J.; Osswald, T.A.; and Sanz-Uribe, J.R. (2003). "An Integrated Model for Statistical and Vision Monitoring in Manufacturing Transitions". *Quality and Reliability Engineering International* 19, pp. 461-476.

Orwoll, E.; Oviatt, S.; and Biddle, J. (1993). "Precision of Dual-Energy X-Ray Absorptiometry: Development of Quality Control Rules and Their Application in Longitudinal Studies". *Journal of Bone and Mineral Research* 8, pp. 693-699.

Pearson, D. and Cawte, S., A. (1997). "Long-Term Quality Control of DXA: A Comparison of Shewhart Rules and CUSUM Charts". *Osteoporosis International* 7, pp. 338-343.

Pearson, D. and Lawson, N. (2007). "Laboratory and Instrument Quality Control". In *Clinical Trials in Osteoporosis*. London: Springer, pp. 141-159.

Pereira, A. C.; Reis, M. S.; and Saraiva, P. M. (2009). "Quality Control of Food Products Using Image Analysis and Multivariate Statistical Tools". *Industrial and Engineering Chemistry Research* 48, pp. 988-998.

Rogerson, P. and Yamada, I. (2009). *Statistical Detection and Surveillance of Geographic Clusters*. Chapman & Hall/CRC: Boca Raton, FL.

Schmitt, K. M.; Young, R. C. D.; Riddington, J. R.; Budgett, D. M.; and Chatwin, C. R. (2000). "Image Processing Applied to Brick Quality Control". *The International Journal of Advanced Manufacturing Technology* 16, pp. 434-440.

Simmons, A.; Moore, E.; and Williams, S. (1999). "Quality Control for Functional Magnetic Resonance Imaging Using Automated Data Analysis and Shewhart Charting". *Magnetic Resonance in Medicine* 41, pp. 1274-1278.

Sonesson, C. (2007). "A CUSUM Framework for Detection of Space-time Clusters Using Scan Statistics". *Statistics in Medicine* 26, pp. 4770-4789.

Stöcker, T., Schneider, F., Klein, M., Habel, U., Kellerman, T., Zilles, K., and Shah, N. J. (2005). "Automated Quality Assurance Routines for fMRI Data Applied to a Multicenter Study". *Human Brain Mapping* 25, pp. 237-246.

Styner, M.; Oguz, I.; Xu, S.; Pantazis, D.; and Gerig, G. (2007). "Statistical Group Differences in Anatomical Shape Analysis Using Hotelling T^2 Metric". *Progress in Biomedical Optics and Imaging* 8(3).

Tan, J.; Chang, Z.; and Hsieh, F. (1996). "Implementation of an Automated Real-Time Statistical Process Controller". *Journal of Food Process Engineering* 19, pp. 49-61.

Taniguchi, K., Ueta, K., and Tatsumi, S. (2006). "A Mura Detection Method". *Pattern Recognition* 39 (6), pp. 1044-1052.

Tong, L.-I.; Wang, C.-H.; and Huang, C.-L. (2005). "Monitoring Defects in IC Fabrication Using a Hotelling T^2 Control Chart". *IEEE Transactions on Semiconductor Manufacturing* 18, pp. 140-147.

Tunák, M. and Linka, A. (2008). "Directional Defects in Fabrics". *Research Journal of Textile and Apparel* 12, pp. 13-22.

Tunák, M.; Linka, A.; and Volf, P. (2009). "Automatic Assessing and Monitoring of Weaving Density". *Fibers and Polymers* 10(6), pp. 830-836.

Vihonen, J.; Jylha, J.; Ala-Kleemola, T.; Ruotsalainen, M.; Kauppila, J.; Huotilainen, T.; Rauhamaa, J.; and Visa, A. (2008). "Directional Filtering for Sequential Image Analysis". *IEEE Signal Processing Letters 15*, pp. 902-905.

Wang, K. and Tsung, F. (2005). "Using Profile Monitoring Techniques for a Data-Rich Environment with Huge Sample Size". *Quality and Reliability Engineering International* 21, pp. 677-688.

Western Electric Company (1956). *Statistical Quality Control Handbook*. Indianapolis, IN.

Wheeler, D. J. and Chambers, D. S. (1992). *Understanding Statistical Process Control*. Knoxville, TN: SPC Press.

Woodall, W. H. (2000). "Controversies and Contradictions in Statistical Process Control". *Journal of Quality Technology* 32, pp. 341-350.

Woodall, W. H. (2007). "Current Research on Profile Monitoring". *Produção* 17, pp. 420-425.

Woodall, W. H.; Spitzner, D. J.; Montgomery, D. C.; and Gupta, S. (2004). "Using Control Charts to Monitor Process and Product Quality Profiles". *Journal of Quality Technology* 36, pp. 309-320.

Woodall, W. H. and Adams, B. M. (1998). Statistical Process Control. Chapter 7 in H. M. Wadsworth (ed.) *Handbook of Statistical Methods for Engineers and Scientists*. Second Edition. New York: McGraw-Hill.

Yu, H. and MacGregor, J.F. (2004). "Monitoring Flames in an Industrial Boiler Using Multivariate Image Analysis". *AIChE Journal* 50, pp. 1474-1483.

Yu, H.; MacGregor, J.F.; Haarsma, G.; and Bourg, W. (2003). "Digital Imaging for Online Monitoring and Control of Industrial Snack Food Processes". *Industrial and Engineering Chemistry Research* 42, pp. 3036-3044.

Zuech, N. (2000). *Understanding and Applying Machine Vision*. New York: Marcel Dekker.

3 A Spatiotemporal Method for the Monitoring of Image Data

3.1 Abstract

Machine vision systems are increasingly being used in industrial applications due to their ability to quickly provide information on product geometry, surface defects, surface finish, and other product and process characteristics. Previous research for monitoring these visual characteristics using image data has focused on either detecting changes within an image or between images. Extending these methods to include both the spatial and temporal aspects of image data would provide more detailed diagnostic information, which would be of great value to industrial practitioners. Therefore, in this paper we show how image data can be monitored using a spatiotemporal framework that is based on an extension of a generalized likelihood ratio (GLR) control chart. The performance of the proposed method is evaluated through computer simulations and experimental studies. The results show that our proposed spatiotemporal method is capable of quickly detecting the emergence of a fault. The computer simulations also show that our proposed GLR control charting method provides a good estimate of the change-point and the size/location of the fault, which are important fault diagnostic metrics that are not typically provided in the image monitoring literature. Finally, we highlight some research opportunities and provide some advice to practitioners.

3.2 Introduction

A common challenge faced by practitioners is the selection of a control charting method that best fits the type of quality characteristics being monitored. In addition, this challenge becomes more difficult when dealing with a manufacturing process where the product's main quality characteristics are of a sensory (e.g. color and appearance) nature. Common examples of such products include liquid crystal display (LCD) monitors, tiles, kitchen countertops, and food products. Traditionally, as stated in Megahed et al. (2011), the quality of these products have been estimated through "go" or "no-go" manual visual inspection. However, these types of product characteristics are increasingly being assessed using machine vision systems (MVS), which are computer systems integrated

with image-capturing devices (e.g. digital cameras) to provide image data for analysis and interpretation.

The ever increasing dependence on MVS in industrial applications raises the question of how these images can be utilized within the framework of statistical process control (SPC). It is well known that the purpose of SPC is not only to detect a process shift as soon as it happens, but also to provide information to enable the process to be returned to its in-control state as quickly as possible. The quick detection of process shifts is typically done through the use of control charts that monitor product and/or process quality characteristics over time, and provide signals when a statistically significant deviation has occurred. On the other hand, there has been less research on process recovery since it is typically considered to be a process-based problem. We believe that the efficient use of digital images can significantly reduce the time required for fault diagnosis/correction since digital images can provide a vast amount of process/product data. Accordingly, this data should be analyzed more effectively such that practitioners can have a control charting scheme that reflects the dual-objective of SPC, i.e., rapid fault detection capability and an ability to provide diagnostic information after the detection of process shifts.

The objective of this paper is to develop a control charting scheme for images of industrial products whose quality is either characterized by uniformity (e.g. when trying to detect unevenness defects in LCD monitors) or by a specific pattern (e.g. manufactured tiles) that has to be followed and deviations from this pattern are to be detected. We do not consider industrial problems where the MVS is used for obtaining the dimensions of industrial parts, since dimensional data can be monitored through standard univariate and/or multivariate SPC methods. In this paper, we only consider grayscale images which represent the majority of images used in industrial applications, since they are cheaper to obtain and analyze.

For our control charting scheme, it is assumed that there is a steady stream of readily available images from the process. This imaging stream can be based on either 100% inspection or a continuous sampling rate that is less than the production rate. We also

assume that the stream of images is captured at a constant resolution such that the total amount of data (i.e. number of pixels) is constant between images. The related quality control literature (discussed in more detail in Section 3.3) has focused on either detecting changes in the image (spatial aspect) or the time when the change has occurred. Extending these control charts to include both the spatial and temporal aspects would provide more detailed diagnostic information, which would allow industrial practitioners to identify process defect(s) faster than when only one of these aspects is identified. Therefore, in this paper, we demonstrate how spatiotemporal methods predominately used in public-health surveillance can be used to monitor sensory quality characteristics of manufactured parts through the use of image data. The use of spatiotemporal methods allows for the identification of a fault's location within the image and the estimated time, i.e. image or part number, at which the process shift has occurred. This information assists practitioners in ensuring a quick process recovery.

It is assumed that the reader is familiar with the construction and use of control charts (for detailed introductions, see Wheeler and Chambers (1992), Woodall and Adams (1998), or Montgomery (2008)). On the other hand, it is assumed that the reader is not familiar with the structure of image data and image-based control charting techniques. Therefore, we present the necessary background in Section 3.3. Then, we discuss how industrial images can be monitored in a spatiotemporal framework based on generalized likelihood ratio methods. This is followed by an introduction of the performance metrics needed to evaluate the spatiotemporal method. Afterwards, we evaluate the statistical performance of the proposed methodology based on computer simulations. This is followed by an experimental example where we provide guidelines that assist industrial practitioners in successfully implementing our proposed method. Finally, we provide our conclusions and ideas for future research.

3.3 Background

3.3.1 Image Data Analysis

An image is often represented as a function f(x, y), where x and y represent the spatial coordinates on the image plane, and the value (or values) at any location (x, y) is

commonly known as the intensity (or intensities). In digital images the intensities take only non-negative integer values, e.g., in grayscale images, f(x, y) can take any integer value between 0 (black) and 255 (white) for 8-bit images or between 0 (black) and 65535 (white) for 16-bit images; in our paper only 8-bit images are being considered. It should be noted that the number of pixels (i.e., pairs of x and y) within an image increases with the image capturing device's resolution.

To incorporate image data in SPC monitoring activities, the captured images should be preprocessed. This step is often referred to in the machine vision literature as low-level processing. Low-level processes are typically comprised of the basic operations of noise reduction, image compression, and contrast enhancement, where the inputs and outputs are images. Sometimes more advanced image processing is required to overcome changes in lighting conditions and part positioning. The purpose of this preprocessing step is to ensure that the image data is suitable for use in product/process monitoring applications. The reader is referred to Gonzalez and Woods (2007) for a more detailed discussion on preprocessing operations.

3.3.2 Image-based Monitoring

A The use of image-based control charting is somewhat different from traditional control charting applications. Megahed et al. (2011) noted that these differences can be attributed to several factors, which include the type of data being monitored and how the control charts are applied. The need for image data preprocessing can also become a factor with 100% inspection since the data preprocessing time can be longer than the production cycle time.

Recall that we only focus on applications of image monitoring where practitioners are concerned with the uniformity within the image or the ideal image has a specific pattern and deviations from this pattern are to be detected and located. Previous research focused on either: 1) detecting the location/size of a fault through the use of spatial control charts (such as: Jiang and Jiang (1998), Armingol et al. (2003), Jiang et al. (2005), Lu and Tsai (2005), Lin and Chiu (2006), and Tunák and Linka (2008)); or 2) the quick detection of these faults for a well-defined statistical monitoring method that is evaluated by its average run performance over a wide variety of shifts (e.g. Wang and Tsung (2005)). We

believe that simultaneous consideration of these two areas of focus is needed for the most effective detection of process changes.

In order to evaluate a monitoring technique's ability to assist practitioners in achieving a rapid process recovery for the previously mentioned applications, we introduce several metrics that reflect the spatiotemporal nature of image data. We divide these metrics into the following three components: 1) estimating the change-point in the process, i.e., estimating the time of the shift in the process parameters that led to an out-of-control signal; 2) determining the location of the fault; and 3) identifying the size of the fault. Table 3.1 illustrates the contributions of the proposed spatiotemporal method when compared to previous research.

Table 3.1: Fault Detection and Diagnosis Measures Captured by Various Image-Monitoring Methods

	Phase I/II Distinction	Spatiotemporal Metrics			Phase II Evaluation
		Fault Location	Fault Size	Change-Point	
Jiang and Jiang (1998)	-	✓	✓	-	-
Armingol et al. (2003)	-	✓	✓	-	-
Jiang et al. (2005)	-	✓	✓	-	-
Lu and Tsai (2005)	-	✓	✓	-	-
Wang and Tsung (2005)	✓	-	-	-	✓
Lin and Chiu (2006)	-	✓	✓	-	-
Tunák and Linka (2008)	-	✓	✓	-	-
Proposed Method	✓	✓	✓	✓	✓

From Table 3.1, it can be seen that the previous works captured, at most, two of the possible three spatiotemporal components. In addition, with the exception of Wang and Tsung (2005), the performance of these techniques was only evaluated through practical case studies, which cannot be easily generalized. Therefore, the use of spatiotemporal monitoring techniques will allow us to tackle all three factors (location, size and time) while ensuring quick detection of the fault. We believe that the information gained from our proposed method could reduce the amount of time needed by practitioner to identify the root-cause for any process shift.

3.4 GLR Spatiotemporal Framework for Image Monitoring

Our framework is developed for two image monitoring applications (uniformity within an image or comparing to a specific pattern); therefore, any non-uniform specified pattern should be eliminated prior to the application of the control chart. A simple, yet effective, method to standardize these two types of image monitoring situations is to subtract a nominal image from each captured image. This subtraction allows us to have a resulting image that is less dependent on the nominal image and therefore, we can consider both applications using the same control charting technique. Hereafter, the word intensity (or intensities) is used to denote the grayscale intensity value resulting from the subtraction of the nominal image from each captured image. Due to this subtraction, the range of pixel intensities is now [-255, 255] instead of the original range of [0, 255].

Consider an $l \times w$ image; the image space can be represented by the set I, where $I = \{(x, y): 0 < x \leq l,\ 0 < y \leq w,\ \forall\ (x, y) \in \mathbb{Z}\}$, and $\mathbb{Z}$ is the set of pairs of possible integers determined by the resolution of the camera. Generally speaking, a process shift can affect the intensity (or intensities) of any pixel (or group of pixels) that are subset of I. Let SF be all possible $\mathbf{1}$ to $l \times w$ pixel combinations of (x, y). For a 10×10 image, the size of SF will be in the order of 2^{100} subsets that need to be evaluated for each image, which is computationally infeasible. More importantly, the reader should note that a typical 10.1 megapixel camera produces a 2736×3648 image. Accordingly, only a few predefined subsets of SF should be monitored, which we refer to as regions of interest (ROIs). The set of ROIs should be determined according to the type of faults that are to be detected. In this paper, we restrict the ROIs to be square-shaped regions, which are allowed to overlap. This reduces the number of ROIs to a more manageable number, p. Allowing the regions to overlap enables us to have a better estimate of the size/location of the fault, which is useful from a diagnostic perspective. We provide a detailed description of the ROI generation heuristic in Section 3.6.

The introduction of the ROIs also allows for an increased efficiency in computer storage since only the mean intensities (deviations from nominal) for each of these p ROIs need

to be calculated and stored. Therefore, the t^{th} image can be reduced to the following p-variate vector:

$$\bar{\boldsymbol{X}}_{(t)} = \left(\bar{X}_{(t)}(1), \bar{X}_{(t)}(2),\ \bar{X}_{(t)}(3), \ldots,\ \bar{X}_{(t)}(k), \ldots, \bar{X}_{(t)}(p)\right). \tag{3.1}$$

In the absence of a process shift, the mean intensity for the k^{th} ROI is assumed to follow the known distribution $N\left(\mu_{0,k}, \sigma_k^2\right)$, which was found to be reasonable in our experimentation. If the distribution parameter values are unknown, we assume that they can be accurately estimated during a Phase I monitoring period such that any estimation error can be neglected. We also assume that no more than one defect can exist in an image, which has two implications on the ROIs. First, there exist ROIs that do not capture the fault at all, i.e., their mean intensities would still follow their respective in-control distributions. Second, defects can be partially captured by one or more ROIs since the ROI size and defect shape need not match. Hence, each of the affected ROIs intensities' would shift to a different and unknown $\mu_{1,k}$ value, resulting from a mixture of in-control and out-of-control pixels. Therefore, it is desirable to effectively detect a wide range of shift sizes away from $\mu_{0,k}$ since the exact magnitude of the mean shift will be unknown. For simplicity, we do not consider changes in σ_k.

We are developing a Phase II spatiotemporal surveillance scheme that is capable of detecting a wide range of shifts in the mean intensities of ROIs. Therefore, for each image there exists two states (defect/no defect) and it is our objective to identify whether all the regions follow the in-control distribution or there exists one (or more) ROIs whose mean intensity has shifted. This is somewhat similar to a more classical problem in SPC, where it is desirable to effectively detect a wide range of process mean shifts. Reynolds and Lou (2010) provided a detailed discussion on how this problem is tackled in univariate SPC, where they classified the research into the following three categories: 1) the use of multiple control charts; 2) the use of an adaptive control chart; and 3) the use of generalized likelihood ratio (GLR) control charts. They showed that the GLR control chart provides a very attractive option for detecting a wide range of mean shifts and that it can overcome some of the difficulties faced by practitioners when trying to implement the other two methods. Accordingly, we extend the GLR control charting technique

investigated by Reynolds and Lou (2010) to image data. Our control charting technique is also closely related to several spatiotemporal monitoring methods used in public health surveillance (for detailed reviews, see Tsui et al. (2011a, b)). For example, it extends Sonesson's (2007) method to the case where the magnitude of the shift is unknown and the regions' intensities follow normal rather than Poisson distributions.

Since we assume that there exists a stream of images from the process, it is appropriate to consider that the sample size (n) is equal to one i.e. we do not combine images to obtain sample statistics for the ROIs. Therefore, the control chart statistics presented here are for the case where $n = 1$. Assuming that the current image number is s, then we have the following p-variate vectors representing the mean intensities for all the ROIs of each captured image: $\bar{\boldsymbol{X}}_{(1)}$, $\bar{\boldsymbol{X}}_{(2)}, \dots, \bar{\boldsymbol{X}}_{(s)}$ where each vector is defined in Equation (3.1). Consider the hypothesis that the process shift has occurred after image τ, where $\tau < s$. Then, the likelihood function at image s for ROI k is defined as

$$L\left(\tau, \mu_{1,k}, k \middle| \bar{X}_{(1)}(k), \bar{X}_{(2)}(k), \dots, \bar{X}_{(s)}(k)\right)$$
$$= \left(\frac{1}{\sqrt{2\pi\sigma_k^2}}\right)^s \times exp\left(-\frac{1}{2\sigma_k^2}\left(\sum_{i=1}^{\tau}\left(\bar{X}_{(i)}(k) - \mu_{0,k}\right)^2 + \sum_{i=\tau+1}^{s}\left(\bar{X}_{(i)}(k) - \mu_{1,k}\right)^2\right)\right). \quad (3.2)$$

If there has not been a process shift, the likelihood function at image s can be simplified to

$$L\left(\tau, \mu_{0,k}, k \middle| \bar{X}_{(1)}(k), \bar{X}_{(2)}(k), \dots, \bar{X}_{(s)}(k)\right)$$
$$= \left(\frac{1}{\sqrt{2\pi\sigma_k^2}}\right)^s \times exp\left(-\frac{1}{2\sigma_k^2}\sum_{i=1}^{s}\left(\bar{X}_{(i)}(k) - \mu_{0,k}\right)^2\right). \quad (3.3)$$

Since it is assumed that only one fault can occur, it is appropriate to use the maximum log likelihood ratio statistic for determining whether there has been a mean shift. Our maximum log likelihood ratio statistic is defined as

$$R_s = \max_{\tau, \mu_1, k} \frac{L(\tau, \mu_{1,k}, k \mid \bar{X}_{(\tau+1)}(k), \bar{X}_{(\tau+2)}(k) \cdots \bar{X}_{(s)}(k))}{L(\tau, \mu_{0,k}, k \mid \bar{X}_{(\tau+1)}(k), \bar{X}_{(\tau+2)}(k) \cdots \bar{X}_{(s)}(k))}. \quad (3.4)$$

Similar to the results in Reynolds and Lou (2010), R_s can be reduced to:

$$R_s = \max_{0 \le \tau < s, k} \frac{n_k (s-\tau)}{2\sigma_k^2} \left(\hat{\mu}_{1,\tau,s}(k) - \mu_{0,k} \right)^2, \tag{3.5}$$

where $\hat{\mu}_{1,\tau,s}(k) = (s-\tau)^{-1} \sum_{i=\tau+1}^{s} \overline{X}_{(i)}(k)$ and n_k is the number of pixels in ROI k. It should be noted that our approach extends the GLR method to include spatial information.

Reynolds and Lou (2010) stated the previous formulation is disadvantageous since we must keep track of all past data and find the maximum value of R_s over $0 \le \tau < s$ for each sampled image. This can become very computationally inefficient with image data when s is large. Therefore, we consider a modification of Equation (3.5), where the maximum is taken over a window of the past m images (refer to Willisky and Jones (1976) and Reynolds and Lou (2010) for more details). The modified statistic is as follows:

$$R_{m,s} = \begin{cases} \max\limits_{0 \le \tau < s, k} \dfrac{n_k (s-\tau)}{2\sigma_k^2} \left(\hat{\mu}_{1,\tau,s}(k) - \mu_{0,k} \right)^2 & s = 1, 2, 3, ..., m \\ \max\limits_{s-m \le \tau < s, k} \dfrac{n_k (s-\tau)}{2\sigma_k^2} \left(\hat{\mu}_{1,\tau,s}(k) - \mu_{0,k} \right)^2 & s = m+1, m+2, ... \end{cases}. \tag{3.6}$$

The GLR control chart signals at image s if $R_{m,s} > h_{GLR}$, where the control limit (h_{GLR}) is chosen to give a specified in-control performance, which we obtain through computer simulations as discussed later in the paper. From Equation (3.6), it can be seen that the $R_{m,s}$ statistic is maximized over all possible ROIs and the previous $s-m$ images. Moreover, we have established that a fault can affect more than one ROI. Accordingly, it can be seen that the use of the $R_{m,s}$ statistic allows us to determine the most likely ROI that represents the fault. This ROI provides our best estimate of the size, shape and location of the fault within an image. Therefore, returning the ROI that caused the signal provides diagnostic information about the fault, which is useful for a rapid process recovery. In addition, estimates of the change-point and the fault location/size can be easily obtained by defining $\hat{\tau}$ and $\hat{k}$ to be the respective values of τ and k at which the maximum for the $R_{m,s}$ in Equation (3.6) is obtained. This maximum $R_{m,s}$ can be represented as

$$R_{m,s} = \frac{n_{\hat{k}}(s-\hat{\tau})}{2\sigma_{\hat{k}}^2}\left(\hat{\mu}_{1,\hat{\tau},s}(\hat{k}) - \mu_{0,\hat{k}}\right)^2. \quad (3.7)$$

If an appropriate fault detection rate can be obtained, while having a predefined rate of false alarms, the GLR chart would provide an attractive option for image monitoring. One limitation of the $R_{m,s}$ statistic provided in Equation (3.7) is it will not indicate whether a signal is a result of an increase or decrease in the intensities. However, if this is a concern to practitioners, the magnitude of change can be identified by examining the mean intensity (deviation from nominal) for the ROI that caused the signal. Another alternative is to modify the $R_{m,s}$ statistic so it can account for the direction of change in the ROI's intensity. More details on the latter approach can be found in Reynolds and Lou (2010).

3.5 Metrics Used for Evaluating the Proposed GLR Spatiotemporal Method

The use of our proposed control charting scheme in Phase II surveillance can be thought of as a two step process. The GLR control chart is first used to detect the occurrence of a process shift. Once the GLR chart detects the shift, we expect the diagnostic aspect of the proposed method to provide good estimates of all three spatiotemporal metrics (accuracy of the change-point and fault location/size estimation), which are fundamental in achieving a fast process recovery. In this section we provide the metrics needed for evaluating the detection and diagnostic aspects of the proposed method.

To evaluate the detection capability of the GLR control chart, we use the steady-state median run length (SSMRL) metric. We chose a steady-state model, as opposed to the traditional zero-state approach, since the steady-state model is more useful for analyzing the performance of the change-point estimator when the process is assumed to be out of control. Consider the scenario where a zero-state model is assumed and thus the performance is based on sustained shifts that occur under the initial startup conditions of the control chart. Accordingly, from a change-point perspective there are only two possible scenarios, either the change-point is estimated correctly or lags the true change-point. However, we also want to allow for the scenario where the change-point is

estimated incorrectly such that it leads the true change-point. Therefore, the use of a steady-state model allows for all three scenarios to be considered. In addition, the steady-state model provides a more realistic depiction of the occurrence of process shifts in applications since shifts would rarely occur when the control chart statistics are set to their original values.

We use the median run length (MRL) instead of the traditional average run length (ARL) metric, because of the computational load required for simulating a spatiotemporal GLR method for image data. Recall that the ROIs are selected to cover a wide range of fault sizes and locations. Accordingly, it is not unusual to have a few hundred ROIs. In our computer simulations $p = 1580$. More importantly, calculations will be made for each of these p ROIs over the last m images as shown in Equation (3.6). Therefore, it seems reasonable to expect that computer simulations for such techniques will be characterized by a small number of replication runs due to the associated computational complexity. Steiner and Jones (2010) suggested that the median run length should be used instead of the average run length when the number of replications is small since the median is less sensitive to outliers. For more details about the use of the MRL, the reader is referred to Steiner and Jones (2010).

To evaluate the diagnostic aspect of the proposed method, we first utilize typical metrics used in the evaluation of $\hat{\tau}$. More specifically, Pignatiello and Samuel (2001) provided an add-on approach for control charts that enables industrial practitioners to estimate the change-point under the assumption that the in-control parameters are known. To evaluate the performance of their technique, they reported the mean and standard deviation for their estimated change-point, calculated from the simulation replications. Similarly, we return both statistics, in addition to the median, since our simulation replications are relatively small in number. We believe that these three statistics should provide a good representation of the relationship between $\hat{\tau}$ and τ.

Finally, we use the Dice similarity coefficient (DSC) to evaluate the performance of our methodology in determining the size and location of the fault. The DSC, first proposed by Dice (1945), is often used in the evaluation of spatial clustering in medical (e.g. Zou et al.

(2004)) and ecological (Jackson et al. (1988)) applications. The DSC can only take values between 0 and 1. Consider Figure 3.1a, where we denote the image space, fault, and selected ROI with I, F and R respectively. In addition, we represent the intersection between F and R as FR. Accordingly, the DSC is defined as

$$DSC = \frac{2 \times FR}{F + R}. \tag{3.8}$$

Based on Equation (3.8), it can be easily seen that if the region does not intersect the fault, then $DSC = 0$. For $DSC = 1$, both the region and the fault must be of equal size and perfectly overlapping. Therefore, higher values of the DSC represent better coverage, while the lower values represent worse coverage. However, there are no set cut-off values to describe the quality of coverage; $DSC = 0.5$ can be useful in practice. For example, consider the scenario in Figure 3.1b. The ROI presents an excellent estimate of the size of the fault while providing a relatively accurate depiction of its location; however, the DSC value is 0.5. It is also important to note that we do not include the time dimension in our evaluation of the fault size/location. This is because we assume that the fault location remains the same until it is detected and therefore, it is sufficient to only consider the spatial component.

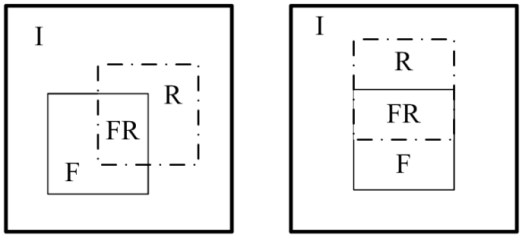

(a) (b)

Figure 3.1: a) Schematic representation of the DSC metric and b) Example scenario with $DSC = 0.5$.

3.6 A Description of the Simulation Studies

To evaluate the statistical properties of the GLR spatiotemporal framework, we ran computer simulations of various intensity shift sizes, magnitudes, and locations with 1000 replications for each combination. For each of these simulations, we assumed that any environmental effects on image quality have been neutralized via appropriate image

processing and that we are interested in detecting faults in nonwoven textile images. A typical image of an industrially produced nonwoven is shown in Figure 3.2. We assume that it is of interest to maintain a similar pattern during the production process.

Figure 3.2: Nonwoven fabric of interest

We refer to this study as a simulation even though an industrial image was used to evaluate the performance of our proposed method. We used one nonwoven image to generate the images needed for our simulations utilizing typical digital image processing techniques, which are described later in this section. We believe that the use of a real industrial image as a basis for our simulations is advantageous since it allows us to replicate some inherent properties and correlations within the image, which might be missed if we just assume a specific distribution for the intensities of each ROI.

Since nonwovens are porous in nature, the acquired image in Figure 3.2 represents both the nonwoven fabric as well as the background. Therefore, we estimated the background intensity of the image as explained in Gonzalez and Woods (2007). We then generated the true image of the fabric by subtracting the background from the image shown in Figure 3.2. To reduce the computational load, the image was also resized (compressed) from 921×613 to 250×250 pixels. We refer to this true (i.e. background-free) and resized image as the nominal image, which is illustrated in Figure 3.3.

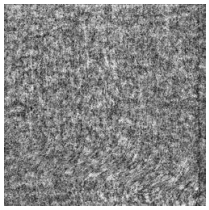

Figure 3.3: Nominal image for the nonwoven fabric

Using the nominal image depicted in Figure 3.3, similar images were generated for the simulation runs by adding noise. In digital image processing, there are two commonly used methods of generating noise in an image. First, the nominal image can be used and then artificial randomly generated noise of a pre-specified distribution is added to each of the pixels. This results in a generated image that is quite similar to the nominal image, especially since the noise is usually generated as a normal distribution with a mean of zero and a small variance. The other method is to assume that the noise of each pixel is a function of the pixel value. For this method, a common approach is to assign a Poisson distribution to every pixel, where the mean of the distribution is the pixel value. Then, new images are generated such that its pixel intensities follow a Poisson distribution whose mean corresponds to the intensity of the corresponding pixels in the nominal image. For example, if $f(23,77) = 10$ (i.e. the intensity of the pixel located at row 23 and column 77 is equal to 10) in the original image, then for each generated image (g), $f_g(23,77)$ will be generated from a Poisson distribution with mean 10 with an upper limit of 255 since the pixel values are bounded by [0, 255]. Researchers should note that both methods are commonly found in image processing software, which makes the generation of images for the simulation runs relatively straightforward. For our simulations, we used the Poisson noise approach since it is a discrete distribution and therefore, it provides a more realistic representation of each pixel's intensity distribution. Faults can be easily generated by changing the mean intensity of pre-specified neighboring pixels.

In order to identify the p square-shaped overlapping ROIs, a simple heuristic was used. Not only is the heuristic easy to implement, it has also been shown to provide good statistical performance for our proposed scheme as shown in Section 3.7. The ROI generation heuristic is comprised of three steps, which are based on the principle that the ROIs are centered around grid points. First, the grid points are overlaid onto the image, where the ratios between the number of pixels and the number of grid points along each of the height and width are set to a number between 25 and 100. For our 250×250 image, we selected the ratio to be 25 in each direction, resulting in having 100 grid points equally distributed within the image. Second, one should decide on the smallest ROI size, which is based on the smallest fault size to be detected. To determine the size of the smallest fault size (in pixels), one has to consider the camera's resolution and zoom, the

position of the camera with respect to the manufactured part, and the degree of compression applied in the image processing/resizing steps. Third, for each grid point, the ROIs are generated as follows: a) initialize the grid point by adding its first ROI, which has the predefined smallest ROI size; b) sequentially generate new ROIs by increasing from the previous ROI size by a predefined ROI step; and c) continue generating ROIs until the image border has been reached (or passed). The code for our ROI generating procedure can be provided by the first author upon request.

The reader should note that our ROI generating procedure is different than what is done in public-health surveillance. There, they typically generate ROIs based on Kulldorff's (2001) circular scan statistic, which is based on moving a "circular window" of various sizes over the geographic map. Consequently, Kulldorff's method creates several distinct circular windows representing his regions of interest, i.e., possible size/location for an outbreak of a cluster. The use of the Kulldorff's method is intuitive in public-health surveillance since the objective is to detect an outbreak and its radius. However, in image data, pixels represent rectangular/square shaped regions. Therefore, it is more intuitive to use a rectangular method to generate the ROIs.

We used 1000 in-control images (after subtracting the background) of size 250×250 pixels for generating the historical distribution required for Phase I. For our proposed spatiotemporal method, we used the ROI heuristic for determining the regions of interest, where 100 grid points equally distributed in the image region were used. The number of ROIs per grid point is a function of the location of the grid point within the image, i.e., grid points near the edge of the image will have fewer ROIs centered around them when compared to those grids points towards the center of the image. In addition, we set the other parameters for our ROI generating procedure to the following: the smallest ROI size is a square of area 22×22 pixels, and the ROI step size was 4 pixels, for both the width and height. The corresponding total number of ROIs (p) was equal to 1580. For each of these ROIs, we estimated the in-control mean and standard deviation. In order to reduce the computation load required for these simulations the history window (m) was chosen to be 10.

As for the Phase II parameters, we let the simulations run for 20 images prior to introducing a fault. If a signal occurred prior to image 21, we restarted this simulation replication. The in-control SSMRL was set to approximately 150. We used several fault locations, sizes, and magnitudes to evaluate the performance of our proposed method. Previous applications of spatiotemporal methods have typically focused only on varying shift sizes and magnitudes. However, the location is an important factor to be considered when monitoring image data due to two issues. The primary issue is that an image can only take non-negative integer values which are bounded between [0 (black), 255(white)] in the case of an 8-bit image. Therefore, there exist certain pixels whose value would not change when a cluster appears; for example, a pixel whose intensity is equal to 0 cannot get any darker. The other issue arises due to how the regions are generated. In our case, it would be easier to detect faults whose center is on one of the grid-points since the probability that the ROI and the fault perfectly overlap would increase. Accordingly, it is important to vary the location, size and magnitude of the fault to ensure that our simulation results can be generalized.

3.7 Simulation Results

Table 3.2 contains the steady-state median run length values for the proposed GLR spatiotemporal method. The performance of our GLR method was evaluated based on 150 fault testing conditions (3 fault centers × 5 fault sizes × 10 intensity shifts). Based on Table 3.2, our proposed method provides an accurate and robust fault detection capability when the fault size is greater in size than the smallest ROI size. For these fault sizes, the SSMRL is less than or equal to seven for all considered intensity shifts. In addition, the SSMRL results show that the proposed GLR spatiotemporal control chart provides a good fault detection rate for the cases when the fault size is less than the smallest ROI size. This is significant since it shows that our method can perform well even when the smallest ROI (which represents the smallest expected fault size to be detected) is larger than the actual fault size.

Table 3.2: SSMRL values with in-control SSMRL = 148

Fault Center's Location	Fault Size	Δ (Magnitude of Intensity Shift)*									
		-10	-5	-3	-2	-1	1	2	3	5	10
(125, 125)	10×10	2	8	31	78	141.5	134.5	81	29	7	2
	15×15	1	3	6	16	89	92	15	6	3	1
	20×20	1	1	3	6	34	30	6	3	1	1
	30×30	1	1	1	2	7	7	2	1	1	1
	50×50	1	1	1	1	2	2	1	1	1	1
(188, 206)	10×10	3	8	37	88	145	138	87	35	8	3
	15×15	1	3	6	15	92	90	16	6	3	1
	20×20	1	1	3	5	27.5	27	5	3	1	1
	30×30	1	1	1	2	6	6	2	1	1	1
	50×50	1	1	1	1	2	2	1	1	1	1
(158,78)	10×10	2	6	23	71	139.5	133	79	29	7	2
	15×15	1	2	5	11	82	83	13	5	2	1
	20×20	1	1	3	5	21	27	5	3	1	1
	30×30	1	1	1	2	6	6	2	1	1	1
	50×50	1	1	1	1	2	2	1	1	1	1

** The pixel intensity values of the nominal image range from 0 to 255.*

The performance of the GLR's change-point estimator is summarized in Table 3.3, where we return several statistics for $\varepsilon_\tau = \hat{\tau} - \tau$. In general, the performance of the proposed change-point method is best when the magnitude of intensity shift and/or the fault size are relatively large. On the other hand, the performance starts to deteriorate significantly when the intensity (deviation from nominal) shift is small and the fault size is 15×15 pixels or less. This is expected for two reasons. First, the magnitude of this intensity shift is too small to allow for an accurate detection. Intensity shifts of 10 or less are barely visible for the human eye as illustrated in Figure 3.4. The other, more important, reason is that our smallest ROI size was set to 22×22, which means that these fault size shifts are less than 50% of the size of our smallest ROI. For a more practical case, one would expect the GLR's change-point performance to be better if the fault size were greater than or equal to the smallest ROI and the intensity shift is reasonable (i.e. $|\Delta| \geq 2$). Therefore, it is important to ensure that the smallest ROI is less than or equal in size to the smallest fault to be detected.

Table 3.3: Error in estimated change-point for different sizes and magnitudes at the location (125, 125)

Δ	Size	Mean of ε_τ (SD of ε_τ)	Median of ε_τ	% Deviations in the parameter ε_τ			
				$\varepsilon_\tau = 0$	$0< \lvert\varepsilon_\tau\rvert \leq 2$	$\varepsilon_\tau < -2$	$\varepsilon_\tau > 2$
-5	15×15	-0.095(0.851)	0	77	20.5	2.2	0.3
	20×20	-0.091(0.593)	0	94.1	5.1	0.8	0
	30×30	-0.007(0.114)	0	99.5	0.4	0.1	0
	50×50	0(0)	0	100	0	0	0
-3	15×15	0.912(2.623)	0	43.5	36.8	3.1	16.6
	20×20	-0.101(0.924)	0	74.3	22.8	2.5	0.4
	30×30	-0.074(0.413)	0	94.5	5	0.5	0
	50×50	0(0)	0	100	0	0	0
-2	15×15	13.795(16.577)	9	9.9	15.7	2.1	72.3
	20×20	0.631(2.291)	0	48.8	34.8	3.7	12.7
	30×30	-0.125(0.805)	0	83.8	14.1	2	0.1
	50×50	-0.008(0.118)	0	99.2	0.8	0	0
-1	15×15	126.028(131.775)	83	0.7	1.7	0.7	96.9
	20×20	37.495(37.773)	27	3	7.1	1.5	88.4
	30×30	1.515(3.509)	0	36.8	36.7	3.2	23.3
	50×50	-0.144(0.892)	0	81	16.5	2.5	0
1	15×15	124.438(123.559)	87.5	0.6	2.3	0.5	96.6
	20×20	36.96(39.431)	24	3.4	8.1	1.6	86.9
	30×30	1.619(3.585)	0	38.7	36	2.4	22.9
	50×50	-0.166(0.722)	0	82.9	15.4	1.7	0
2	15×15	12.735(15.085)	8.5	10	17.5	1.2	71.3
	20×20	0.562(2.185)	0	48.6	36.1	3.3	12
	30×30	-0.086(0.725)	0	81.8	16.6	1.6	0
	50×50	-0.012(0.134)	0	99.1	0.9	0	0
3	15×15	0.821(2.461)	0	43.7	38.2	3.5	14.6
	20×20	-0.116(0.943)	0	76.4	20.3	2.5	0.8
	30×30	-0.062(0.498)	0	96.2	3.2	0.6	0
	50×50	0(0)	0	100	0	0	0
5	15×15	-0.099(0.875)	0	79.2	18	2.4	0.4
	20×20	-0.065(0.457)	0	94.4	5	0.6	0
	30×30	-0.001(0.032)	0	99.9	0.1	0	0
	50×50	0(0)	0	100	0	0	0

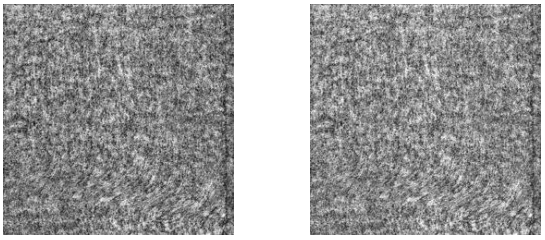

Figure 3.4: Nominal image (Left) and a superimposed global shift of 10 on the nonwoven (Right)

To evaluate the ability of the proposed method in effectively estimating the fault's location and size, we proposed the use of the DSC metric in Equation (3.8). Recall that the DSC metric is for an individual simulation replication. Accordingly, we return the median DSC (MDSC) to provide an overall representation of the method's ability to estimate the fault's location/size for a given test condition. More importantly, the DSC metric is defined independently of the ROI generating heuristic, and therefore it is implicitly assumed that any fault can be perfectly represented with an ROI when $DSC = 1$. However, the use of our ROI generating heuristic significantly limits that possibility. For example, consider the case that we are interested in detecting a 15×15 fault using the ROIs used in our simulations. In this case, the maximum achievable DSC (MADSC) is 0.635 (i.e. $\frac{2\times(15\times15)}{(15\times15)+(22\times22)}$) assuming there is an ROI whose center is the same as the fault's center. Table 3.4 demonstrates the method's ability in estimating a fault's location/size under various intensity shifts. For simplicity, we do not account for the possible mismatch between the fault and ROI's center in calculating the MADSC.

Table 3.4: MDSC/MADSC comparison for select testing conditions for the fault centered at (188, 206)

Δ	Size	MDSC	$\frac{MDSC}{MADSC}$	Δ	Size	MDSC	$\frac{MDSC}{MADSC}$
-5	10×10	0.163	0.477	5	10×10	0.163	0.477
	15×15	0.270	0.426		15×15	0.270	0.426
	20×20	0.385	0.426		20×20	0.385	0.426
	30×30	0.581	0.581		30×30	0.581	0.581
	50×50	0.765	0.765		50×50	0.765	0.765
-3	10×10	0.147	0.430	3	10×10	0.147	0.430
	15×15	0.270	0.426		15×15	0.270	0.426
	20×20	0.385	0.426		20×20	0.378	0.418
	30×30	0.567	0.567		30×30	0.567	0.567
	50×50	0.745	0.745		50×50	0.745	0.745
-2	10×10	0.009	0.026	2	10×10	0.008	0.022
	15×15	0.270	0.426		15×15	0.270	0.426
	20×20	0.385	0.426		20×20	0.378	0.418
	30×30	0.552	0.552		30×30	0.552	0.55
	50×50	0.743	0.743		50×50	0.725	0.725
-1	10×10	0	0	1	10×10	0	0
	15×15	0.006	0.010		15×15	0.014	0.023
	20×20	0.348	0.385		20×20	0.333	0.368
	30×30	0.550	0.550		30×30	0.550	0.550
	50×50	0.721	0.721		50×50	0.704	0.704

Prior to considering the specific results of Table 3.4, the reader should note that the ratio $\left(\frac{MDSC}{MADSC}\right)$ is conservative. This is because we assumed that the fault and the ROI's center coincide in the construction of the MADSC metric. We know that this is not the case based on our ROI heuristic parameters, which makes the nearest ROI to the fault to be centered at (200,200). As for the results, the ratio is higher for larger $|\Delta|$ values for a given fault size, which is expected. In addition, it is remarkable that our conservative $\frac{MDSC}{MADSC}$ ratio is greater than 0.5 for all fault sizes greater than that of our smallest ROI. This value is important since we have shown in Figure 3.1b that a DSC value of 0.5 can be of value to practitioners. Therefore, we can conclude that the spatial identification of the fault is robust for all fault sizes' greater than our smallest ROI. On the other hand, it should not be surprising that $MDSC = 0$ when $|\Delta| = 1$ and the fault size is (10×10) since the MRL for these cases was very close to the in-control MRL. This implies that the majority of these signals were false alarms rather than signals due to the shift, and therefore we expect the coverage metric to be very low.

The results provided in this section show that our method is extremely accurate when the fault size is greater than the smallest ROI. For these fault sizes, the SSMRL is less than or equal to seven for all intensity shifts. More importantly, for these cases, the spatiotemporal method provides accurate estimates for the change-point, estimated fault size, and fault location as shown in Table 3.3 and 3.4. First, the estimate ($\hat{\tau}$) was within ±2 of the true change-point for approximately 70% of the simulation replications when the intensity shift is ±1. The estimate's accuracy improved significantly for larger $|\Delta|$, where it reached 100% accuracy for $|\Delta| \geq 5$. In addition, the ratio $\left(\frac{MDSC}{MADSC}\right)$ was at least 0.5 for fault sizes greater than our smallest ROI. Therefore, one can conclude that the performance of the proposed GLR spatiotemporal framework is useful for both fault detection and diagnosis.

3.8 A Practitioner's Guide for Implementing the Proposed Method

Thus far we have focused on providing a detailed description of the statistical basis and properties of our proposed Phase II GLR spatiotemporal control chart. However, several

practical issues arise when applying such a control charting technique in industry. Specifically, it is important to minimize the image-to-image variation resulting from environmental conditions (i.e. lighting conditions, part location, etc.) and image processing stage. Accordingly, we provide a detailed step-by-step methodology that assists industrial practitioners in successfully implementing the proposed monitoring technique. This step-by-step methodology is comprised of four stages, as shown in Figure 3.5. We start by highlighting some of the factors that should be considered in setting-up the MVS. Then, we provide some basic steps that should be followed during the image processing stage. These steps allow the image data to be used in our control charting scheme. Afterwards, we discuss some Phase I analysis and control chart design decisions. Finally, we end the methodology by the steps needed to apply the control charting scheme for monitoring and diagnosing the production process in real-time. In this section, we focus on the first two stages since we provided a detailed discussion of the ROI generation and the steps needed for Phase II monitoring earlier in the paper.

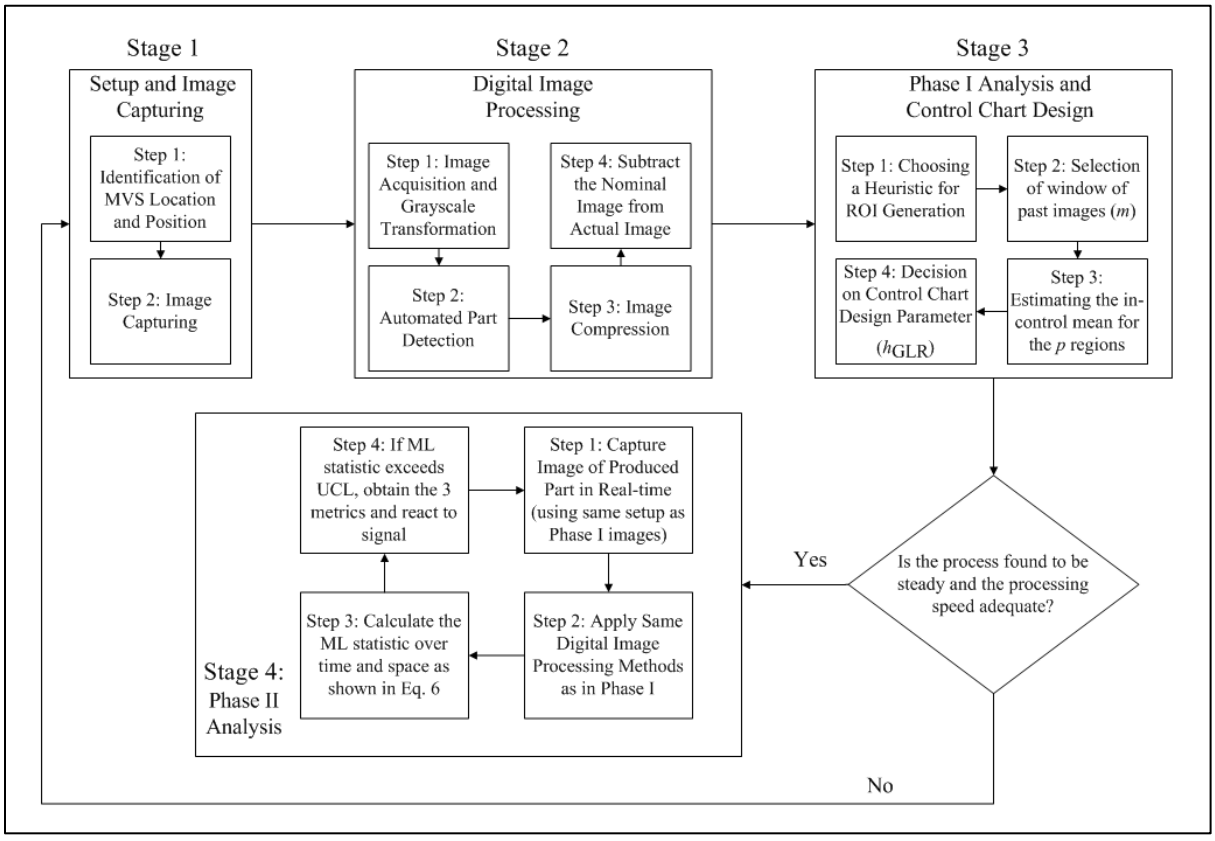

Figure 3.5: A practitioner's guide to spatiotemporal image monitoring

Prior to the image capturing stage, practitioners should identify a suitable location within their facility to install the MVS. There might be several possible locations on the shop floor. The decision to install the image capturing device should be based on factors that take into account both the production process and the environmental conditions needed for optimal image quality.

The MVS should be installed in a location where there would be no need for repositioning of the camera. This is because any slight change in the location will lead to a recalibration of the MVS, which includes taking Phase I images to re-estimate the in-control parameters of the ROIs. This need for recalibration is uncommon with typical measurement devices since they are less sensitive to changes in environmental conditions.

Another important consideration is related to selecting the location with the best available lighting conditions for image capturing. Ideally, there should not be any spatial or temporal variations in the lighting conditions in the neighborhood of the capturing device and the part to be monitored. However, this is not always possible in industrial facilities. Therefore, practitioners may need to perform a lighting survey, also known as a lighting audit, to determine the variability in illumination. This should be done by first documenting the basic layout of the area surrounding the capturing device (including the positioning of all lighting sources). Then, photometers can be used to collect illumination readings at equally spaced positions over this area. Finally, one should repeat this process a few times throughout the expected image monitoring period to record the temporal differences in illumination. Upon analyzing the lighting surveys for candidate areas, practitioners should select the location(s) with minimum variations. The reader should refer to Sanders and McCormick (1993) for more details on the development of lighting surveys.

Practitioners can further reduce the effect of changes in illumination through the installation of uniform and temporally constant light sources as described in Miller and Shridhar (1994). In addition, jigs and fixtures can be used to fix the location of the produced parts. This allows for constant positioning of the part, which eliminates the

need to account for variations in image positioning during the image processing stage. This reduces the computational time involved in image processing step, which may be important if 100% sampling is to be employed. Megahed and Camelio (2010) provided a more detailed discussion on some of the practical considerations in using MVSs for quality purposes.

After the image is captured, some basic image processing steps should be applied. Here we focus on four basic operations that are typically done in any image-based quality monitoring system. The first of these steps is image acquisition, where the image(s) is (are) fed into the software environment for processing. The difference between image capturing and image acquisition is that the latter marks the beginning of using computer software to extract the needed information from the image data. In the acquisition step, the image is changed from its raw form into a matrix form (A) as shown in the following equation:

$$A = \begin{bmatrix} f(1,1) & f(1,2) & \cdots & f(1,w) \\ f(2,1) & f(2,2) & \cdots & f(2,w) \\ \vdots & \vdots & \vdots & \vdots \\ f(l,1) & f(l,2) & \cdots & f(l,w) \end{bmatrix}. \tag{3.9}$$

As noted earlier in the chapter, (x, y) are the spatial co-ordinates of the image and the function f returns the intensity of that particular pixel. The values of l and w depend on the resolution of the camera used, where l and w increases as the resolution, number of megapixels, increases. Practitioners should note that captured images are often in a RGB (Red, Green, and Blue) color format. Since our methodology is developed for grayscale images, these color images should be transformed into a grayscale format. The majority of image processing software has standard functions to achieve this transformation, which marks the end of the image acquisition step.

Now that the image is in a format that can be easily read and manipulated by the software, it is important to remove any unneeded information in the image. This typically encompasses two steps. First, it is important to ensure that only quality-related information is extracted from the image through a part detection step. It is typical to

follow the part detection step with an image compression (resizing step). This step utilizes the inherent inter-pixel redundancy (i.e. neighboring pixels typically have similar intensity values) in the image, and as a result, the image can be resized without any significant information loss, but with a substantial gain in computational efficiency. Megahed and Camelio (2010) provided a detailed discussion on the effect of part detection and image compression on the computational speed in a quality monitoring framework.

After the image is compressed, the nominal image should be subtracted so that the obtained data can be used for our proposed method. It is very important that an appropriate fixture/jig is used to ensure that the parts are properly aligned during the image capturing stage so that the data obtained from the subtraction provides a true representation of the product-to-product variation rather than deviations resulting from the alignment. This subtraction marks the end of the image processing stage. Now, the image data is suitable to be used for the application of the proposed fault detection and diagnostic scheme.

3.9 Experimental Lab Study

In this section, we provide an example of how the proposed method can be applied in an industrial setting. This case study provides an implementation of the guidelines discussed above to further assist practitioners in understanding the necessary steps for applying our spatiotemporal control charting scheme. More specifically, we show how the proposed method can be applied in detecting induced faults in commercially-available 1 sq. ft. manufactured tiles. Figure 3.6 provides a representation of the conforming and faulty tiles used in the experimental study.

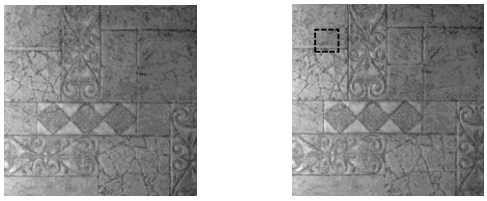

(a) (b)

Figure 3.6: Tiles used in the experimental study. Figure (a) represents the conforming tiles and Figure (b) represents the faulty tiles. The fault in Figure (b) was induced by adding a -10 pixel intensity shift at the location identified by a black dashed square.

The first step in making sure that the captured images are suitable for quality monitoring is to ensure that the image-to-image variation can be mainly attributed to part-to-part variation rather than changes in the environmental conditions such as changes in camera positioning, lighting conditions and part positioning. To ensure that the camera (8.0 megapixel CANON SX 100 IS Power-shot model) was fixed for the duration of the experiment, we mounted it on an approximately 3ft×4ft×3ft aluminum frame. This is a standard setup used in the literature to reduce the possibility of any changes in the camera's position during the experimental study. As for the lighting conditions, the images were taken in a light-controlled environment. There were no temporal variations in the lighting conditions since the room was not illuminated by external lighting. We acknowledge that such a room might not be representative of typical manufacturing environments; therefore, we recommended the formation of lighting surveys to select the location which has the least temporal variations in lighting. Finally, the tiles were fixed using a simple jig to ensure that each tile is in the same location with respect to the camera. A visual representation of the experimental setup and the jig used for ensuring that the tiles are fixed is provided in Figure 3.7. This step marks the end of Stage 1 for our study since the tiles used in the experimentation were commercially available and therefore, it is reasonable to assume that they were produced by a stable manufacturing process.

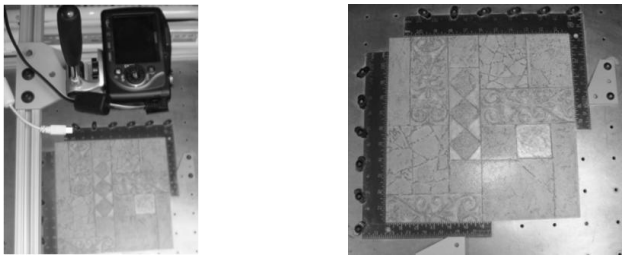

(a) (b)

Figure 3.7: a) Experimental setup and b) Jig used for tile positioning

In this study, 41 images of tiles were captured for Phase I analysis. More specifically, one of these images was randomly selected to be the nominal image and the other 40 were used in Phase I monitoring. Prior to using these forty images in Phase I monitoring, we applied several image processing steps. First, we cropped the tile from the image such that the image contains only the data of interest (i.e. the tile without the table and the

fixture). Afterwards, we resized the cropped grayscale image to 250×250 pixels to allow for real-time processing speeds, which is important if 100% sampling is employed in Phase II. Accordingly, each pixel in the image represents approximately a 2.232×10^{-3} sq. in. region on the tile. Then, each image was subtracted from the nominal tile image to lessen the inherent inter-pixel redundancy. Hereafter, the word "image" refers to a resultant image after all the aforementioned image processing steps are applied. We illustrate these image processing steps in Figure 3.8.

(a) (b) (c) (d)

Figure 3.8: Obtained images from the digital image processing steps where a) Captured grayscale image by the MVS, b) Cropped image of the tile, c) Resized image after image compression and d) Resultant image after Subtraction. It should be noted that these figures were scaled to 4 %, 4%, 24%, and 24% of their actual respective sizes.

As illustrated earlier, one must identify the ROIs prior to Phase I monitoring. For the sake of convenience, we used the same design parameters for the ROI generation procedure as in the simulations, i.e., 100 grid points that are equally distributed across the image, $m = 10$, the smallest region size is a square of area 22×22 pixels, and the ROIs are incremented by 4 pixels in both height and width until they hit an edge of the image. Based on the aforementioned discussion, we obtained the in-control distribution for each of the ROIs. We then used these in-control distributions to simulate similar image data (ROIs) so that the upper control limit of the GLR chart could be obtained. From our 1000 simulation replications, we found that a $h_{GLR} = 365$ results in a $\text{MRL} = 150$. This control limit value is the only design parameter needed for Phase II monitoring (when the image processing steps, ROI generation heuristic, and m are unchanged).

For Phase II monitoring, we assumed that the process remains in-control for 20 images and then a sustained shift of, where $\mu_1 = 10$ covering a 30×30 pixel region occurs. We used the same setup to capture images of the faulty tiles and then applied the same

digital image processing steps on each of the Phase II images. Then, based on Equation (6), we calculated the $R_{m,s}$ statistic for each image. The GLR control chart signaled at image 24, where $\hat{\mu}_1 = 7.63$. More importantly, the estimated change-point reflected that the change occurred after image 20 and the spatial identification of the fault provides a good representation of the fault's location and size. We summarize the results of implementing the GLR control charting scheme to the case study in Figure 3.9, where it can be easily seen that the proposed method could be useful in detecting and diagnosing faults in industrial settings.

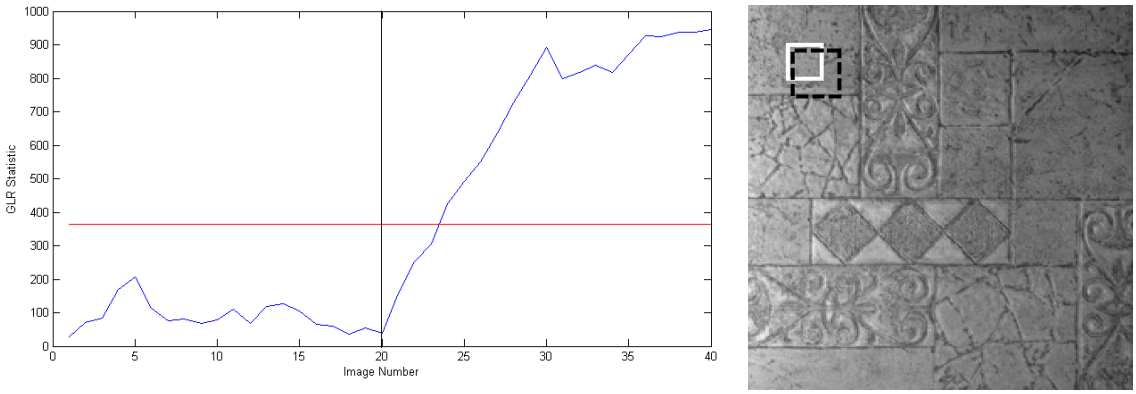

(a) (b)

Figure 3.9: Results of the application of the proposed GLR scheme to the case study. Figure (a) shows the GLR control chart and Figure (b) shows the identified fault (white solid square) with respect to the actual fault location (black dashed square).

3.10 Conclusions and Recommendations

We developed a spatiotemporal GLR control charting scheme that can be used for monitoring grayscale images of industrial parts which are characterized by uniformity within the image or by a specific desired pattern. We showed that the use of the generalized likelihood ratio control chart allows for rapid fault detection. More importantly, the proposed GLR spatiotemporal framework provides a good estimate for the change-point and the size/location of the fault, which are important diagnostic metrics to achieve a rapid fault recovery. Moreover, we provided some factors that should be considered by practitioners if they were to use our proposed method on the shop floor.

Some research opportunities in the analysis of image data for SPC applications include extending our proposed method to the detection and diagnosis of multiple faults within the image. Also, the effect of the choice of the window size, m, on the performance of the method could be investigated. In addition, it can be easily seen that the performance of our proposed method is highly dependent on the ROI generation step. In this paper, we have only focused on providing a simple approach for generating the ROIs. Accordingly, further improvements on our reported performance can be achieved by exploring how the generation of the ROIs can be improved, which includes the decoupling of the spatial identification of the fault from the monitoring method. It should also be noted that there are no studies in the literature that discuss the effect of estimation error on the performance of image-based control charts. Another promising area of research is how to extend the application of our proposed GLR spatiotemporal framework to three-dimensional image-based systems. For example, Megahed et al. (2010) demonstrated that the use of three-dimensional laser scanning systems can be very useful for quality monitoring purposes since three-dimensional scanners can rapidly provide millions of data points representing the entire geometry of a part. This is somewhat analogous to image data except that each sampling location represents a dimensional deviation from nominal rather than an intensity value. Therefore, it seems reasonable that spatiotemporal monitoring can play an important role for improving the effectiveness of using such systems for quality monitoring and improvement.

3.11 References

Armingol, J. M.; Otamendi, J.; de la Escalera, A.; Pastor, J. M.; and Rodriguez, F. J. (2003). "Statistical Pattern Modeling in Vision-Based Quality Control Systems". *Journal of Intelligent and Robotic Systems* **37**, pp. 321-336.

Dice, L. R. (1945). "Measures of the Amount of Ecologic Association between Species". *Ecology* **26**, pp. 297-302.

Gonzalez, R. C. and Woods, R. E. (2007). *Digital Image Processing*. Harlow: Prentice Hall.

Jackson, D. A.; Somers, K. M.; and Harvey, H. H. (1988). "Similiarity Coefficients: Measures of Co-occurrence and Association or Simply Measures of Occurrence?" *The American Naturalist* **133**(3), pp. 436-453.

Jiang, B.C. and Jiang, S.J. (1998). "Machine Vision Based Inspection of Oil Seals". *Journal of Manufacturing Systems* **17**, pp. 159-166.

Jiang, B.C.; Wang, C.-C.; and Liu, H.-C. (2005). "Liquid Crystal Display Surface Uniformity Defect Inspection Using Analysis of Variance and Exponentially Weighted Moving Average Techniques". *International Journal of Production Research* **43**, pp. 67-80.

Kulldorff, M. (2001). “Analysis and Interpretation of Disease Clusters and Ecological Studies”. *Journal of the Royal Statistical Society Series A (Statistics in Society)* **164**(1), pp. 61-72.

Lin, H.-D. and Chiu, S. (2006). "Computer-Aided Vision System for Mura-Type Defect Inspection in Liquid Crystal Displays". *Lecture Notes in Computer Science* **4319**, pp. 442-452.

Lu, C.-J. and Tsai, D.-M. (2005). "Automatic Defect Inspection for LCDs Using Singular Value Decomposition". *The International Journal of Advanced Manufacturing Technology* **25**, pp. 53-61.

Megahed, F. M. and Camelio, J. A. (2010). “Real-Time Fault Detection in Manufacturing Environments Using Face Recognition Techniques”. *Journal of Intelligent Manufacturing*, Available Online At: www.springerlink.com/index/dl61x21j072k1j06.pdf

Megahed, F. M.; Wells, L. J.; and Camelio, J. A. (2010). “The Use of 3D Laser Scanners in Statistical Process Control”. *SAE Conference on Aerospace Manufacturing and Automated Fastening Conference & Exhibition*, Wichita, Kansas.

Megahed, F. M.; Woodall, W. H.; and Camelio, J. A. (2011). “A Review and Perspective on Control Charting with Image Data”. *Journal of Quality Technology* **43**(2), pp. 83-98.

Miller, J. W. V. and Shridhar, M. (1994). “Hardware Considerations for Illumination-Invariant Image Processing,” *SPIE Machine Vision Applications, Architectures, and Systems Integration Conference III*, Oct. 31-Nov. 4, Boston, MA.

Montgomery, D. C. (2008). *Introduction to Statistical Quality Control*. Sixth Edition. Hoboken, N.J.: John Wiley & Sons.

Pignatiello, J. J., and Samuel, T. R. (2001), "Estimation of the Change Point of a Normal Process Mean in SPC Applications," *Journal of Quality Technology* 33, 82-95.

Reynolds, M. R., Jr. and Lou, J. (2010). “An Evaluation of a GLR Control Chart for Monitoring the Process Mean”. *Journal of Quality Technology* **42**(3), pp. 287-310.

Sanders, M. S. and McCormick, E. J. (1993). *Human Factors in Engineering and Design*. Seventh Edition. New York: McGraw-Hill.

Sonesson, C. (2007). “A CUSUM Framework for Detection of Space-Time Disease Clusters Using Scan Statistics”. *Statistics in Medicine* **26**, pp. 4770-4789.

Steiner, S. H. and Jones, M. (2010). “Risk-Adjusted Survival Time Monitoring with an Updating Exponentially Weighted Moving Average (EWMA) Control Chart”. *Statistics in Medicine* **29**(4), pp. 444-454.

Tsui, K-L; Han, S. W.; Jiang, W.; and Woodall, W. H. (2011a). “A Review and Comparison of Likelihood Based Charting Methods”, to appear in *IIE Transactions*.

Tsui, K-L; Wong, S. Y.; Jiang, W.; and Lin, C-J. (2011b). “Recent Research and Developments in Temporal and Spatiotemporal Surveillance for Public Health”. *IEEE Transactions on Reliability* **60**(1), pp.49-58.

Tunák, M. and Linka, A. (2008). "Directional Defects in Fabrics". *Research Journal of Textile and Apparel* **12**, pp. 13-22.

Wang, K. and Tsung, F. (2005). "Using Profile Monitoring Techniques for a Data-Rich Environment with Huge Sample Size". *Quality and Reliability Engineering International* **21**, pp. 677-688.

Wheeler, D. J. and Chambers, D. S. (1992). *Understanding Statistical Process Control*. Knoxville, TN: SPC Press.

Woodall, W. H. and Adams, B. M. (1998). Statistical Process Control. Chapter 7 in H. M. Wadsworth (ed.) *Handbook of Statistical Methods for Engineers and Scientists*. Second Edition. New York: McGraw-Hill.

Zou, K. H.; Warfield, S. K.; Bharatha, A.; Tempany, C. M. C.; Kaus, M. R., Haker, S. J.; Wells, W. M.; Jolesz, F. A.; and Kikinis, R. (2004). “Statistical Validation of Image Segmentation Quality Based on a Spatial Overlap Index”. *Academic Radiology* **11**(2), pp. 178-189.

4 The Use of 3D Laser Scanners in Process Monitoring

4.1 Abstract

Statistical process control (SPC) methods have been extensively applied to monitor the quality performance of manufacturing processes such that out-of-control conditions can be quickly detected and corrected. The success of SPC tools in detecting process shifts can be primarily attributed to control charts, which were originally developed in the 1920s. For the first few decades of control charting research, the focus was on optimizing the fault detection capability for shifts in a single quality characteristic. More recent SPC research has aimed to incorporate multiple data streams for a better understanding of process variation. However, SPC methods have yet to take full advantage of all available measurement technologies; for example, there is little to no research on how 3D laser scanners can be used in process monitoring. This is unfortunate as these scanners can rapidly provide millions of data points representing the entire surface geometry of manufactured parts, which is a significant advantage over competing technologies that typically provide only hundreds of data points. Consequently, 3D laser scanners are better suited to detect unexpected faults, i.e., faults that are not captured by measuring a small number of predefined dimensions of interest. Therefore, this paper presents a framework for performing process monitoring using point cloud data obtained through a 3D laser scanner. In addition, several research and application opportunities for using this technology in SPC are discussed. The results of this framework can significantly improve the monitoring of modern manufacturing parts that are characterized by complex surface geometries.

4.2 Introduction

In industrial statistical process control (SPC) applications, the quality of manufactured products is evaluated by key product characteristics (KPCs) identified by manufacturing engineers. Traditionally, these characteristics are physical measures, such as dimensions or part feature locations. These dimensional quality characteristics are of fundamental importance in assembly, since out-of-specification parts may lead to significant problems during the assembly process, resulting in poor performance of the final product. This

concept is well documented in the SPC literature; e.g., Montgomery (2008) highlighted the importance of conforming to standards in the automotive industry as the final assembly is composed of thousands of parts. Consequently, it is vital that each part is within the specification limits for ease of assembly; ideally, the product's quality characteristics should be as close as possible to their corresponding target values.

Traditionally, the choice of the KPCs was restricted by the capabilities of the available measurement technologies. For example, consider the assembly of car doors, where an inadequate door fit leads to a loss of quality, possibly characterized by excessive door closing effort, increased wind noise, and/or decreased aesthetics. Wu et al. (1994) noted that the quality of a door's fit is a function of dimensional variations in the doors, body openings, and fitting and hanging processes. Quality can also be affected by the general assembly. To assess the fitting quality, practitioners must decide on what to measure on the assembly and how to interpret the data. Typically, practitioners select between 15 to 25 sampling points per door, track these points using coordinate measuring machines (CMMs), and then apply SPC methods to assess if the observed vehicle-to-vehicle variation is significant, see e.g. see Wells et al. (2011). However, these sampling points may not capture all possible variation sources since only some gaps between the door and the body are measured. Therefore, it is important to develop SPC methods that can better monitor the quality of such complex products, especially since increased variation in product quality is often an indication of process deterioration (Panagiotidou and Tagaras (2010)), which can ultimately lead to costly process failure/downtime.

Advanced measurement technologies provide the opportunity to collect millions of data points, allowing for a product's entire surface geometry to be represented. With this type of data, fault detection is no longer limited by traditional measurement system capabilities. By monitoring the entire surface geometry one can detect the occurrence of unexpected fault patterns, i.e. faults that would not normally impact preset CMM measurement points. Three-dimensional (3D) laser scanners have recently emerged as a measuring technology that can rapidly provide such information. Son et al. (2002) showed that the current focus for 3D scanners resides in reverse engineering applications and providing one-to-one comparisons between as-built parts and their corresponding

computer aided design (CAD) representations. Despite the importance of such comparisons, they only provide information for a single scanned product, rather than capturing the item-to-item variation, which is necessary for an accurate depiction of the state of the manufacturing process. Therefore, in this paper we explore how 3D scanners can be used for process monitoring by utilizing their ability to collect real-time representations of a product's entire geometry. By using accumulated item-to-item scans, practitioners can better address the data rich but information poor problem highlighted in Wang and McGreavy (1998) and Choudhary et al. (2009). As a result, shop-floor decision-making and productivity can be significantly enhanced.

In the following section, an overview of laser scanning systems and relevant SPC research is provided. Afterwards, some of the practical issues with the use of laser scanning technologies in industrial facilities are highlighted. Then, the proposed methodology for quality monitoring is presented. From the proposed methodology several different control charting methods are developed. The applicability of these proposed control charts and a comparison study of their performance are obtained through simulation studies. This is followed by an experimental study, where the use of the proposed method for monitoring the quality of manufactured parts is demonstrated. Finally, a discussion of recommendations for future research and conclusions are given in the last two sections, respectively.

4.3 Background and Significance

This section introduces the technological and statistical bases for the proposed SPC method for monitoring point cloud data. Specifically, it is divided into three subsections: the first provides an overview of 3D laser scanning systems, demonstrating their advantage over current measurement techniques; the second presents an overview of statistical process control; and the last subsection provides some background on related SPC methods, especially control charts used for high-density data.

4.3.1 Overview of 3D Laser Scanner Systems

Coordinate measuring machines and optical coordinate measuring machines (OCMMs) are the most widely used dimensional measurement tools in industry; however, they are

limited in the number and location of measurable sample points when compared to laser scanners, illustrated in Figure 4.1. As mentioned earlier, the inability of CMMs and OCMMs to capture a part's entire surface allows for many defects to remain undetected, especially if the defects do not affect key quality characteristics. This problem is overcome by using 3D laser scanners as they are able to capture the entire product geometry.

(a) (b) (c)

Figure 4.1: Representation of (a) a CAD model of a manufactured part; (b) a CMM or OCMM measurement systems that only measures a set of specified points; and (c) an actual laser scan that captures all product characteristics

Three-dimensional laser scanning systems project laser strips onto the measured item where the reflected beams are captured by optical sensors (such as cameras), as shown in Fig. 2. Using image processing techniques, the 3D coordinates for each collected point are acquired. Zussman et al. (1994) highlighted several difficulties associated with using 3D laser scanners for measuring, which can be attributed to their optical sensors and mechanical moving parts. Despite these difficulties, 3D scanning technologies represent the next generation of manufacturing measurement systems since 1) they rapidly record thousands or millions of 3D data points that characterize all product geometric features; and 2) 3D laser scanners, often referred to as noncontact scanning techniques, have faster operational times when compared to current measurement systems, especially when dealing with complex part geometries, as discussed in Martinez et al. (2010).

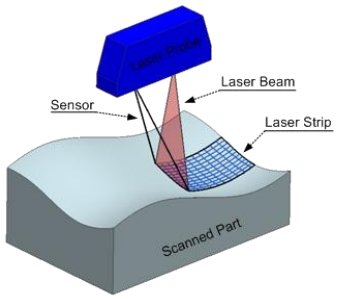

Figure 4.2: Simple Representation of a Common 3D Scanning System

Data obtained from 3D scanners is often referred to as a point cloud, which consists of a set of measured points from a given object typically given in a Cartesian coordinate system. It should be noted that the total number of scan points is a function of the scanner's resolution (scan points per line of scanning), the dimensions of the item being measured, and the scanning path. Therefore, it is quite common (especially for manual scanning operations) for the number of scanned points for one part (even when using the same scanner) to be significantly different from one scan to another, as scan paths can vary significantly.

Currently, there are two major areas of 3D laser scanning research. The first area aims to improve the accuracy of laser scanners (see e.g. Feng et al. (2001), Isheil et al. (2011), Xi et al. (2001), and Tamura et al. (1994)), while the other area focuses on how scanning data can be used in manufacturing environments. Son et al. (2002) divided the latter research into two categories, reverse engineering and product inspection. In reverse engineering, scanning systems transform manufactured parts into CAD models (Hisao and Chuang (2003), Mohaghegh et al. (2007), Várady et al. (1997)). Várady et al. (1997) provided several examples of the significance of this transformation, which includes the ability to evaluate the manufacturability of a product's design. In such instances, it is important to compare a part's as-built scan with its corresponding CAD geometry to identify areas of the product that do not meet specifications.

The use of 3D laser scanners for product inspection typically involves separating "bad" items from "good" items based on deviations of the scanned part from the nominal CAD model as in Shi et al. (2007), Shi and Xi (2008), Mohib et al. (2009), and Reinhart and Tekouo (2009). It should be noted, however, that these inspection approaches neglect the item-to-item variation and therefore, cannot be used to detect manufacturing process shifts effectively. Consequently, more proactive techniques must be developed to exploit the full potential of 3D scanning technologies. One such technique is presented in our paper.

4.3.2 An Overview of Statistical Process Control

The main objective of SPC is to rapidly detect the occurrence of unexpected process shifts and provide practitioners insight toward identifying the root-cause(s) of these shifts. Once the root-cause has been identified, appropriate corrective actions should be implemented to prevent the production of additional non-conforming items. Control charting is the primary SPC technique used for this purpose. A typical control chart is shown in Figure 4.3. This chart plots the values of a statistic that summarizes measurement(s) of important part/process quality characteristics as a function of time. Control limits are then used to determine if the variability of the statistic over time can be solely attributed to the inherent randomness in the production process (statistic plots inside the control limits), or if an assignable cause for that variation may be present (statistic plots outside the control limits). The choice of the control limits, i.e., how wide they are from the center line, is based on some statistical considerations that are described in more detail later in this chapter.

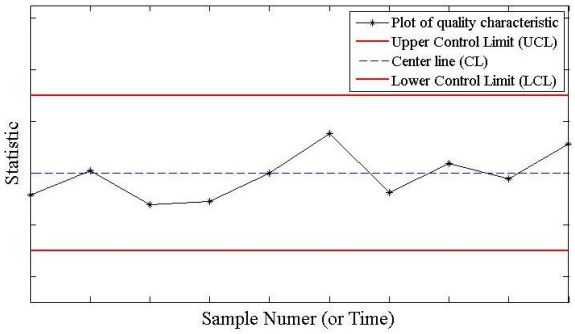

Figure 4.3: A Typical Control Chart

The selection of which control charting technique to use often depends on two important practical considerations; the situation in which the control chart is being implemented and the amount of data being collected. Even though control charts are always used to draw conclusions about the process or product's quality performance, these conclusions differ depending on whether the applied monitoring approach is a Phase I or Phase II application. In Phase I, historical data of the process are analyzed to understand the variation of the process over time, evaluate process stability, and estimate the in-control parameters of the process/product. On the other hand, in Phase II, the process/product is monitored in real-time to quickly detect shifts from the baseline established in Phase I.

Accordingly, Phase I and Phase II techniques are evaluated differently; Phase I methods are usually evaluated by the overall probability of a signal, and run-length performance is typically used for comparison purposes in Phase II. More discussion on Phase I and Phase II techniques, and their evaluation metrics can be found in Woodall (2000).

To clarify how the data analysis can affect the choice of control charting method, consider three possible scenarios for the car door assembly example discussed in the Introduction. For this example, it is assumed that the number and locations of door gap measurements are held constant. First, a practitioner can define the door quality through its maximum gap deviation. This statistic, i.e. maximum gap deviation, can be monitored by a univariate control chart such as a Shewhart or an exponentially weighted moving average (EWMA) control chart. A second option could be to monitor both the maximum and minimum deviations; therefore, the quality of each door can be represented by a vector containing maximum and minimum gap deviations. This vector can then be monitored by two univariate control charts or a multivariate chart, e.g., multivariate exponentially weighted moving average (MEWMA). The third alternative is to use all collected data points in the analysis, making use of all the available data. In this case, profile monitoring techniques can be used to monitor the variation in the measurements over time. The reader is referred to Montgomery (2008) for a detailed introduction on univariate and multivariate control charting techniques.

4.3.3 Profile Monitoring and its Application to High-Density Data Problems

To handle the challenge of monitoring 3D laser scanning data, the proposed technique transforms the point cloud data using profile monitoring techniques, which are better suited to characterize current manufacturing operations (Woodall et al. (2004)), especially for data-intensive processes (Wang and Tsung (2005)). Therefore, in this subsection a brief introduction of profile monitoring techniques is given. Following this introduction, current profile monitoring techniques applied to CMM and image data are discussed. CMM data are very similar in structure to point clouds, whereas image data represent a fairly similar data-intensive situation.

Profiles occur when a quality characteristic is functionally dependent on one or more independent variables. In this case, instead of observing a single measurement on each product, the practitioner observes "a set of values over a range, when plotted, takes the shape of a curve" (Montgomery (2008)). In other words, there exists a response variable *y* that is measured along with corresponding values of one or more independent/explanatory variables. For the simple linear regression case, Woodall et al. (2004) showed that profile monitoring techniques track the relationship between the response and an explanatory variable by estimating the regression parameters of the lines, mainly the slope, *y*-intercept, and error variance. Practitioners can then monitor the response stability through applying standard univariate or multivariate control charting methods on these parameters. The reader is referred to the review papers by Woodall et al. (2004) and Woodall (2007) for reviews of existing profile monitoring methods.

Woodall (2007) suggested that the monitoring of product shapes is a very promising area of profile monitoring research since the shape of manufactured items is usually an important aspect of quality. Colosimo et al. (2010) showed how profile monitoring techniques can be applied to three dimensional surfaces using CMM data, where a regression model with spatially correlated noise was combined with univariate and multivariate control charts. It should be noted that they assumed that the 3D surface profile of the part can be characterized by a parametric model. Having an accurate parametric model representing the 3D surface of the part might not be possible for complex shapes.

For data-rich manufacturing processes where a parametric model might not be possible, Wang and Tsung (2005) suggested characterizing each sample by a quantile-quantile (Q-Q) plot. A Q-Q plot is a standard graphical technique that is used to determine if two datasets come from the same distribution (Gunter (1994) and NIST/SEMATECH (2003)). Q-Q plots are generated by plotting the quantiles of one dataset against the quantiles of a second dataset. If one of the datasets is fixed as a reference (plotted on the x-axis), then the Q-Q plot can be used to compare the differences between many datasets through one-to-one comparisons with the reference dataset. When a compared dataset follows the same distribution as the reference dataset, a linear relationship will be

observed. Wang and Tsung (2005) noted that this relationship can be monitored as a linear profile, which can be characterized by its *y*-intercept and slope, and monitored by two EWMA control charts. This method was implemented on image data for detecting defects in liquid crystal displays (LCDs). Their results showed that this method is capable of rapidly detecting process shifts. In our paper, we investigate using a similar approach to monitor 3D laser scanning data. Additional profile monitoring techniques for image data are discussed in Megahed et al. (2011).

4.4 Proposed Method for Monitoring High-Density Data

This section proposes a Phase II method for monitoring high-density 3D laser scanner data. The statistical bases for this method are described over three subsections. First, the rationale behind using Q-Q plots for the problem of interest is demonstrated, including the need for extending the approach of Wang and Tsung (2005). The second subsection provides several methods to parameterize the Q-Q plot such that typical univariate control charts can be used to detect any process change. The third subsection compares the performance of different charting approaches based on a simulated example.

4.4.1 Rationale for Using Q-Q plots and the Need for Extending Previous Research

Point cloud data cannot be directly used for quality monitoring purposes since the point cloud consists of measured points of the scanned part in a Cartesian coordinate system, and the number and location of sampled points vary from scan to scan. Therefore, it is a common practice to compare point clouds against a part's nominal CAD geometry, which transforms the point cloud to a distribution of deviations from nominal. Hereafter, we refer to distribution of deviations from nominal of a scanned part by the term 'distribution'. Q-Q plots provide a powerful method for visualizing distributional data (Gunter (1994)). Consequently, Q-Q plots are used to compare each distribution to the nominal distribution so that practitioners can better understand the part-to-part variation.

As discussed earlier, Wang and Tsung (2005) suggested using two EWMA control charts to monitor the slope and the y-intercept of Q-Q plots of high-density image data. For their calculations, they used a generalized least squares (GLS) model (Kendall et al. (1994)) to

estimate the parameters of the fitted line for the Q-Q plot. This model becomes extremely complex with high-dimensional data, where the number of quantiles (n) used to generate the Q-Q plot can significantly increase. Since the fitted line requires estimating the covariance matrix for the quantile vector, $\mathbf{z} = (z_1, z_1, \cdots, z_n)$ this calculation becomes extremely inefficient, as n increases, even with Wang and Tsung's (2005) assumption of multivariate normality for **z**. Therefore, in this paper, the ordinary least squares (OLS) approach is used instead, since it is impractical to repeatedly calculate the covariance matrix of **z** when n is large.

Based on the above discussion, it can be easily seen that the conclusions of Wang and Tsung (2005) may not hold for our application since the regression model is different. Therefore, this paper reconsiders how the Q-Q plot can be parameterized. More specifically, the Q-Q plot can be characterized by its slope, y-intercept and the variance about the line, as recommended by Kim et al. (2003) for linear profiles. In addition, the use of residuals of the Q-Q plot from the nominal line, suggested by Kang and Albin (2000) and Mahmoud et al. (2010), is explored. To differentiate between these two types of residuals, they will be referred to as 'RI' and 'RII', respectively.

4.4.2 Phase II Monitoring of the Regression Parameters of the Q-Q Plots

The objective of this paper is to explore how 3D laser scanners can be used in Phase II process monitoring applications. Moreover, the need for using OLS to fit the regression line for the Q-Q plot instead of GLS has been presented. Accordingly, this subsection provides a mathematical representation of the linear regression model used to linearly fit the Q-Q plot, and the control limits for monitoring in Phase II.

For a linear profile of n (predictor, response) pairs, the Phase II simple linear regression model is defined as

$$Y_{ij} = A + BX_i + \varepsilon_{ij}, \quad i = 1, 2, \ldots, n \quad \text{and} \quad j = 1, 2, \ldots. \tag{4.1}$$

In our case, Y_{ij} and X_i, represent the i^{th} quantile of the j^{th} observation and the i^{th} quantile of the reference distribution, respectively. In addition, ε_{ij} is assumed to be independently and identically distributed, i.i.d, $N(0, \sigma_\epsilon^2)$ random variables. We also assume that the in-

control values of the intercept (A_0), slope (B_0) and variance (σ_ε^2) are known, or can be accurately estimated by a sufficiently large Phase I sample. For a given observation *j*, the OLS estimators for A and B can be easily calculated by

$$a_j = \overline{Y}_j - b_j \overline{X}_j \quad \text{and} \quad b_j = \frac{S_{XY}^{\{j\}}}{S_{XX}}, \tag{4.2}$$

where $\overline{Y}_j = \sum_{i=1}^{n} \frac{Y_{ij}}{n}$, $\overline{X} = \sum_{i=1}^{n} \frac{X_i}{n}$, $S_{XY}^{\{j\}} = \sum_{i=1}^{n} \left(X_i - \overline{X} \right) \left(Y_{ij} - \overline{Y}_j \right)$, and $S_{XX} = \sum_{i=1}^{n} \left(X_i - \overline{X} \right)^2$, as shown in Mahmoud et al. (2010). The variance of the residuals, σ_ε^2, is traditionally estimated by the mean squared error, $MSE_j = \frac{SSE_j}{n-2}$, where $SSE_j = \sum_{i=1}^{n} \varepsilon_{ij}^2$, referred to as RI. Here, ε_{ij} is obtained by

$$e_{ij} = Y_{ij} - a_j - b_j X_i, \quad i = 1, 2, \ldots, n \text{ and } j = 1, 2, \ldots. \tag{4.3}$$

It should be noted that in this paper we code the X-values such that their mean is equal to zero, i.e., $\overline{X} = 0$, to make the least square estimators of A and B independent, which allows us to monitor them individually using univariate control charts as shown in Kim et al. (2003). Additional discussion on the advantages of rescaling the X-values is provided in Mahmoud et al. (2010).

In addition to monitoring the residuals of the fitted linear profile, there exists an alternative error measure of the linear profile, referred to as RII, which is the average deviation from the in-control line. It should be noted that the use of RII was first investigated by Kang and Albin (2000) and Mahmoud et al. (2010). The deviation of the i^{th} quantile from the in-control regression line for observation j is given by

$$d_{ij} = Y_{ij} - A_0 - B_0 X_i, \quad i = 1, 2, \ldots, n. \tag{4.4}$$

Consequently, the mean squared deviations (MSD_j) from the in-control line for sample *j* can be calculated by

$$MSD_j = \frac{SSD_j}{n}, \text{ where } SSD_j = \sum_{i=1}^{n} d_{ij}^2 . \tag{4.5}$$

Now that the Q-Q plot's parameters are estimated, their use in the monitoring of Phase II data must be defined. Choosing an adequate monitoring strategy is a function of the parameters that have been selected for monitoring and the type of control chart used to monitor each of these parameters. In this paper, EWMA control charts are used to monitor each of the different parameterizations of the Q-Q plot, which are summarized in Table 4.1. The reader should note that the general formulation for each of the EWMA control charts used in these cases is given by

$$\begin{aligned} E(t) &= r \times S + \left[(1-r) \times E(t-1)\right] \\ UCL &= \mu + k \times \sigma \times \sqrt{\frac{r}{2-r}} \\ LCL &= \mu - k \times \sigma \times \sqrt{\frac{r}{2-r}} \end{aligned} , \tag{4.6}$$

where E is the EWMA statistic, t is the observation number, S is the value of the parameter (i.e. slope (m), y-intercept (b), MSE or MSD) at observation t, and r is the EWMA smoothing parameter (set at 0.2, a typical value). In addition, UCL and LCL are the upper and lower control limits for a given EWMA chart, k is the EWMA design parameter, and μ and σ are the mean and standard deviation of the statistic under consideration. Here, the control chart will signal if its EWMA statistic exceeds its respective control limit. It should be noted that the EWMA charts for *MSE* and *MSD* are one-sided, because the charts are bounded by zero and are only designed to detect increases in variation. Furthermore, $E(0)$ is taken as μ.

Table 4.1: Possible Parameterizations of the Q-Q Plot

Cases	Slope (m)	*Y*-intercept (b)	MSE	MSD
Case 1	✓	✓		
Case 2	✓	✓	✓	
Case 3	✓	✓		✓
Case 4	✓	✓	✓	✓

EWMA control charts were selected since they provide a simple, yet highly effective method to monitor linear profiles (Kim et al. (2003), Wang and Tsung (2005), and

Mahmoud et al. (2010)). It should be noted that increasing the number of parameters being simultaneously monitored, i.e., the number of control charts, does not necessarily lead to an improved quality performance. Increasing the number of charts can result in more false alarms when the process is in-control, while not improving the fault detection capability when the process becomes out-of-control (Montgomery (2008)). The performance of different Phase II control charting procedures is typically evaluated through the use of the average run length (ARL) metric, which is defined as the average number of samples (i.e. scanned parts) taken until a control chart signals. In the following subsection, we use computer simulations to select the most effective parameterization of the Q-Q plots based on the cases summarized in Table 4.1.

4.4.3 Selection of the Most Effective Parameterization of the Q-Q Plot

To identify the most effective parameterization of the Q-Q plot for monitoring 3D scans, we simulated the deviations of the manufactured part from the CAD geometry, as captured by 3D laser scanners. In our simulations, each observation (i.e. deviations of the part from the CAD) consists of 1000 sampling points that follow the standard normal distribution. These sampling points were then arranged in an ascending order, and their quantiles were calculated as explained in NIST/SEMATCH (2003). Moreover, the reference distribution's quantiles are calculated as

$$X_i = \Phi^{-1}\left(\frac{i-0.5}{n}\right), \tag{4.7}$$

where Φ^{-1} is the standard normal inverse cumulative distribution function. It should be noted that the *X*-values were coded such that their mean is equal to zero and that the number of quantiles (*n*) for each observation, as well as the reference distribution, was set to 1000. To obtain the in-control values for each of the parameters listed in Table 4.1, we simulated 10,000 in-control observations and calculated their respective quantiles. OLS regression was then performed to obtain the slope, y-intercept, and MSE for that observation. In addition, the historical values for the MSD parameter were calculated as explained in Equation (4.5). The resulting means and standard deviations for these four parameters are summarized in Table 4.2.

Table 4.2: Summary of the Historical in-Control Parameters

Cases	Slope (m)	*Y*-intercept (b)	MSE	MSD
μ	0.999	0.0000512	0.00166	0.00317
σ	0.00226	0.0317	0.000740	0.00176

Using the historical in-control values in Table 4.2, the control limits of the EWMA charts were calculated from Equation (4.6). Specifically, each case (in Table 4.1) was designed to have a combined average run length (ARL) equal to 200. This was achieved by designing the ARL of each individual EWMA chart to be equal to $200\times p$ by adjusting the EWMA design parameter k, where p is equal to the number of charts in a given case. For example, in Case 4, the four individual EWMA charts were designed to each have an in-control ARL (ARL_0) equal to 800. The resulting control charting scheme using all four charts would have an ARL_0 of approximately 200, if these charts are independent. We summarize the design parameters for our four cases in Table 4.3. The reader should note that these values are based on 50,000 simulation replications.

Table 4.3: EWMA Design Parameters and ARL_0 Estimates for the Four Cases

	Case 1	Case 2	Case 3	Case 4
k_m	2.849	2.966	2.990	3.002
k_b	2.886	3.012	2.925	3.122
k_e		3.661		3.756
k_d			2.732	3.939
ARL_0	200.06	199.94	199.92	200.06

Since we are interested in identifying which parameterization of the Q-Q plot is better suited for detecting process shifts, we evaluated the performance of the four cases under six different scenarios, summarized in Table 4.4. These scenarios can be classified into two categories: global and localized shifts. Global shifts replicate a point cloud, where all the deviations of the as-built part have shifted from their corresponding nominal values, from the CAD geometry. A global shift can occur due to a loose or worn out fixture. On the other hand, localized shifts replicate a point cloud where only a specific area of the part being measured has shifted from nominal, such as a failure caused by a worn out die. For the six scenarios, the sampling points (either entirely or only 10 or 50 points) were

drawn from the distribution $N\left(\delta_{\mu'},(1+\delta_{\sigma'})^2\right)$. It should be noted that for a given scenario, we only increased one of the distribution's parameters.

Table 4.4: A Description of the Six Scenarios of Process Shifts Introduced in the Simulations

Scenario	Size of shift	Shift Introduced
I	Global	$\delta_{\mu'}$
II	Global	$1+\delta_{\sigma'}$
III	Localized (10 points)	$\delta_{\mu'}$
IV	Localized (10 points)	$1+\delta_{\sigma'}$
V	Localized (50 points)	$\delta_{\mu'}$
VI	Localized (50 points)	$1+\delta_{\sigma'}$

We provide the out-of-control ARL for the first two scenarios in Figure 4.4. It should be noted that the bars are in an ascending order of the cases, for each shift value. Based on Figure 4.4a, it can be seen that Case 1 performs best for small shifts and performs only slightly worse than the other three cases for the relatively large shifts, i.e. when $\delta_{\mu'} \geq 1$. For Scenario II, Figure 4.4b shows that Case 1 uniformly outperforms the other three cases for all variance shifts considered. Therefore, if a practitioner were only to focus on detecting global shifts in the part, our results indicate that Case 1 would lead to the best performance.

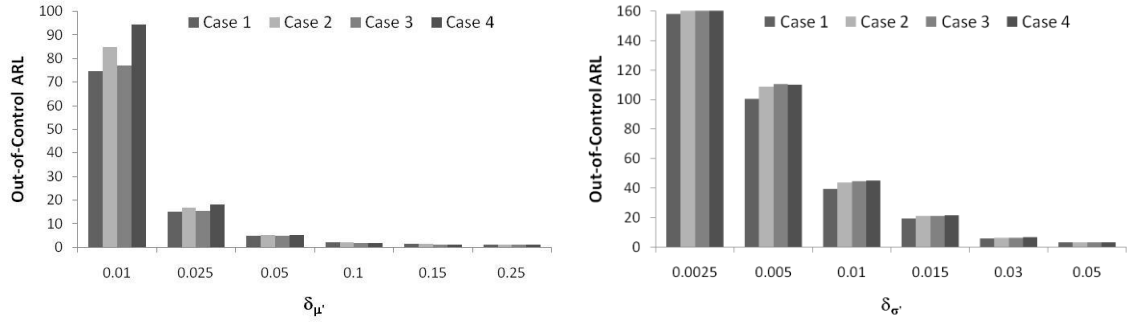

(a) (b)

Figure 4.4: Out-of-control ARL Comparisons for the Four Cases for: (a) Scenario I, and (b) Scenario II

Similar to the global shifts, we investigated the performance of the four cases for the localized shift scenarios using the average run length metric. Our results are summarized in Figure 4.5. Similar to Figure 4.4, the bars are in an ascending order of the cases, for

each shift value. For the localized mean shits, i.e. Figures 4.5a and 4.5c, we can see that the performance is quite similar to the global mean shift. Case 1 performs best at smaller shifts and slightly lags the other three cases for shifts $\delta_{\mu'}>1$. For the localized variance shifts, Figure 4.5b indicates that Case 3 performs best for smaller shifts, while Figure 4.5d shows that Case 1 performs best for smaller shifts. For the relatively large shifts, Cases 2 and 4 have the lowest out-of-control ARL, as depicted in Figures 4.5b and 4.5d. These results are different than what was obtained in Scenario II, where Case I outperformed the other three cases for both small and larger shifts.

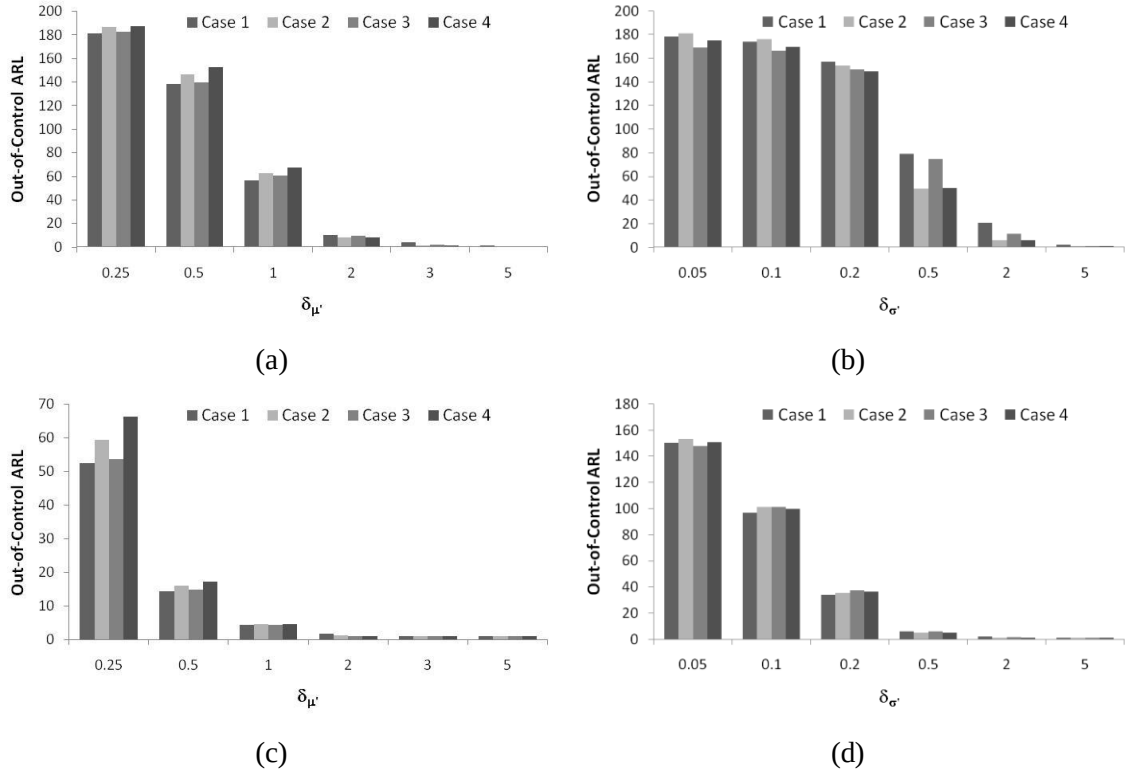

Figure 4.5: Out-of-control ARL Comparisons for the Four Cases for: (a) Scenario III, (b) Scenario IV, (c) Scenario V, and (d) Scenario VI.

Based on the above discussions, there is not any case which uniformly performs best for all of the scenarios considered. Accordingly, a practitioner should take into consideration two factors when designing/selecting his/her control charting scheme for point cloud monitoring. First, one must consider the number of simultaneous charts to be used. Increasing the number of charts may provide better performance; however, this requires being able to design each chart, such that they individually and collectively meet certain

performance criteria. Second, the type of process/product being monitored should be accounted for when selecting the control charting scheme. More specifically, the most critical or highest probable types of shifts should be identified and accounted for in the design of the control charting scheme. For example, when producing compliant (non-rigid) parts higher priority should go toward detecting shifts in the variance.

4.5 Pilot Lab Study

In this section, our proposed method was applied to detect defects in commercially available metal brackets, which are used to fix 2'' pipes onto wood frames. The major nominal dimensions of the bracket are shown in Figure 4.6a. In this study, a total of 50 conforming and defective brackets were used to emulate the in-control and out-of-control states of a production process, respectively. To represent the out-of-control conditions, three unique deformation modes were introduced into the system by modifying a total of 20 brackets (8, 8, and 4 for failure modes 1, 2 and 3, respectively). These deformation modes can be visualized in Figure 4.6b-d, where the nominal CAD geometry and the deformed part are represented by the dark solid geometry and the light wireframe geometry, respectively. These failure modes are representative of typical global and local deformation modes for a bracket. Failures 1 and 2 are global deformation modes; the first is resulting from excessive bending of the bracket's 2" diameter sleeve, and the latter is caused by an incorrect angle (not orthogonal) between the side and bottom of the bracket's mounting plate. Failure 3 is a localized deformation mode at the end of the bracket's mounting plate. This section is divided into four subsections describing the major steps in implementing our proposed method in a lab environment, and the subsequent fault diagnosis using laser scanning software.

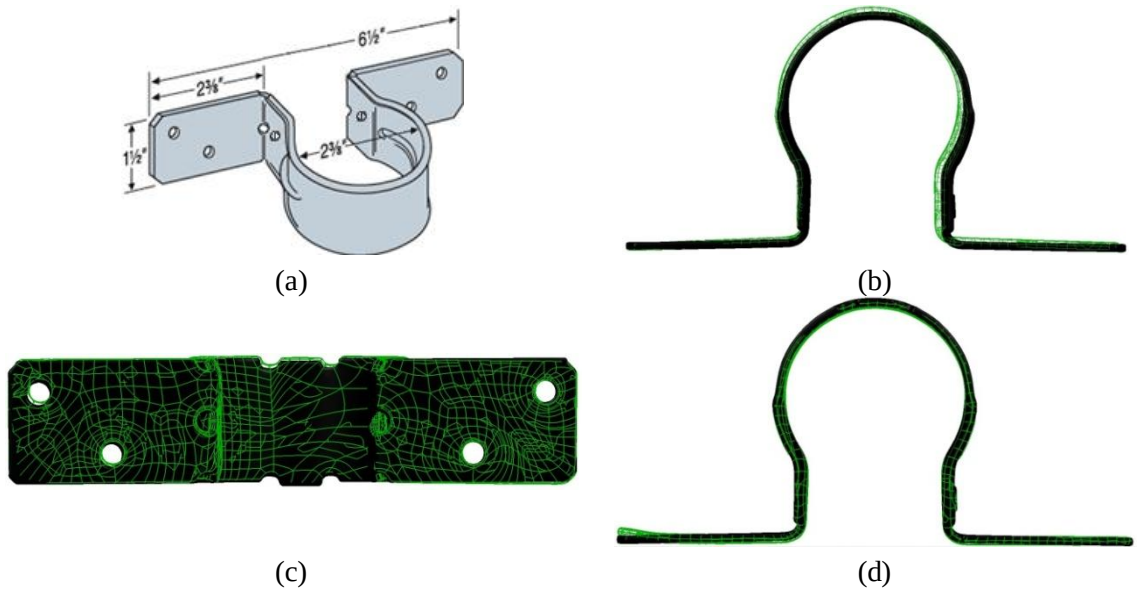

Figure 4.6: CAD Geometry of (a) Nominal bracket; Nominal Geometry versus (b) Failure Mode 1, (c) Failure Mode 2, and (d) Failure Mode 3

4.5.1 Part Scanning and Generating the Distribution of Deviations from Nominal

The scans were captured using a version 2.0 Faro Laser ScanArm®, which was mounted on a Faro Platinum Arm®. The arm itself was fixed to an optical table to ensure that the scanner had a consistent coordinate system. The optical table also ensures that the scanner needs to be calibrated only once during the data collection process. In addition, the brackets themselves were attached to a fixture mounted to the optical table in order to avoid any misalignments in the CAD-to-part comparison.

Geomagic's Qualify® software was used to uniformly sample each of the scans to ensure that the sample point density within each scan is almost constant. This is important in applying SPC to scanned data, since all regions of the point cloud will have an equal weight. Not only does this ensure consistency between scans, but it also prevents cases where deviations from nominal are concentrated in a subset of the scan. As a result, the monitored scans can be compared over time since they are equally representative of the part's geometry. In addition, the uniform sampling reduces the number of sampled points, which helps reduce data redundancy and ease the computational burden. In our study, the number of scanned points in the uniform sample was set to be approximately 50,000 points. It should be noted that in other applications the number of sample points can be

significantly different depending on the size of the scanned part and the desired minimum fault size to be detected.

After sampling, a 3D compare method in Geomagic's Qualify® software was used to obtain the deviations of the part from nominal. It is important to note that, in process monitoring applications, preset alignment methods should not be used since these predefined functions attempt to get the best alignment possible, which can distort the true distribution of the absolute deviations from nominal. Accordingly, this technique cannot be used for monitoring. Instead, the coordinate system for the CAD geometry was aligned with that of the fixture (used to attach the brackets to the optical table).

4.5.2 Control Charting Scheme Selection and Design

Our simulations showed that there is not any one control charting scheme which uniformly performs best for all the process shifts considered. Consequently, we suggested that the practitioner should select the control charting scheme based on the application. For our lab study, the part being monitored is fairly rigid and therefore, it is not likely to exhibit significant variation shifts. Therefore, we should focus on the control charting schemes which are best able to detect mean shifts. In the previous section, we have noted that Cases 1 and 3 have the best overall performance for detecting shifts in the mean. However, Case 3 requires the simultaneous monitoring of three parameters, as opposed to Case 1 which requires only two. As a result, we apply the control charting scheme based on Case 1, since it is easier to design and fits best with the types of faults that can occur with this part.

In our simulations, the baseline quantiles were generated from the standard normal distribution as explained in Equation (4.7). The rationale behind the choice of this distribution is mainly due to mathematical convenience. In practice, however, the use of the standard normal for the baseline may not be a valid assumption. Therefore, in our lab study, we chose one of the 30 conforming parts at random to be the baseline by obtaining its deviations from nominal distribution and observing n=1,001 quantiles. These 1,001 quantiles were then used as the baseline quantiles. It should be noted that we coded these quantiles to have a mean of zero, as explained earlier in the chapter. To acquire the

historical distribution, 24 of the remaining 29 good parts were chosen at random, which allowed us to plot 24 Q-Q plots and use OLS to obtain the slope and the y-intercept for each of these plots. The mean and standard deviation for each of these two estimators were then calculated, see Table 4.5, to be used in constructing the control limits for the two EWMA control charts.

Table 4.5: Historical Values of the In-control Parameters of the Q-Q plots

Cases	Slope (m)	Y-intercept (b)
μ	1.2027	0.000769
σ	0.2643	0.0038

In order to implement the control charting method, appropriate control limits need to be determined to achieve a desired ARL_0. For this lab study, an in-control ARL of 250 was selected. Under the normality assumption for the slope and y-intercept, the EWMA design parameter, k, was set to 2.962, which would result in an in-control ARL of 500 (Lucas and Saccucci (1990)). Since the estimators of the slope and Y-intercept are independent, this charting scheme would have the desired in-control ARL of approximately 250.

For the Phase II analysis, it is assumed that the process is in-control for five parts (the remaining in-control scans not used for generating the historical data) followed by sustained process shift, corresponding to one of the defects shown in Figure 4.6b-d. It is important to stress that the purpose of this Phase II experimentation is to show how the method works rather than the actual results, since the results are pertinent to this experiment only. On the other hand, the aforementioned defects are carefully selected to show the ability of the proposed method to detect both global (Fault modes 1 and 2) and localized faults (Fault mode 3) in manufactured parts. This ability is demonstrated in Figure 4.7, where at least one of the control charts signaled to detect an out-of-control condition within two scanned parts.

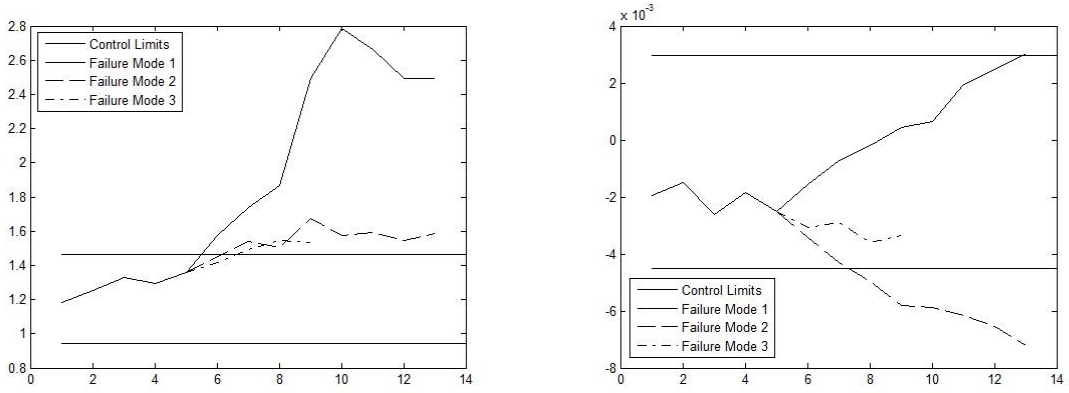

(a) (b)

Figure 4.7: EWMA control Chart for (a) the slopes, and (b) the y-intercepts of the Q-Q plots

It is evident from this small sample size experiment that the utilization of point cloud data can be very useful as it allows for using thousands of sample points to judge whether the process is in-control or out-of-control. Even though some of these sample points are highly correlated, the overall use of this method can be seen in its ability to represent the part being monitored completely rather than approximate it with a few pre-defined quality characteristics.

4.5.3 Fault Diagnosis using 3D Scanning Software

From a practitioner's perspective, the detection of an out-of-control condition serves only as a first step in returning the process to its in-control performance. Once a shift happens, the practitioner would then perform a root-cause analysis to identify the underlying cause for the shift, and then perform the required corrective actions for process recovery. In SPC, control charts are only typically used for fault detection, since it is assumed that the fault diagnosis state is process specific. However, in practice, the fault diagnosis stage is often the most critical since practitioners are required to isolate the faulty subsystem and identify what "went wrong", which often results in a lengthy diagnosis stage. This is problematic since the production line can be shut down when the control chart signals to prevent the production of additional non-conforming parts. This downtime can be very costly, reaching tens of thousands of dollars per minute in the automotive industry. Therefore, it is important to provide diagnostic measures to assist practitioners in the fault diagnosis stage.

When using Q-Q plots for monitoring point cloud data, there is no direct method to identify the location of the fault on the part, since the spatial aspect of the data is lost when transforming the scans into Q-Q plots. However, diagnosis can be performed by inspecting the scans at and/or immediately prior to the signaling of the control charts. For example, Fig. 8, shows the deviations of the as-built part to the CAD geometry for the part that lead to the control chart signal. Additionally, Figure 4.8 shows that the control chart signal is resulting from a localized fault on the left side of the part. When we viewed these results by their XYZ coordinates, we concluded that the fault is a bending of the left side of the part in the positive *z* direction. This conclusion should save the practitioners' time in identifying the location/size of the fault, since they can combine this conclusion with their process knowledge to have a more rapid process recovery.

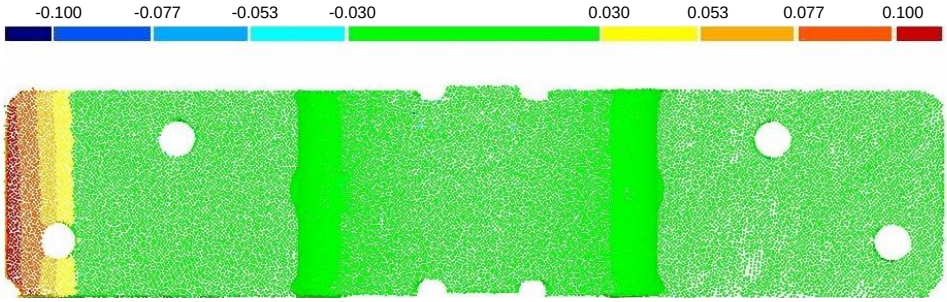

Figure 4.8: Point Cloud Deviations from Nominal for Failure Bode 3 (measurements are in inches)

4.6 Future Research

In this chapter, we have shown how software can be used to complement our proposed control charting method to assist practitioners in visualizing the fault location, which is an important first-step in achieving a rapid process recovery. We believe that the diagnostic aspect of our paper can be further enhanced through the use of spatiotemporal monitoring methods, which are widely used in public health surveillance for cluster detection, see e.g. Sonesson (2007), Tsui et al. (2011), and Jiang et al. (2011). The potential of using such methods is further supported by the work of Megahed et al. (2011) who developed a spatiotemporal monitoring technique for identifying the time as well as the location/size of the fault in image data, which are quite similar to point clouds in terms of high-dimensionality and structure.

Another promising research topic includes exploring how to combine the information from different measurement systems that vary in speed and information provided to improve the existing quality practices. In practice, it is often the case that different measurement devices are used for the same purpose; however, the association between these devices is often overlooked. As an illustration, we provide an example that the authors are currently researching. Consider a quality system, where low-cost high-frequency measurements, such as the door gap measurements presented in Figure 4.9a, along with expensive low-frequency measurements, such as the laser scanner example shown in Figure 4.9b, are used in parallel. If a strong association is present between the laser scanner and the gap measurements, it may be possible to infer the optimal placement for gap measurements from inherent associations within the data. This inference would enable industrial practitioners to utilize their existing measurement capabilities in a more effective and efficient way. Consequently, a better process understanding resulting in an increase in productivity and a reduction in operational cost can be achieved.

(a) (b)

Figure 4.9: Door Measurements: a) High Frequency Sampling, and b) Low Frequency Sampling

4.7 Conclusions

The method proposed in this chapter can be seen as an introductory method for quality monitoring using of 3D laser scan data. In addition, this chapter has the following contributions: 1) it provides a structured methodology for industrial practitioners to utilize 3D laser scan data within the current SPC framework; 2) it utilizes deviations from nominal instead of the raw point cloud data to overcome the aforementioned difficulties in point clouds, which provides an important insight on the importance of data preparation, often overlooked in the existing SPC literature; 3) it demonstrates how these

deviations from nominal can be monitored using profile monitoring techniques; and 4) it provides researchers a benchmark method for comparison, which does not currently exist in the literature.

Monitoring of point cloud data is a very promising area of application within statistical quality control. It is a natural extension of profile monitoring, an application and research area of increasing importance. Point cloud monitoring also adds the capability of monitoring a wide variety of quality characteristics, such as dimensional data, product geometry, surface defect patterns, and surface finish, in real-time. As the use of laser scanners increases, there will be an increasing number of practical applications where the concepts of statistical quality control can play an important role.

4.8 References

Choudhary, A. K., Harding, J. A., & Tiwari, M. K. (2009). Data mining in manufacturing: a review based on the kind of knowledge. *Journal of Intelligent Manufacturing, 20*(5), 501-521, doi:10.1007/s10845-008-0145-x.

Colosimo, B. M., Mammarella, F., & Petro, S. (2010). Quality control of manufactured surfaces. In H.-J. Lenz, & P.-T. Wilrich (Eds.), *Frontiers of Statistical Quality Control* (Vol. 9). Vienna: Springer.

Feng, H.-Y., Liu, Y., & Xi, F. (2001). Analysis of digitizing errors of a laser scanning system. *Precision Engineering, 25*, 185-191.

Gunter, B. (1994). Q-Q plots. *Quality Progress, 27*(2), 81–86.

Hisao, S.-W., & Chuang, J. C. (2003). A Reverse Engineering Based Approach for Product Form Design. *Design Studies, 24*(2), 155-171.

Isheil, A., Gonnet, J. P., Joannic, D., & Fontaine, J. F. (2011). Systematic error correction of a 3D laser scanning measurement device. *Optics and Lasers in Engineering, 49*(1), 16-24.

Jiang, W., Han, S. W., Tsui, K. L., & Woodall, W. H. (2011). Spatiotemporal surveillance methods in the presence of spatial correlation. *Statistics in Medicine, 30*(5), 569-583, doi:10.1002/sim.3877.

Kang, L., & Albin, S. L. (2000). On-line monitoring when the process yields a linear profile. *Journal of Quality Technology, 32*(4), 418-426.

Kendall, M. G., Stuart, A., Ord, J. K., Arnold, S. F., & O'Hagan, A. (1994). *Kendall's advanced theory of statistics*. London; New York: Edward Arnold ; Halsted Press.

Kim, K., Mahmoud, M. A., & Woodall, W. H. (2003). On the monitoring of linear profiles. *Journal of Quality Technology, 35*(3), 317-328.

Lucas, J. M., & Saccucci, M. S. (1990). Exponentially Weighted Moving Average Control Schemes - Properties and Enhancements. *Technometrics, 32*(1), 1-12.

Mahmoud, M. A., Morgan, J. P., & Woodall, W. H. (2010). The monitoring of simple linear regression profiles with two observations per sample. *Journal of Applied Statistics, 37*(8), 1249-1263.

Martinez, S., Cuesta, E., Barreiro, J., & Alvarez, B. (2010). Analysis of laser scanning and strategies for dimensional and geometrical control. *The International Journal of Advanced Manufacturing Technology, 46*(621-629).

Megahed, F. M., Wells, L. J., Camelio, J. A., & Woodall, W. H. (2011). A Spatiotemporal Monitoring Method for Image Data. Submitted for publication.
Megahed, F. M., Woodall, W. H., & Camelio, J. A. (2011). A Review and Perspective on Control Charting with Image Data. *Journal of Quality Technology, 43*(2), 83-98.
Mohaghegh, K., Sadeghi, M. H., & Abdulla, A. (2007). Reverse engineering of turbine blades based on design intent. *International Journal of Advanced Manufacturing Technology, 32*(9-10), 1009-1020.
Mohib, A., Azab, A., & Elmaragy, H. (2009). Feature-Based Hybrid Inspection Planning: A Mathematical Programming Approach. *The International Journal of Computer Integrated Manufacturing, 22*(1), 13-29.
Montgomery, D. C. (2008). *Introduction to statistical quality control* (6th ed.). Hoboken, N.J.: Wiley.
NIST/SEMATECH (2003). e-Handbook of Statistical Methods. http://www.itl.nist.gov/div898/handbook/.
Panagiotidou, S., & Tagaras, G. (2010). Statistical processs control and condition-based maintenance: a meaningful relationship through data sharing. *Production and Operations Management, 19*(2), 156-171.
Reinhart, G., & Tekouo, W. (2009). Automatic Programming of Robot-Mounted 3D Optical Scanning Devices to Easily Measure Parts in High-Variant Assembly. *CIRP Annals - Manufacturing Technology, 58*(1), 25-28.
Shi, Q., & Xi, N. (2008). *Automated Data Processing for a Rapid 3D Surface Inspection System.* Paper presented at the IEEE International Conference on Robotics and Automation,
Shi, Q., Xi, N., & Spagnuluo, C. (2007). A Feedback Design to a CAD-Guided Area Sensor Planning System for Automated 3D Shape Inspection. *Computer-Aided Design & Applications, 4*, 209-218.
Son, S., Park, H., & Lee, K. H. (2002). Automated laser scanning system for reverse engineering and inspection. *International Journal of Machine Tools & Manufacture, 42*(8), 889-897.
Sonesson, C. (2007). A CUSUM framework for detection of space-time disease clusters using scan statistics. *Statistics in Medicine, 26*, 4770-4789.
Tamura, S., Kim, E.-K., Close, R., & Sato, Y. (1994). Error correction in laser scanner three-dimensional measurement by two-axis model and coarse-fine parameter search. *Pattern Recognition, 27*(3), 331-338.
Várady, T., Martin, R. R., & Cox, J. (1997). Reverse Engineering of Geometric Models--an Introduction. *Computer-Aided Design, 29*(4), 255-268.
Wang, K., & Tsung, F. (2005). Using profile monitoring techniques for a data-rich environment with huge sample size. *Quality and Reliability Engineering International, 21*(7), 677-688.
Wang, X. Z., & McGreavy, C. (1998). Automatic classification for mining process operational data. *Industrial & Engineering Chemistry Research, 37*(6), 2215-2222.
Wells, L. J., Megahed, F. M., Camelio, J. A., & Woodall, W. H. (2011). A framework for variation visualization and understanding in complex manufacturing systems. *Journal of Intelligent Manufacturing*, doi:10.1007/s10845-011-0529-1.
Woodall, W. H. (2000). Controversies and contradictions in statistical process control. *Journal of Quality Technology, 32*(4), 341-350.
Woodall, W. H. (2007). Current research on profile monitoring. *Produção, 17*, 420-425.
Woodall, W. H., Spitzner, D. J., Montgomery, D. C., & Gupta, S. (2004). Using control charts to monitor process and product quality profiles. *Journal of Quality Technology, 36*(3), 309-320.
Wu, S.-K., Hu, J., & Wu, S. M. (1994). A fault identification and classification scheme for an automobile door assembly process. *The International Journal of Flexible Manufacturing Systems, 6*, 261-285.

Xi, F., Liu, Y., & Feng, H.-Y. (2001). Error compensation for three-dimensional line laser scanning data. *The International Journal of Advanced Manufacturing Technology, 18*, 211-216.

Zussman, E., Schuler, H., & Seliger, G. (1994). Analysis of the geometrical feature detectability constraints for laser-scanner sensor planning. *The International Journal of Advanced Manufacturing Technology, 9*, 56-64.

5 Conclusions and Future Work

5.1 Dissertation Contributions

The control charting tools presented in this dissertation set the foundations needed for effectively incorporating high-density image data into SPC. In today's competitive global market, quality, cost and timeliness are key competitive advantage differentiators for manufacturing facilities. The developed tools will transform high-density data into high-content information, which will provide industrial practitioners with a deeper understanding of the state of their manufacturing process, especially since SPC has not effectively used aesthetic and 3D surface geometries in process monitoring. From this research, there several main contributions to the field of statistical quality control, which include the following: 1) classifying the research areas for image-based control charting techniques; 2) developing performance metrics needed to evaluate image-based control charting techniques; 3) creating a spatiotemporal framework for monitoring image data that is not only capable of detecting out-of-control conditions quickly, but provides the estimates of the changepoint and the fault location/size; 4) building a framework for point cloud monitoring such that all surface defects can be detected rather than the ones that are captured by the CMM measurements; and 5) using point cloud data to identify the magnitude and location of product faults through comparing the CAD model to the as-built product. These contributions, described in more detail in the subsections below, should have a substantial effect on the ability of current SPC tools to capture process shifts in the ever-increasing complexity in current production systems. In addition, the developed tools will encourage researchers to further investigate how high-density measurement systems can be used in statistical process control.

5.1.1 Reviewing, Analyzing and Classifying Image-Based Monitoring

Chapter 2 provides a review and perspective on the state of the literature on image-based control charting. Since the literature on image-based control charting was fragmented (i.e. methods were developed in isolation independent of previous work), this chapter brings these methods into better focus. More specifically, these methods were separated into the following categories: univariate methods, multivariate methods, spatial control charts, multivariate image analysis, and medical applications. In addition, the term "spatial

control chart" was coined and it was found that there are no existing methods that are used to monitor point cloud data.

The corresponding paper was very well received by the SPC community. This work was invited to be presented in three SPC-related conferences (INFORMS 2010, QPRC 2011, and INFORMS 2011). More importantly, this paper allowed me to organize an invited session on the monitoring of image-data with Prof. Kaibo Wang, Tsinghua University, in the 2011 INFORMS Annual Meeting. This session showcased some of the latest work on image-based control charting and presented some future research directions in this area. The dissemination of this work through these conferences have increased the impact of this work and resulted in an increased awareness of the potential benefits and opportunities in this field. This may have contributed to having this paper as the most downloaded *Journal of Quality Technology* paper in 2011.

5.1.2 Performance Metrics for the Evaluation of Image-Based Charts

As shown in Chapter 2, the majority of the literature on using control charts for image data focused on a given application/dataset, which reduces the impact since it is difficult to compare the different methods. It is customary in SPC that this comparison is based on computer simulations where the data can be replicated. The in-control performance is set to be similar and then the out-of control ARL is used to determine which control charting methodology is superior when detecting various shifts. In Chapter 3, it was shown that the image-based control charting methodologies should be considered as a two-step process. First, they can be used to detect the occurrence of a process problem. Since image-data computations can be computationally intensive, we recommended the use of the steady-state median run length metric as opposed to the commonly used ARL metric. Second, diagnostic metrics for evaluating the estimation of the change-point and the size/location of the fault were proposed. These metrics allow for the ability to evaluate the performance of different control charting methods for image data. In addition, they can also be used to compare the performance of public-health surveillance techniques that were highlighted in Chapter 3. It should be noted that the use of diagnostic metrics allows us to truly know if the signaling of the GLR chart should be considered as a false alarm

or is it due to an actual process issue. This analysis was never done in the SPC literature and it is very beneficial in linking fault detection and diagnosis.

5.1.3 A Spatiotemporal Framework for Image Monitoring

Building on the previous subsection, it is important to show how the information extracted from image data can be more beneficial than discrete measurements. Not only does image data contain both sensory and dimensional measurements, but it can also be used to significantly reduce the time required for fault diagnosis/correction. Accordingly, the use of the spatiotemporal GLR control charting technique allowed for having a rapid fault detection capability and an ability to provide diagnostic information after the detection of process shifts. The combination of these two features had never been done for grayscale imaging, which represents the majority of images captured at the shop-floor of manufacturing processes. To increase the applicability of this control charting methodology, each captured image is to be subtracted from its nominal. This allows the spatiotemporal framework to be applied to images of industrial products whose quality is either characterized by uniformity (e.g. when trying to detect unevenness defects in LCD monitors) or by a specific pattern (e.g. manufactured tiles) that has to be followed and deviations from this pattern are to be detected. Finally, it should also be noted that the ability to apply the same control charting methodology to more than one image-based application is unique. This will enable this framework to have a greater impact in many industries.

5.1.4 Detection of Unspecified Faults through the Use of 3D Scanning

Dimensional specifications play an important role in assembly operations. Typically, practitioners select a few sampling points per part, track these points using CMMs, and then apply SPC methods to assess if the observed part-to-part variation is significant. However, these sampling points may not capture all possible variation sources since only a few points on the part are measured. 3D scanning technologies provide an opportunity to overcome this deficiency since a product's entire surface geometry can be represented. By monitoring the entire surface geometry, unexpected fault patterns can be detected. Through the use of QQ plots, we have shown that these faults can be detected. This work is the first time that variation from one scanned part to another has been captured and

analyzed to accurately depict the state of the manufacturing process. More generally, the use of the accumulated item-to-item scans allows us to better address the data rich but information poor problem highlighted in the literature. This can result in an improved shop-floor decision-making, which results in better productivity.

5.1.5 Identifying Process Issues through Spatial Analysis of Point Clouds

Not only does the use of QQ plots allow us to detect unspecified faults, but it also allows us to detect deterioration in the process performance prior to the occurrence of an out-of-specification product. Specifically, the majority of current manufacturing processes have very high process capability indices, which means that deterioration in the process may not initially result in a non-conforming part. The use of control charting on 3D scans increases the possibility of such an effect to be observed, and the identification of the location on the part allows practitioners to use their process knowledge to determine more quickly which subsystem in the process is out-of-control. This is very important since costly process failures/downtime can be reduced.

5.1.6 Summary of Contributions

The overall goal of this dissertation is to develop control charting methods for high-density data to better capture both the aesthetic and dimensional quality characteristics of manufactured products. One can consequently have a rapid fault detection capability and an ability to provide diagnostic information after the detection of process shifts. Even though this research problem is broad and complex, this dissertation presents an opportunity to move quality monitoring to the next level as depicted in Figure 5.1.

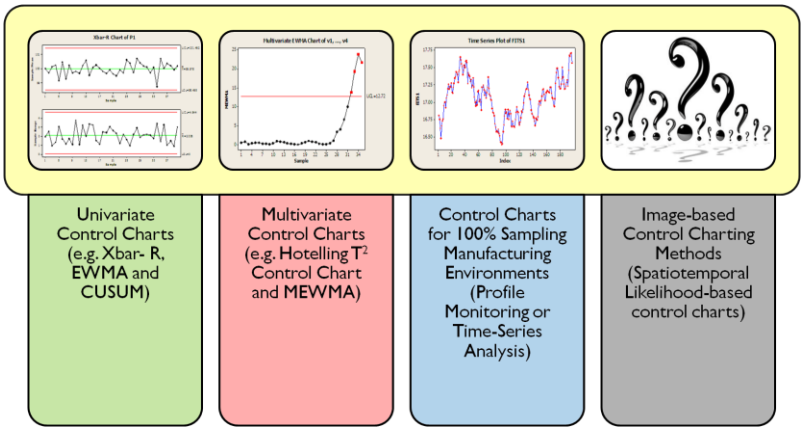

Figure 5.1: The Expected Paradigm Shift in SPC Methodology

5.2 Future Work

In general, this dissertation provides a methodology to utilize data captured from high density image devices for fault detection and diagnosis in manufacturing environments. Based on this work, there exist several research opportunities that should be investigated. Some of these opportunities are highlighted in the subsections below.

5.2.1 Effect of Estimation Error on High Density Data Methods

In both Chapters 2 and 3, it was assumed that the in-control parameters for both the ROIs and the Q-Q plots were known. However, in practice, the in-control parameters are typically unknown and must be estimated in order to construct the necessary control chart limits. Therefore, one should investigate the effect of parameter estimation on the performance of both the spatiotemporal GLR charts and the EWMA control charts for monitoring the slope and y-intercept of the Q-Q plot. This can be done through calculating the expected value of the average run length and the standard deviation of the average run length to determine how large of a Phase I sample is needed such that any estimation error can be neglected. Consequently, industrial practitioners can be guaranteed of satisfactory performance of these charts for both the in-control and out-of-control situations.

5.2.2 Visualizing Variation in High Density Data Environments

The reason for the wide-spread use of SPC is the simplicity of visualizing statistical fluctuations by the engineers, the managers and the technicians on the shop-floor. More specifically, when monitoring only one quality characteristic, a typical univariate control chart makes it very easy to understand what an out-of-control signal means. However, with the increase in the amount of data being monitored current SPC methods have failed to enable that visualization. Therefore, SPC researchers should consider investigating incorporating visual analytics with SPC to simplify the visualization process so that shop-floor personnel can incorporate their process knowledge with the information captured by the control charts. One approach to achieve this aforementioned goal is to examine how different data streams can be used to visualize the variation propagation among the different stages of the manufacturing process. This builds on the work carried out in this

dissertation, where practitioners were directed in their diagnosis based on the identification of the fault location on a manufactured part.

5.2.3 Estimating the Life-Cycle Performance of Manufactured Parts through Correlating Process and Product Variables

Another future topic involves conducting research on the application of data analytics for manufacturing system control with an emphasis on quality and reliability improvement. The goal is to create quality systems that store the measured process parameters and correlate them to both product life-cycle data and process failures. The objective of this system is to effectively utilize the capabilities of computing and sensor systems that are already available in manufacturing facilities today to predict when both the product and process will fail. Such a system has the potential to transform decision-making at both the management and shop-floor levels. More specifically, it would enable company executives to accurately forecast the lifespan of each product based on the exact process parameters that were used in manufacturing. In addition, engineers on the shop-floor can set more effective controls accounting for process shifts and machine aging.

5.3 References

Fitchett , D. and Sondalini, M. (2006). *True Downtime Cost Analysis: The Best Way to Discover and Justify Removing Manufacturing Waste*, 2nd Edition.

Reilly, K. (2005) "Auto Manufacturers Can Save Millions by Reducing Defect Detection-to-Correction Time," AMR Research Report, Boston, MA.

Report to the President on Ensuring American Leadership in Advanced Manufacturing compiled by the President's Council of Advisors on Science and Technology (PCAST), June 2011.

"Too Much Buzz: Social Media Provides Huge Opportunities, but Will Bring Huge Problems." *The Economist*. Dec 2011. http://www.economist.com/node/21542154.

Appendix A: Journal of Quality Technology Copyright Permission

COPYRIGHT PERMISSION AGREEMENT

Title of Article: "A Review and Perspective on Control Charting with Image Data", by Fadel M. Megahed, William H. Woodall, and Jaime A. Camelio; *Journal of Quality Technology*, Vol. 43, No. 2, April 2011

Requested by: Fadel Megahed, Virginia Tech

Purpose of Request: Republish article in dissertation; dissertation will be available online via Virginia Tech's ETD (Electronic Theses and Dissertations) system

Projected Date of Use: 2012

Permission Granted: Yes No further distribution allowed without permission; This edition only

Fee: $0.00 (Our accounting department will send you an invoice shortly. Do not send any payment until you receive the invoice from ASQ .)

Billing Address: **_____NO FEE_____**

A one-time permission is hereby granted to reprint the material described above in the specified publication. Any unauthorized reproduction is a violation of U.S. copyright law and is subject to a penalty of $100,000 per violation. As a condition of this approval, you agree to publish the following copyright line in conjunction with this material:

Reprinted with permission from ***Journal of Quality Technology*** ***©2011*** American Society for Quality. No further distribution allowed without permission.

I agree to the terms listed above.

Please sign here and fax to 414-765-8660 or email signed copy to address below.

Name *Fadel M. Megahed* Title PhD Candidate Date: 3/14/2012

If you have any questions, please contact Katie Kvien at kkvien@asq.org.
Signed by: Katie Kvien, March 14, 2012

Appendix B: Quality and Reliability Engineering International Copyright Permission

JOHN WILEY AND SONS LICENSE
TERMS AND CONDITIONS
Mar 14, 2012

This is a License Agreement between Fadel M Megahed ("You") and John Wiley and Sons ("John Wiley and Sons") provided by Copyright Clearance Center ("CCC"). The license consists of your order details, the terms and conditions provided by John Wiley and Sons, and the payment terms and conditions.

All payments must be made in full to CCC. For payment instructions, please see information listed at the bottom of this form.

License Number	2867620040075
License date	Mar 14, 2012
Licensed content publisher	John Wiley and Sons
Licensed content publication	Quality & Reliability Engineering International
Licensed content title	A Spatiotemporal Method for the Monitoring of Image Data
Licensed content author	Fadel M. Megahed, Lee J. Wells, Jaime A. Camelio, William H. Woodall
Licensed content date	Jan 1, 2012
Start page	n/a
End page	n/a
Type of use	Dissertation/Thesis
Requestor type	Author of this Wiley article
Format	Electronic
Portion	Full article
Will you be translating?	No
Order reference number	
Total	0.00 USD
Terms and Conditions	

TERMS AND CONDITIONS

This copyrighted material is owned by or exclusively licensed to John Wiley & Sons, Inc. or one of its group companies (each a "Wiley Company") or a society for whom a Wiley Company has exclusive publishing rights in relation to a particular journal (collectively WILEY"). By clicking "accept" in connection with completing this licensing transaction, you agree that the following terms and conditions apply to this transaction (along with the billing and payment terms and conditions established by the Copyright Clearance Center

Inc., ("CCC's Billing and Payment terms and conditions"), at the time that you opened your Rightslink account (these are available at any time at http://myaccount.copyright.com)

Terms and Conditions

1. The materials you have requested permission to reproduce (the "Materials") are protected by copyright.

2. You are hereby granted a personal, non-exclusive, non-sublicensable, non-transferable, worldwide, limited license to reproduce the Materials for the purpose specified in the licensing process. This license is for a one-time use only with a maximum distribution equal to the number that you identified in the licensing process. Any form of republication granted by this licence must be completed within two years of the date of the grant of this licence (although copies prepared before may be distributed thereafter). The Materials shall not be used in any other manner or for any other purpose. Permission is granted subject to an appropriate acknowledgement given to the author, title of the material/book/journal and the publisher. You shall also duplicate the copyright notice that appears in the Wiley publication in your use of the Material. Permission is also granted on the understanding that nowhere in the text is a previously published source acknowledged for all or part of this Material. Any third party material is expressly excluded from this permission.

3. With respect to the Materials, all rights are reserved. Except as expressly granted by the terms of the license, no part of the Materials may be copied, modified, adapted (except for minor reformatting required by the new Publication), translated, reproduced, transferred or distributed, in any form or by any means, and no derivative works may be made based on the Materials without the prior permission of the respective copyright owner. You may not alter, remove or suppress in any manner any copyright, trademark or other notices displayed by the Materials. You may not license, rent, sell, loan, lease, pledge, offer as security, transfer or assign the Materials, or any of the rights granted to you hereunder to any other person.

4. The Materials and all of the intellectual property rights therein shall at all times remain the exclusive property of John Wiley & Sons Inc or one of its related companies (WILEY) or their respective licensors, and your interest therein is only that of having possession of and the right to reproduce the Materials pursuant to Section 2 herein during the continuance of this Agreement. You agree that you own no right, title or interest in or to the Materials or any of the intellectual property rights therein. You shall have no rights hereunder other than the license as provided for above in Section 2. No right, license or interest to any trademark, trade name, service mark or other branding ("Marks") of WILEY or its licensors is granted hereunder, and you agree that you shall not assert any such right, license or interest with respect thereto.

5. NEITHER WILEY NOR ITS LICENSORS MAKES ANY WARRANTY OR REPRESENTATION OF ANY KIND TO YOU OR ANY THIRD PARTY, EXPRESS, IMPLIED OR STATUTORY, WITH RESPECT TO THE MATERIALS OR THE ACCURACY OF ANY INFORMATION CONTAINED IN THE MATERIALS,

INCLUDING, WITHOUT LIMITATION, ANY IMPLIED WARRANTY OF MERCHANTABILITY, ACCURACY, SATISFACTORY QUALITY, FITNESS FOR A PARTICULAR PURPOSE, USABILITY, INTEGRATION OR NON-INFRINGEMENT AND ALL SUCH WARRANTIES ARE HEREBY EXCLUDED BY WILEY AND ITS LICENSORS AND WAIVED BY YOU.

6. WILEY shall have the right to terminate this Agreement immediately upon breach of this Agreement by you.

7. You shall indemnify, defend and hold harmless WILEY, its Licensors and their respective directors, officers, agents and employees, from and against any actual or threatened claims, demands, causes of action or proceedings arising from any breach of this Agreement by you.

8. IN NO EVENT SHALL WILEY OR ITS LICENSORS BE LIABLE TO YOU OR ANY OTHER PARTY OR ANY OTHER PERSON OR ENTITY FOR ANY SPECIAL, CONSEQUENTIAL, INCIDENTAL, INDIRECT, EXEMPLARY OR PUNITIVE DAMAGES, HOWEVER CAUSED, ARISING OUT OF OR IN CONNECTION WITH THE DOWNLOADING, PROVISIONING, VIEWING OR USE OF THE MATERIALS REGARDLESS OF THE FORM OF ACTION, WHETHER FOR BREACH OF CONTRACT, BREACH OF WARRANTY, TORT, NEGLIGENCE, INFRINGEMENT OR OTHERWISE (INCLUDING, WITHOUT LIMITATION, DAMAGES BASED ON LOSS OF PROFITS, DATA, FILES, USE, BUSINESS OPPORTUNITY OR CLAIMS OF THIRD PARTIES), AND WHETHER OR NOT THE PARTY HAS BEEN ADVISED OF THE POSSIBILITY OF SUCH DAMAGES. THIS LIMITATION SHALL APPLY NOTWITHSTANDING ANY FAILURE OF ESSENTIAL PURPOSE OF ANY LIMITED REMEDY PROVIDED HEREIN.

9. Should any provision of this Agreement be held by a court of competent jurisdiction to be illegal, invalid, or unenforceable, that provision shall be deemed amended to achieve as nearly as possible the same economic effect as the original provision, and the legality, validity and enforceability of the remaining provisions of this Agreement shall not be affected or impaired thereby.

10. The failure of either party to enforce any term or condition of this Agreement shall not constitute a waiver of either party's right to enforce each and every term and condition of this Agreement. No breach under this agreement shall be deemed waived or excused by either party unless such waiver or consent is in writing signed by the party granting such waiver or consent. The waiver by or consent of a party to a breach of any provision of this Agreement shall not operate or be construed as a waiver of or consent to any other or subsequent breach by such other party.

11. This Agreement may not be assigned (including by operation of law or otherwise) by you without WILEY's prior written consent.

12. Any fee required for this permission shall be non-refundable after thirty (30) days from

receipt.

13. These terms and conditions together with CCC's Billing and Payment terms and conditions (which are incorporated herein) form the entire agreement between you and WILEY concerning this licensing transaction and (in the absence of fraud) supersedes all prior agreements and representations of the parties, oral or written. This Agreement may not be amended except in writing signed by both parties. This Agreement shall be binding upon and inure to the benefit of the parties' successors, legal representatives, and authorized assigns.

14. In the event of any conflict between your obligations established by these terms and conditions and those established by CCC's Billing and Payment terms and conditions, these terms and conditions shall prevail.

15. WILEY expressly reserves all rights not specifically granted in the combination of (i) the license details provided by you and accepted in the course of this licensing transaction, (ii) these terms and conditions and (iii) CCC's Billing and Payment terms and conditions.

16. This Agreement will be void if the Type of Use, Format, Circulation, or Requestor Type was misrepresented during the licensing process.

17. This Agreement shall be governed by and construed in accordance with the laws of the State of New York, USA, without regards to such state's conflict of law rules. Any legal action, suit or proceeding arising out of or relating to these Terms and Conditions or the breach thereof shall be instituted in a court of competent jurisdiction in New York County in the State of New York in the United States of America and each party hereby consents and submits to the personal jurisdiction of such court, waives any objection to venue in such court and consents to service of process by registered or certified mail, return receipt requested, at the last known address of such party.

Wiley Open Access Terms and Conditions

All research articles published in Wiley Open Access journals are fully open access: immediately freely available to read, download and share. Articles are published under the terms of the Creative Commons Attribution Non Commercial License. which permits use, distribution and reproduction in any medium, provided the original work is properly cited and is not used for commercial purposes. The license is subject to the Wiley Open Access terms and conditions:
Wiley Open Access articles are protected by copyright and are posted to repositories and websites in accordance with the terms of the Creative Commons Attribution Non Commercial License. At the time of deposit, Wiley Open Access articles include all changes made during peer review, copyediting, and publishing. Repositories and websites that host the article are responsible for incorporating any publisher-supplied amendments or retractions issued subsequently.
Wiley Open Access articles are also available without charge on Wiley's publishing platform, **Wiley Online Library** or any successor sites.

Use by non-commercial users

For non-commercial and non-promotional purposes individual users may access, download, copy, display and redistribute to colleagues Wiley Open Access articles, as well as adapt, translate, text- and data-mine the content subject to the following conditions:

- The authors' moral rights are not compromised. These rights include the right of "paternity" (also known as "attribution" - the right for the author to be identified as such) and "integrity" (the right for the author not to have the work altered in such a way that the author's reputation or integrity may be impugned).
- Where content in the article is identified as belonging to a third party, it is the obligation of the user to ensure that any reuse complies with the copyright policies of the owner of that content.
- If article content is copied, downloaded or otherwise reused for non-commercial research and education purposes, a link to the appropriate bibliographic citation (authors, journal, article title, volume, issue, page numbers, DOI and the link to the definitive published version on Wiley Online Library) should be maintained. Copyright notices and disclaimers must not be deleted.
- Any translations, for which a prior translation agreement with Wiley has not been agreed, must prominently display the statement: "This is an unofficial translation of an article that appeared in a Wiley publication. The publisher has not endorsed this translation."

Use by commercial "for-profit" organisations

Use of Wiley Open Access articles for commercial, promotional, or marketing purposes requires further explicit permission from Wiley and will be subject to a fee. Commercial purposes include:

- Copying or downloading of articles, or linking to such articles for further redistribution, sale or licensing;
- Copying, downloading or posting by a site or service that incorporates advertising with such content;
- The inclusion or incorporation of article content in other works or services (other than normal quotations with an appropriate citation) that is then available for sale or licensing, for a fee (for example, a compilation produced for marketing purposes, inclusion in a sales pack)
- Use of article content (other than normal quotations with appropriate citation) by for-profit organisations for promotional purposes
- Linking to article content in e-mails redistributed for promotional, marketing or educational purposes;
- Use for the purposes of monetary reward by means of sale, resale, licence, loan, transfer or other form of commercial exploitation such as marketing products
- Print reprints of Wiley Open Access articles can be purchased from: corporatesales@wiley.com

Other Terms and Conditions:

BY CLICKING ON THE "I AGREE..." BOX, YOU ACKNOWLEDGE THAT YOU HAVE READ AND FULLY UNDERSTAND EACH OF THE SECTIONS OF AND PROVISIONS SET FORTH IN THIS AGREEMENT AND THAT YOU ARE IN AGREEMENT WITH AND ARE WILLING TO ACCEPT ALL OF YOUR OBLIGATIONS AS SET FORTH IN THIS AGREEMENT.

v1.7

If you would like to pay for this license now, please remit this license along with your payment made payable to "COPYRIGHT CLEARANCE CENTER" otherwise you will be invoiced within 48 hours of the license date. Payment should be in the form of a check or money order referencing your account number and this invoice number RLNK500739161.
Once you receive your invoice for this order, you may pay your invoice by credit card. Please follow instructions provided at that time.

Make Payment To:
Copyright Clearance Center
Dept 001
P.O. Box 843006
Boston, MA 02284-3006

For suggestions or comments regarding this order, contact RightsLink Customer Support: customercare@copyright.com or +1-877-622-5543 (toll free in the US) or +1-978-646-2777.

Gratis licenses (referencing $0 in the Total field) are free. Please retain this printable license for your reference. No payment is required.
